multi-Risk sciEnce for resilienT commUnities undeR a changiNg climate

Codice progetto MUR: **PE00000005** – CUP LEAD PARTNER: I33C22006910006

Deliverable title: Models for degradation prediction of infrastructure components and residual life estimates

Deliverable ID: DV 6.4.3

Due date: February 2025

Submission date: February 2025

AUTHORS

Carlo Pellegrino (UNIPD), Flora Faleschini (UNIPD), Lorenzo Hofer (UNIPD), Laura Niero (UNIPD), Paolo Zampieri (UNIPD), Aldo Milone (UNINA), Raffaele Landolfo (UNINA), Giuseppe Quaranta (UNIROMA1), Maria Sambito (UNIKORE), Gabriele Freni (UNIKORE), Cristiana Bragalli (UNIBO); Elena Toth (UNIBO); Lorenzo Carmelo Zingali (UNIBO)

1. Technical references

Project Acronym	RETURN
Project Title	multi-Risk sciEnce for resilienT commUnities undeR a changiNg climate
Project Coordinator	Domenico Calcaterra UNIVERSITA DEGLI STUDI DI NAPOLI FEDERICO II domcalca@unina.it
Project Duration	December 2022 – November 2025 (36 months)

Deliverable No.	DV4.3
Dissemination level*	
Work Package	WP4 – Modelling and experimental technologies (including AI) for vulnerability assessment
Task	T4.3 – Modelling of degradation phenomena and residual life estimates
Lead beneficiary	UNIPD
Contributing beneficiary/ies	UNIBO, POLITO, UNIROMA1, UNIPD, UNINA, UNIKORE, AlmavivA

* PU = Public

PP = Restricted to other programme participants (including the Commission Services)

RE = Restricted to a group specified by the consortium (including the Commission Services)

CO = Confidential, only for members of the consortium (including the Commission Services)

Document history

Version	Date	Lead contributor	Description
0.0	01.02.2025	Carlo Pellegrino (UNIPD)	Table of contents
0.1	17.02.2025	Carlo Pellegrino (UNIPD), Flora Faleschini (UNIPD), Lorenzo Hofer (UNIPD), Laura Niero (UNIPD), Paolo Zampieri (UNIPD), Aldo Milone (UNINA), Raffaele Landolfo (UNINA), Giuseppe Quaranta (UNIROMA1), Maria Sambito (UNIKORE), Gabriele Freni (UNIKORE), Cristiana Bragalli (UNIBO); Elena Toth (UNIBO); Lorenzo Carmelo Zingali (UNIBO)	First draft
0.2	20.02.025		Critical review and proofreading
0.3	25.02.2025		Edits for approval
1.0	28.02.2025		Final version

2. ABSTRACT

The assessment of degradation phenomena and the development of predictive models for the residual life of existing structures and infrastructures play a crucial role in ensuring the safety, durability, and effective management of aging infrastructure. This study focused on the main structural typologies found in Italy—critical reinforced concrete elements, masonry, and steel structures—analyzing their specific degradation mechanisms and vulnerabilities. This deliverable highlights how these mechanisms impact safety and performance over time, providing a detailed framework for understanding and addressing these challenges. The main outcomes include a comprehensive review of degradation processes, the development of predictive models for residual characteristic estimation, tailored methodologies for structural assessment, and practical applications to representative case studies across Italy, offering actionable insights to enhance infrastructure resilience and management strategies.

First, Section 5.1 investigates the damage in half-joints, known also as Gerber saddles. There are various causes that make Gerber saddles so susceptible to deterioration. One cause is the absence of specific regulations and prescriptions for the design of half-joints at the time of maximum use of this construction technique. This led to the creation of elements with deficiencies in reinforcement detail. Furthermore, the durability requirement was introduced in more recent times; in fact, it is often found that the concrete cover is reduced and insufficient to protect the reinforcement from physical and chemical attacks. This condition is further worsened by the complexity in the creation of Gerber chairs cast on site, with a concrete cover thickness that is non-uniform. In this context, a method for the evaluation of the load-bearing capacity of saddles subject to degradation and corrosion is proposed and results explained.

In Section 5.2, the main physical, chemical, and biological deterioration mechanisms affecting the long-term structural performance of masonry bridges are first introduced. The defects induced by these degradation processes are then systematically classified, highlighting their correlation with specific deterioration mechanisms. Subsequently, a comparative analysis of commonly used modeling approaches for the assessment of masonry bridges is presented, emphasizing the advantages and limitations of different defect modeling strategies. For each approach, reference is made to well-documented case studies to illustrate whether defects are modeled directly or indirectly.

In Section 5.3, typical degradation phenomena for steel bridges are addressed, i.e., with either reference to environmental and man-induced effects. Namely, metallic corrosion and fatigue cracking occurring in structural components belonging to steel critical infrastructures are addressed from both a phenomenological and a modelling perspective, i.e., at material and structural scale, respectively.

In Section 5.4, a numerical modelling approach is presented to investigate the deterioration of integral abutment bridges (IABs), essential for understanding their long-term durability and safety. In this context, the research unit at Sapienza University of Rome is developing a comprehensive numerical model to simulate the combined effects of traffic loads, thermal gradients, chloride-induced corrosion (in both ordinary reinforcement and post-tensioned tendons), and aging phenomena such as steel relaxation, creep, and shrinkage of concrete. This report presents the selected case study, highlighting the structural model and the numerical approaches employed to simulate corrosion processes triggered by airborne chlorides. The adopted numerical framework is designed to capture key corrosion mechanisms, including chloride diffusion through concrete, the initiation and propagation of steel corrosion, and the resulting loss of cross-sectional area in both reinforcement and tendons. Additionally, the model accounts for time-dependent and spatially

varying chloride exposure, enabling accurate predictions of localized corrosion effects on structural components.

Then, the focus of Section 6.1 concerns the deterioration and residual life prediction for water distribution networks. Modeling the water pipe failure rates and residual life prediction requires to assemble and validate data on physical properties about individual pipes (diameter, age, length, depth) and their operation (pressure, velocity) and data on external pressure, as climate data and external loads due to traffic. The analysis will first consist in collecting and validating data from multiple sources containing statistical and dynamical drivers. In the modeling activity, machine-learning approaches will be applied to the large-scale real-world Water Distribution Network maintenance dataset for attempting to interpret the degradation phenomena and therefore provide information on the residual life.

Finally, Section 6.2 is focused on urban drainage infrastructure deterioration and investigating the efficiency of prediction models. After a classification and the identification of advantages and disadvantages of different approaches, the chapter focuses on the data needs of each approach and the definition of compelling developments of existing approaches to be applied to urban drainage pipes.

3. Table of contents

List of Tables

List of Figures

4.Introduction

4.1 Context and importance of Residual Life Estimate in Italian Infrastructure

The residual life estimate is a fundamental topic for the stability and safety of our society. In Italy, many historical structures, such as bridges, tunnels, and aqueducts, have reached or exceeded their nominal lifespan. Over time, these structures are subjected to deterioration processes that can alter their structural characteristics, compromise their functionality, and reduce their safety. Quantifying how degradation affects their performance is essential to plan targeted interventions, mitigate risks, and prevent socio-economic and environmental consequences.

4.2 Motivation for classification based on infrastructure type and construction materials

The aging of infrastructure components poses critical challenges, as degradation processes over time can alter structural characteristics, reduce their capacity, and compromise their functionality. These effects, coupled with man-made hazards such as traffic loads and industrial activities, significantly increase the risk of structural failures. The classification has been developed based on the different types of infrastructure and the construction materials used, recognizing that each material and structural type requires specific analysis to assess the residual life estimate. This assessment is essential for understanding the extent of deterioration, planning targeted interventions, and ensuring long-term safety and functionality. This deliverable provides a comprehensive methodology to address these challenges, emphasizing the importance of quantifying and mitigating degradation to preserve infrastructure resilience.

4.3 Purpose and structure of the document

The primary objective of this document is to assess degradation mechanisms affecting infrastructure components and to develop predictive models for estimating their residual life. This analysis is essential for ensuring the safety, durability, and efficient management of aging infrastructure, particularly in the context of Italian infrastructures.

5. Modeling of deterioration and residual life prediction of Road and Highway Infrastructures

5.1 RC and PC Bridges (Carlo Pellegrino and Flora Faleschini)

5.1.1 Degradation phenomena in critical reinforced concrete elements

The main object of this analysis is the damage in half-joints, known also as Gerber saddles. There are various causes that make Gerber saddles so susceptible to deterioration. One cause is the absence of specific regulations and prescriptions for the design of half-joints at the time of maximum use of this construction technique. This led to the creation of elements with deficiencies in reinforcement detail. Furthermore, the durability requirement was introduced in more recent times; in fact, it is often found that the concrete cover is reduced and insufficient to protect the reinforcement from physical and chemical attacks. This condition is further worsened by the complexity in the creation of Gerber chairs cast on site, with a concrete cover thickness that is non-uniform. Among other causes, the position and geometry of the element can certainly be identified. The saddles are points of discontinuity in the deck and expansion joints are found in correspondence with them. If these joints are not correctly monitored and maintained, they can break and, combined with inadequate rainwater management systems, cause water to percolate onto the element. This problem is aggravated by the use of anti-freeze salts in the winter period which contaminate the water with quantities of chlorides not negligible. This issue is very important especially in support saddles, due to their geometric conformation there is the stagnation of water in the recut area and therefore the predisposition to an accelerated degradation of these areas and of the support devices.

Geometry and steel reinforcement layout favor the formation of more or less extensive crack patterns. According to the studies carried out in literature, the first crack originates from a load approximating approximately 20%-40% of the ultimate load and is usually generated at 45° starting from the attachment point of the saw. It is easy to imagine, thanks to the increases in traffic load that have occurred over the last 50 years, how frequent this condition is on existing bridges. At the time of the inspection it is of fundamental importance to detect the distribution of the crack pattern, useful for a future monitoring program of critical cracks and for a first estimate of the reinforcement actually present.

Figure 1 - Degradation phenomenon in a Gerber saddle.

The degradation of concrete is caused by various phenomena and can develop from the first days after casting, but more often degradation occurs over a long period of time due to environmental actions. The main recognizable phenomena are freeze-thaw attacks, sulphate attacks, alkali-aggregate reactions, mechanical actions and corrosion of reinforcement. Among them, the last is the most important degradation phenomena and is treated in detail. Further, there may happen humidity washout and stains formation, biological colonization, efflorescence phenomena, gravel nests and impact damage.

5.1.2 Steel corrosion – carbon or chlorides-induced corrosion

In standard conditions the steel bars are protected by a highly alkaline solution present in the pores of the concrete, the pH varies between 13 and 14. This condition allows the steel to be kept depassivated. Carbonation or chloride penetration can reduce the pH and make the bars susceptible to corrosion. As indicated in Tuutti's model (*Tuutti 1982*), two phases are recognisable. The first is initialisation, in which the substances (CO2 or chlorides) penetrate the concrete and reach the reinforcements, and the second is propagation in which corrosion develops. Carbon dioxide can react with the alkaline compounds present in the pores, this reaction (Eq. 1) reduces the pH of the concrete, making it close to neutrality. The bars are therefore no longer protected by the passivation film.

$$CO_2 + Ca(OH)_2 \xrightarrow{H_2O, NaOH} CaCO_3 + H_2O \tag{1}$$

The corrosion that develops in this type of process is uniform. Over time the products, which occupy a greater volume than the initial material, accumulate around the bar and can cause cracking and spalling of the concrete cover. The rate of carbonation is negligible in dry or water-saturated concrete, but is maximum for concrete with relative humidity between 60% and 80%. This phenomenon will therefore develop faster in external elements and protected from the elements. Another factor that influences the diffusion of CO2 is porosity, cement paste with a sufficiently low water/cement ratio will have reduced capillary porosity and therefore limited penetration of the carbonated front.

$$x_c(t) = \sqrt{2 \cdot k_e \cdot k_c \cdot (k_t \cdot R_{ACC,0}^{-1} + \varepsilon_t^{\circ}) \cdot C_s} \cdot W(t) \cdot \sqrt{t} \tag{2}$$

There are several methods available in the literature for calculating the depth of carbonation, among which the one reported in fib Bulletin 34 is the most well-known (*fib 2006*). This equation is related to a probabilistic approach to corrosion in non-cracked concrete. x_c is the depth of the carbonated front [mm] at time t, t expressed in years, R_{ACC}^{-1} is the inverse of the effective resistance to carbonation and ε_t is an error parameter. Both of these last parameters are expressed in [(mm^2/year)/(kg/m^3)]. C_s instead is the concentration of CO2 in the air [kg/m^3]. The calculation of the environmental coefficients k_e, transfer k_c, regression k_t and W(t) climate function must be carried out in accordance with the provisions reported in Annex B of Bulletin 34.

The presence of chlorides in the concrete pore solution can cause pitting corrosion in the reinforcement. This type of corrosion is highly localized and causes pits, or pitting, in a specific area of the bar. The initiation phase ends when the chloride content near the armor exceeds the critical level, the protective film breaks. Studies conducted by *Gjorv 2014* have demonstrated the difficulty in accurately describing the penetration of chlorides into concrete and defining its critical content. Also in this case the phenomenon develops more quickly in the external areas protected from the weather, an element subjected to wetting absorbs the water loaded with chlorides by capillarity, while during the drying periods the water evaporates causing an accumulation of chlorides in the concrete. The penetration of chlorides is therefore dependent on the geometry, exposure, environment and properties of the concrete. The phenomenon is usually described in a simplified way through the second Fick equation, an approach also used by *fib Bulletin 34 2006*. The formulation reported in this last Bulletin considers the possibility of having an initial C0 chloride content other than zero.

$$C(x=a,t) = C_0 + (C_{S,\Delta x} - C_0) \cdot \left[1 - erf \frac{(a-\Delta x)}{2 \cdot \sqrt{D_{app,C} \cdot t}}\right] \tag{3}$$

Where $C(x{=}a,t)$ is the chloride content at time t and at the depth a where the reinforcements are located, C_0 is the initial content and $C_{s,\Delta x}$ is the value measured at depth Δx. All these values are indicated in % of the weight of cement. x is the depth at which the phenomenon is studied, a the thickness of the concrete cover and Δx is the depth of the convection zone where the penetration by chlorides differs from Fick's second law, all these expressed in [mm]. t is the time in years and *erf* the error function. The apparent diffusion coefficient $D_{app,C}$ can be obtained from equation (B2.1-2) and (B2.1-3/4) of Bulletin 34. This depends on the type of cement used, the ambient temperature and curing time of the jet. The corrosion rate can be estimated through Faraday's law (Eq.4) starting from data collected in situ or through empirical methods.

$$V_{corr} = 0.0116 \cdot i_{corr} \tag{4}$$

The penetration of the attack is instead determined by (Eq. 5):

$$P_x = V_{corr} \cdot t_p \cdot \alpha \tag{4}$$

where P_x is the penetration of the corrosive attack indicated in [μm], V_{corr} is the speed of evolution of the phenomenon [μm/year], t_p is the time elapsed since depassivation of the bars [years] and α is the pitting factor. t_p can be estimated using the models reported in the previous paragraphs. Various experimental studies have shown that using α=4 allows for the best correlation between analytical and experimental data. In the presence of uniform corrosion α=1. i_{corr} is the current density expressed in [mA/cm^2]. It can be determined experimentally by using an LPT linear polarization test or through empirical models, such as *Liu and Weyers* 1998.

One of the main effects of corrosion degradation of reinforced concrete is the reduction of the resistant section of the reinforcement. As reported in Biondini's studies (*Biondini* 2011), the effects on the reduction of resistant area are different in relation to the type of corrosion, see Figure 2. The remaining resistant area, determined with the equations referred to below, refers to the instant in time in which P_x was evaluated. Different models are available to consider such phenomena, such as those reported in *Gonzales et al.* 1995 and *Val et al.* 1997.

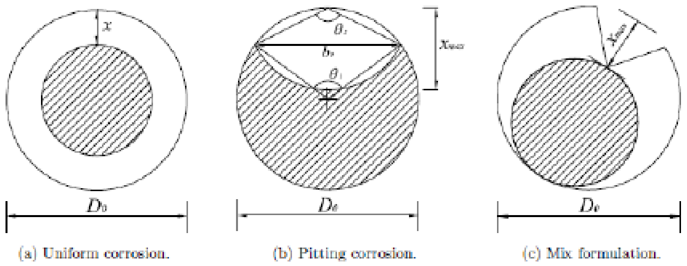

Figure 2 - Effects of corrosion on steel bars (*Biondini* 2011).

A further effect to consider is the variation in the tensile behavior of the steel, an aspect that influences the ductility of the structure. As highlighted in the studies of *Almusallam* 2011, as the degree of corrosion of the bar increases, there is a less extensive plastic branch of the σ-ε bond. A change in behavior from ductile to brittle can be identified for a section loss of approximately 15%, as highlighted in Figure 7.

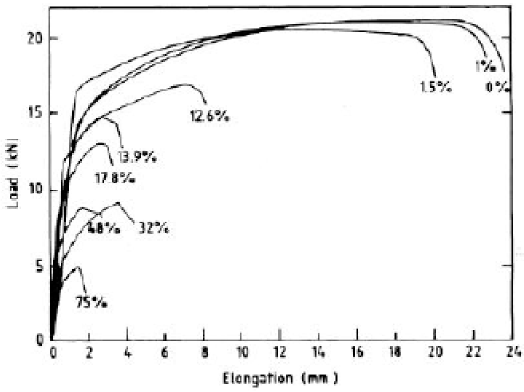

Figure 3 - Effect of corrosion on steel tensile behavior (*Almusallam* 2001)

From the results obtained from tensile tests on corroded bars, a slight reduction in the yield stress and ultimate strength of the steel was noted. This result can be attributed to the irregular shape of the corroded section of the bar; in some points, stress peaks may occur which lead to plasticization of the area earlier than the remaining section. This reduction, although small and often overlooked in the verification phases, can therefore only be found in the presence of pitting corrosion. Numerous models are available in the literature for the definition of reduced ultimate resistance and strain, all based on linear models as a function of section loss.

Lastly, bond capacity between reinforcement and concrete is strongly influenced by the presence of longitudinal cracks and the accumulation of rust around the bar. From experimental tests carried out by *Coronelli and Gambarova* 2004, two phases were highlighted. The first in which there is an increase in resistance capacity due to adhesion, thanks to the confinement offered by the accumulation of corrosion products around the bar. Rust and oxides have a greater volume than the original material and therefore cause compression on the armor. This effect increases up to the point where the tensile stresses generated on the concrete lead to the creation of the longitudinal crack. At this moment the confinement on the bar is lost and the adhesion undergoes a progressive deterioration as the level of corrosion increases. Also worth highlighting is the contribution due to the reduction of the rib area. Models that describe this behavior are covered in the version of *fib Model Code* 2020. Furthermore, these standards will also deal in greater detail with the problem of adhesion for smooth bars with square or spiral sections. Particularly there two models are proposed for calculating the bond strength in the presence of corroded bars. These apply to both ribbed and smooth armor, hooks or bends are not considered.

To evaluate the influence of corrosion phenomena on the load bearing capacity of Gerber saddles, this work was carried out to reproduce numerically some tests carried out in literature, which will be used as a base to carry out further parametric analysis in a second moment. The tests are those reported in *Di Carlo et al.* 2023, briefly reported here. The aim of the experimental test is to study the influence of bars corrosion on strength and ductility of Gerber saddles. Two beams with nibs at both ends are produced and tested; the first one in a non-corroded configuration and the other one subjected to accelerated corrosion process before being loaded. Corrosion is present only in the reinforcement involved in the resistant mechanism. The test configuration is composed by a fixed restraint at midspan created with two transversal steel beams, to simulate structural continuity, and a cylindrical support with 100mm radius positioned 700mm from the fixed section. Load is applied through an hydraulic press to the saddle, its footprint is 200x100mm and is located 800mm from the support. Beams have a total length of 4300mm, with a section of 500x200mm. Nib has a reduced height of 250mm and extends for 300mm. Four upper Ø16 bars and four lower Ø10 bars extend for all the element's length, shear reinforcement is composed by two-arm Ø10 stirrups with 50mm spacing in the central 1050mm of the sample and with a 100mm spacing in the remaining parts. Each beam has two reinforcement layouts in the nib, later called G1 and G2. G1 saddle has two Ø12 horizontal bars, two Ø10 two-arm stirrups in the section change zone and three Ø12 diagonal bars. G2 half-joint has four Ø12 horizontal bars, three Ø10 two-armed stirrups and three Ø12 diagonal bars. Both have two vertical Ø12 stirrups in the nib. Average cubic compression strength of concrete is 52.6MPa, steel yielding and failure stresses depend on the reinforcement type and position and ranges between 455 and 507 MPa for yielding, and 545 and 612 MPa for ultimate strength.

The numerical model is carried out in Abaqus FEA environment. Only half beam is modelled software to reduce analysis computational cost, using a symmetrical scheme with respect of the mid span section. Concrete is modelled with three dimensional elements while reinforcement are truss elements. A perfect adherence constraint is considered between bars and concrete. Concrete compressive behaviour is determined from average compressive strength fcm using the relationships reported in *Eurocode* 2 (2023) at 5.1.6.(3). In absence of experimental data, tensile behaviour is defined via fracture energy GF. Numerous studies on GF are available, and we used the approach present in the Japanese code *JSCE* (2007) which is well-knwon to provide the least error in estimating fracture energy. Starting from that value is possible to determine the σ-w curve of concrete tensile behaviour according to *fib Model Code* 2010.

In FEM software, concrete is modelled as an elastic material up to a tension of $0.4^{*} f_{cm}$ and with Concrete Damage Plasticity in the plastic section. Tensile behaviour is defined with CDP and σ-w curve. Steel is modelled as a bilinear elastic-plastic material with hardening branch. Ultimate strain εu is considered equal to 7.5%. A symmetry restraint is applied to the mid span section of the beam to simulate the behaviour of a complete element. Load is applied as an incremental displacement. An overview of the reinforcement layout is shown in Figure 4.

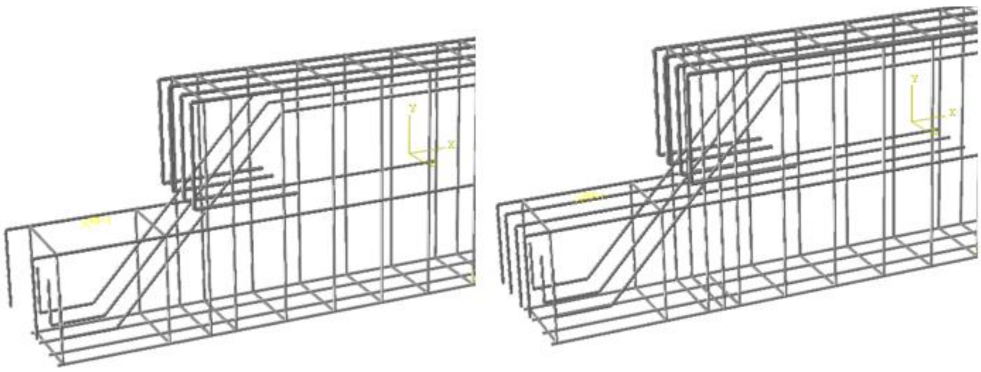

Figure 4 - Reinforcement layout (G1 on the left, G2 on the right).

Saddles subjected to artificial corrosion, G1_c and G2_c, have geometric and material differences. As regards concrete, cover is not considered in the numerical model. In fact, in presence of corrosion with penetration depth higher than 0.4mm, as in the cases studied, it is hypotized that the concrete cover has almost no contribution to consider cracking and spalling effects. Since mechanical properties of corroded steel are not available, they are estimated using Andrade models. The modified constitutive behavior are shown in Figure 5.

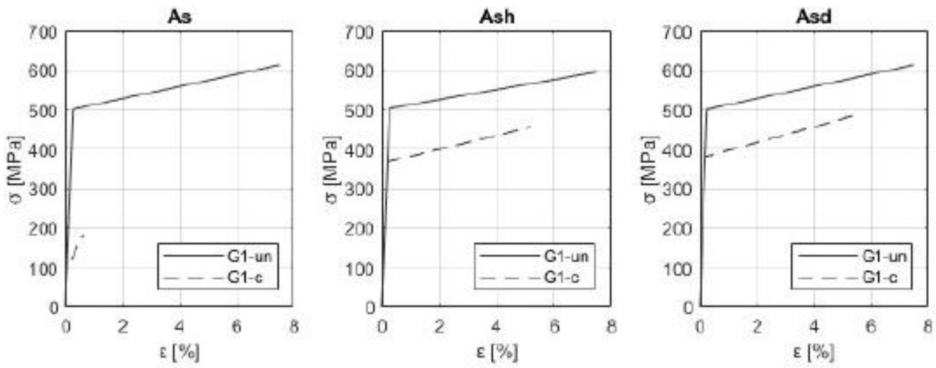

Figure 5 - Modified constitutive behavior for corroded reinforcement.

Comparison between experimental and numerical results is performed only for the failure load value. Studying the sensors configuration used to get displacement and strain in experimental test, some doubts arose about reliability of the data collected, therefore a comparison of force-displacement curve is not carried out.

The full push-down numerical curves are shown in Figure 6.

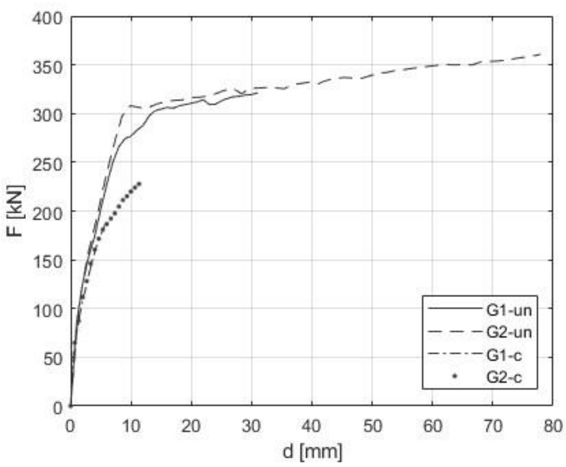

Figure 6 - Push-down numerical curves.

Experimental test highlighted a failure load of 301.5 kN and 331.8 kN for samples G1-un and G2-un. Numerical values obtained for the same saddles are 321.3 kN and 360.6 kN respectively, thus making an error between 6% and 8%. F-d curves of corroded elements exhibit brittle failure without reaching a plateau zone. Numerical shear capacities obtained are 189.9 kN for G1_c and 222.7kN for G2_c, with an error of 14% and 8% respectively. These differences may be caused by following factors:

1. Concrete constitutive model is determined with the formulation given in codes. Using values obtained from load test a better accuracy can be reached.
2. Steel constitutive law is based on codes or values commonly used in practice. Since the analysis are interrupted when steel strain exceeds εu, a correct value for failure strain is essential to define the final analysis step.
3. Section loss has been determined from a graphical reference, introducing a possible data reading error.
4. Model developed b Andrade to consider the effects of corrosion on mechanical parameters of steel is calibrated on section losses between 0% and 11%, values much lower than the ones of this study. Experimental data of corroded bars allow to eliminate these uncertainties.

Results obtained confirm the reliability of the numerical modeling approach to capture the ultimate behavior of corroded saddles, clearly identifying the main variations of their structural behavior not only in terms of ultimate behavior but also in terms of overall response to the external loading. These approach will be used to further carry out simulations to investigate the effect of corrosion extension and effects in the reinforcements of Gerber saddles.

5.2 Masonry Bridges (Carlo Pellegrino)

5.2.1 Review of Deterioration Phenomena at Material Scale

The deterioration of masonry materials is a complex and multifaceted process influenced by a variety of environmental and intrinsic factors. This review examines the phenomena of deterioration at the material scale, emphasizing the mechanisms that degrade structural integrity over time. Figure 7 illustrates the overarching procedure of deterioration, providing a systematic framework to understand the interplay between external actions, deterioration mechanisms, and resulting damage (UIC report 2020). This understanding is essential for identifying the factors that compromise the durability of masonry structures and for proposing effective conservation strategies.

Figure 7 – Representation of the deterioration process in existing masonry bridges.

The degradation processes observed in masonry materials are categorized into three primary types: physical, chemical, and biological deterioration (Figure 8). This classification is based on the type of action causing them, with each type reflecting distinct characteristics and impacts on the material. Physical deterioration results from mechanical stresses induced by environmental factors, chemical deterioration arises from interactions that alter the material's composition, and biological deterioration is caused by organisms that chemically or mechanically degrade the material. These phenomena often act synergistically, amplifying their overall impact on the material.

2.1.1.1. Physical Deterioration

Physical deterioration is primarily driven by mechanical stresses from environmental factors, often intensified by the inherent properties of the masonry material. Freeze-thaw cycles are particularly damaging in climates with frequent temperature fluctuations around freezing (Camuffo et al. 2021). Water infiltration into the material's pores leads to freezing and expansion by approximately 9%, generating significant pressure that causes internal cracking and surface spalling over repeated cycles (Made et al. 2004; Powers 1945). Poor drainage systems and prolonged exposure to moisture exacerbate this process by allowing more water to penetrate the structure. Another major factor is wind abrasion, where windborne particles erode masonry surfaces. The degree of damage depends on the velocity of the wind, particle size, and the material's hardness (UIC report 2020). Over time, this erosion forms characteristic honeycomb patterns, particularly in softer stones or porous surfaces. Salt crystallization is equally detrimental (Granneman et al. 2016). Salts dissolved in water infiltrate the masonry and recrystallize as water evaporates, creating internal pressures that fracture the material. This phenomenon is especially severe in regions with high humidity, where repeated cycles of salt dissolution and crystallization accelerate deterioration (Scherer 1999).

2.1.1.2. Chemical Deterioration

Chemical deterioration arises from a series of interconnected processes that alter the composition and integrity of masonry materials through reactions with environmental agents. One of the most pervasive processes is carbonation, where atmospheric CO_2 dissolves in rainwater to form carbonic acid. This acid reacts with calcium carbonate in the masonry, producing calcium bicarbonate, a soluble compound that dissolves and washes away, weakening the structure

(Ferretti et al. 2006). This phenomenon primarily occurs in carbonate-based materials such as limestone, dolomite, marble, mortars, and plasters. Over time, this reaction can also lead to the formation of surface crusts that initially act as protective layers but often detach, exposing the underlying material to further degradation. Hydrolysis is a chemical weathering process mainly affecting silicate and carbonate minerals. When the original stone comes into contact with rainwater, it disintegrates, leading to the formation of clay minerals that are weaker than the original ones. The rate of solubilization depends on the nature of the material, the acidity of the water, and the climate. Oxidation often accompanies carbonation, particularly in masonry containing iron-rich minerals. When exposed to oxygen and moisture, these minerals oxidize to form iron oxides and hydroxides, which weaken the cohesion of the masonry (Winkler 1973). The reddish-brown stains caused by oxidation are a common early indicator of this deterioration and are frequently linked to progressive structural weakening. Hydration further exacerbates chemical deterioration. Anhydrous minerals such as calcium sulfate absorb water and expand to form hydrated compounds like gypsum. This volumetric expansion creates internal stresses within the masonry, resulting in cracking and surface crusting. These gypsum layers, often darkened by pollutants, compromise both the aesthetic and structural integrity of the material. Finally, acid rain accelerates these processes by introducing additional acidic compounds. Pollutants such as sulfur dioxide and nitrogen oxides react with atmospheric moisture to form sulfuric and nitric acids, which aggressively attack masonry minerals (De Ponti et al. 2021). Acid rain is particularly damaging in urban and industrial environments, where pollutant concentrations are higher, leading to rapid dissolution and degradation of the masonry structure.

2.1.1.3. Biological Deterioration

Biological growth contributes significantly to both chemical and physical weathering. Microbial activity, such as the secretion of organic acids by bacteria, fungi, and lichens, chemically degrade masonry surfaces. For instance, lichens produce oxalic acid that dissolves the outer stone layers. Over time, the growth of these organisms facilitates further chemical and physical attacks (Chen et al. 2000). Vegetation growth is another critical aspect of biological deterioration. Roots from plants and trees penetrate existing cracks, exerting mechanical pressure that widens these cracks. This allows for greater water infiltration and accelerates other degradation processes (Biscarini et al. 2020).

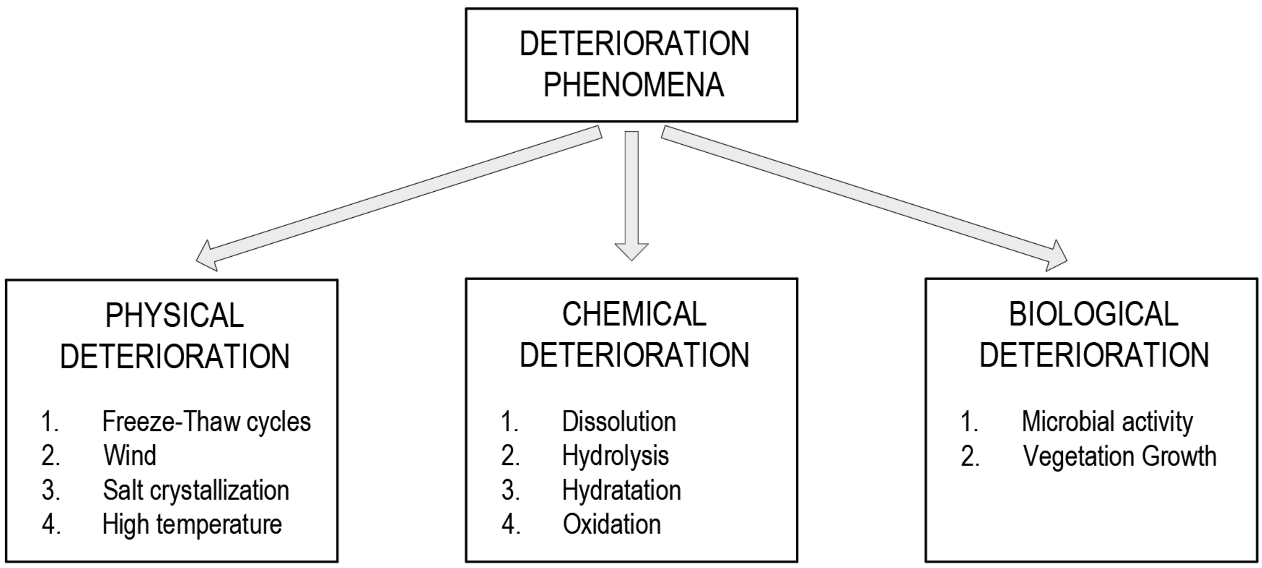

Figure 8 – Representation of typical deterioration phenomena in masonry bridges caused by physical, chemical, or biological actions.

The interaction of deterioration phenomena reveals critical damage patterns that provide insights into the structural health and longevity of masonry materials. Surface changes such as discoloration, efflorescence, and crust formation indicate chemical and biological activity, while spalling, cracking, and fragmentation reflect the effects of physical stresses and the weakening of material cohesion. These damages often extend beyond superficial layers, leading to structural disjunctions, deformations, and compromised load-bearing capacity, making accurate diagnostics vital for addressing their underlying factors.

This analysis of deterioration phenomena provides essential insights that form the foundation for modeling damage and incorporating these factors into the assessment of load-bearing capacity. By understanding the interplay between deterioration processes and structural performance, it becomes possible to develop more accurate predictive models and improve maintenance strategies for masonry structures. Furthermore, the growing impact of climate change amplifies the urgency of conservation efforts. Rising temperatures, more frequent wet-dry cycles, and increased levels of atmospheric pollutants are expected to intensify deterioration processes such as freeze-thaw damage, salt crystallization, and acid rain-induced chemical degradation.

5.2.2 Modeling of Deterioration Phenomena at Structural Scales

Deterioration at the material scale encompasses localized mechanisms of physical, chemical, and biological degradation. Modeling at the structural scale, however, is essential to evaluate how these combined phenomena influence the overall performance of masonry bridges. In many cases, the underlying processes of degradation are not explicitly modeled. Instead, engineers assume certain levels of degradation and focus on investigating their effects on structural response and load-bearing capacity. This approach simplifies complex deterioration mechanisms, translating them into quantifiable changes in mechanical behavior and material properties. Such simplifications enable an efficient analysis of structural safety and serviceability, emphasizing changes in load-bearing capacity, stiffness reduction, and stability under service and extreme conditions.

Figure 9 - Representation of some typical defect types in existing masonry bridges: (a) loss of material in the joints; (b) loss of bricks; (c) longitudinal cracking; (d) transverse cracking.

	Empirical methods	Limit analysis 2D	Limit analysis 3D	FEM 2D	FEM 3D
Infiltration	-	1	1	2	2
Efflorescence	-	1	1	2	2
Vegetation	-	1	1	1	1
Alveolization	-	1	1	1	1
Cracks along joints	-	2	2	2	2
Loss of material in joints	-	2	2	2	2
Cracks in bricks	-	1	1	2	2
Exfoliation	-	2	2	2	2
Missing or broken masonry elements	-	2	2	2	2
Impact damage	-	2	2	2	2
Cracks between arch and vault	-	1	2	1	2

Table 1 – Different types of damage in masonry bridges modeled using empirical methods, limit analysis (2D and 3D), and FEM (2D and 3D). Specifically: - inability to model the damage; 1 simplified damage modeling; 2 direct damage modeling.

Masonry bridges exhibit a wide range of defects that compromise their structural integrity, arising from environmental exposure and mechanical stress. One of the most common issues is moisture infiltration, which leads to material degradation by promoting efflorescence due to salt crystallization. This phenomenon weakens the masonry fabric over time, exacerbating surface deterioration and increasing the risk of exfoliation. The presence of efflorescence is an indicator of salt migration within the masonry, resulting from prolonged exposure to moisture cycles. Similarly, vegetation growth within cracks and joints accelerates deterioration by retaining moisture and exerting mechanical pressure on the surrounding masonry, further promoting disaggregation and mortar loss. Alveolization, a type of surface erosion that manifests as small cavities, typically results from sustained exposure to atmospheric agents, including freeze-thaw cycles and chemical pollutants. This process gradually depletes the protective outer layers of masonry elements, exposing deeper layers to accelerated degradation. Cracking patterns in masonry bridges do not always indicate significant structural issues; however, in some cases, they can be a concern. Cracks along joints (Figure 9c,d) may develop due to mechanical stress, thermal expansion, and differential settlements. When critical, these cracks can impact on the structural stability of the bridge by altering load transfer mechanisms and creating potential points of failure. Material loss is another crucial aspect of degradation, particularly in the form of loss of material within joints (Figure 9a), where mortar erosion weakens the cohesion between masonry units. Exfoliation, delamination, and disaggregation further contribute to the progressive weakening of the structure by reducing the effective cross-section of load-bearing elements. Additionally, missing or broken masonry elements (Figure 9b) introduce local stress redistributions, leading to further instability. Impact-related damage, such as damage from external shocks, typically caused by vehicular collisions or falling debris, results in localized fractures that propagate under repeated loading conditions. Lastly, cracks between the arch and vault indicate significant structural distress, often associated with differential movement, settlements, or changes in internal thrust distribution. The defects commonly observed in masonry bridges are summarized in Table 1, which provides a systematic classification of the most relevant forms of defects affecting these structures.

The following sections analyze two main categories of methods for assessing masonry bridges affected by deterioration phenomena. These methods are summarized in Table 1, which outlines whether a typical defect type can be modeled using a numerical approach, and whether this modeling can be conducted in an approximate or direct manner. Empirical methods, such as the MEXE method, are omitted from the discussion as they are unable to accurately account for the

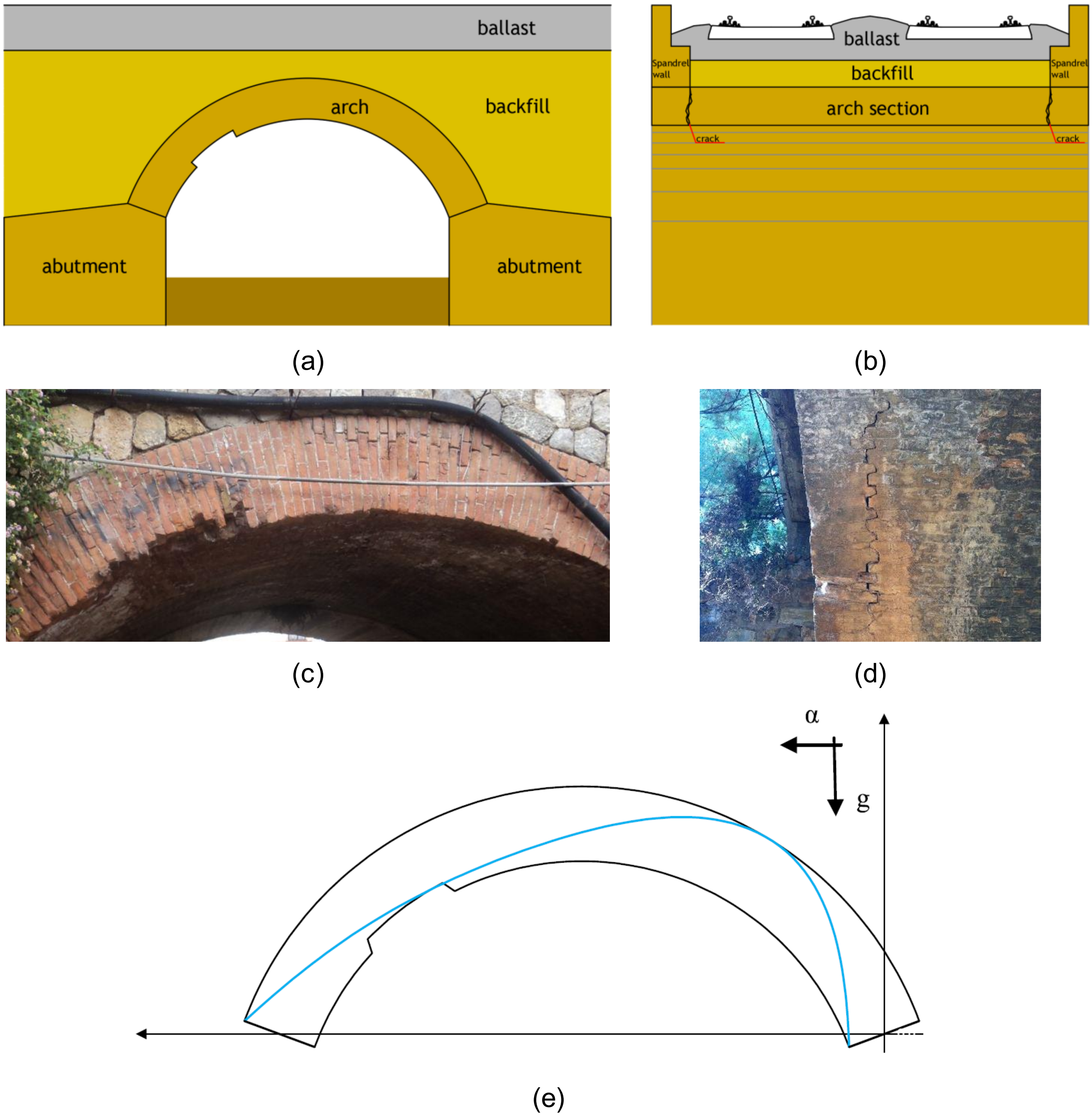

Figure 10 – (a) Bridge longitudinal section; (b) Bridge transverse section; (c) arch local thickness reduction; (d) arch and spandrel wall separation; (e) Thrust line of the case-study. (Zampieri et al. 2016)

detailed degradation phenomena that characterize masonry bridges (UIC 2018). In fact, these methods provide a simplified approach to evaluating structural capacity, relying on global parameters and safety factors to estimate the load-bearing capacity of bridges. While effective for preliminary assessments, empirical methods cannot explicitly account for the complex effects of structural deterioration, such as material loss, cracking, or joint degradation. This limitation necessitates more advanced approaches that can model these effects in detail.

2.1.1.4. Modeling based on Limit Analysis

Limit analysis provides a more refined framework for incorporating deterioration phenomena into structural models, effectively addressing defects that empirical methods fail to consider. The loss of material in mortar joints, missing or broken bricks, surface exfoliation, and impact damage can be represented through reductions in the thickness of structural elements or reductions in the length of contact interfaces between adjacent blocks. These modifications directly affect stress transfer mechanisms within the masonry structure, allowing for a realistic representation of the structural response under degraded conditions. Even localized reductions in the effective cross-section of an arch can significantly impact its load-bearing capacity, as the arch is the primary structural element resisting external loads.

These strategies for modeling defects are exemplified in the works of Gilbert (1993), who modeled mortar joint loss to provide a detailed representation of the contact surface between masonry blocks and its influence on load distribution. Similarly, Zampieri et al. (2016) analyzed impact damage by reducing the thickness of specific portions of the arch to simulate localized damage scenarios (Figure 11). Cavalagli et al. (2017) addressed imperfections in masonry bridge geometry by modifying the thickness, width, and centroid position of the individual blocks constituting the model. This approach allowed for an evaluation of the effects of these irregularities on structural capacity, highlighting the importance of considering such imperfections in numerical models. These studies highlight how modeling strategies can capture the variations in structural response caused by some defects, providing valuable insights into the behavior of masonry bridges under degraded conditions without necessarily requiring overly complex methods.

Specific defects, such as transverse and longitudinal cracking, are often modeled in an approximate manner using these strategies. For instance, transverse cracks may be represented by reducing the interface area between blocks, while longitudinal cracks are typically accounted for by assuming a reduced effective depth of the arch. This simplification reflects the presence of the crack and its influence on load distribution without explicitly modeling the crack itself. The differences in stiffness and the decoupled behavior between the arch and the spandrel walls are often modeled by assigning reduced strength to the contact surface, capturing the loss of connectivity between these structural elements. In addition to geometric changes, deterioration also impacts material properties, reducing key mechanical parameters such as compressive strength, tensile strength, friction, and cohesion. The values of these quantities must be estimated based on experimental data and statistical relationships available in literature, considering the type of masonry and the intensity of the degradation.

These approaches, when integrated with experimental data and statistical relationships, provide a robust framework for addressing the influence of deterioration on the structural response of masonry bridges, offering practical solutions for their assessment and conservation.

2.1.1.5. Modeling based on FEM/DEM

More detailed numerical approaches, such as the Finite Element Method (FEM) and Discrete Element Method (DEM), allow for a more precise representation of defects in existing masonry bridges. These methods enable the direct modeling of material loss, surface exfoliation, and localized damage in either two-dimensional or three-dimensional models, depending on the required level of detail. In such cases, material losses can be explicitly represented, creating a model that closely follows the actual geometry of the bridge, often reconstructed based on photogrammetric surveys that account for irregularities and unique features of the structure. Additionally, the loss of material in superficial joints can be directly modeled depending on the chosen numerical approach. Unlike limit analysis, where cracks are approximated, FEM and DEM allow for the direct introduction of fracture surfaces at their exact locations, enabling a more realistic representation of crack propagation and interaction. Other defects can be incorporated by adjusting the constitutive models of the masonry, modifying key mechanical parameters to reflect deterioration, similarly to how limit analysis approaches approximate the effects of degradation.

Figure 11 illustrates how the yield surface modifies and how constitutive law of uniaxial compression and tension can be represented in the presence of deterioration. It is possible to define reduction parameters for compressive and tensile strength (d_c and d_t), which can be derived from in-situ tests or data reported in the literature. These models provide a framework for understanding the effects of deterioration on structural behavior and refining numerical simulations accordingly. A practical implementation of this approach is found in Saviano et al. (2022), where FEM was used to assess the effects of aging on the in-plane lateral capacity of tuff stone masonry walls. In this study, aging was simulated by progressively reducing compressive strength values to account for

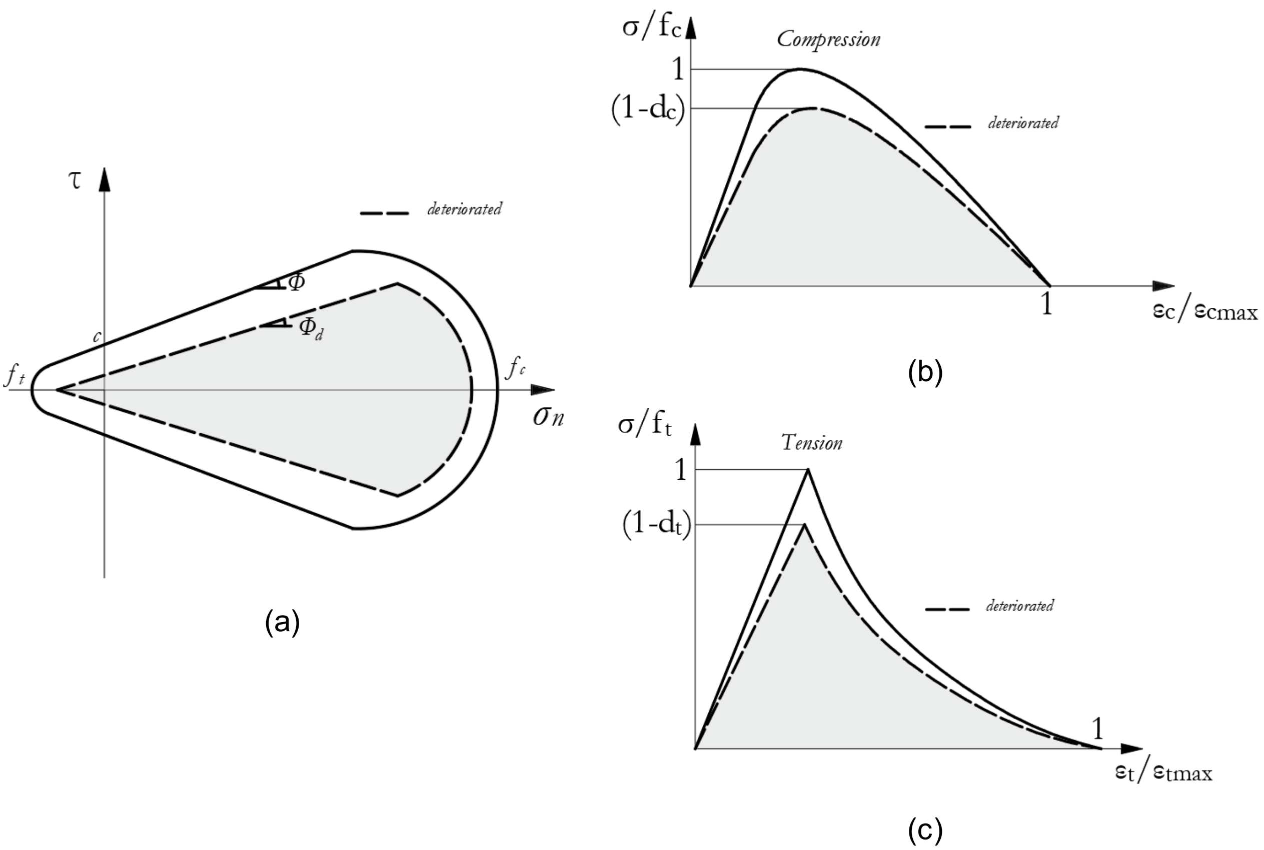

Figure 11 – Variation of the yield surface and representation of constitutive laws for uniaxial compression and tension in presence of deterioration.

material alterations caused by water infiltration and rising damp. Other mechanical parameters, such as tensile strength, elastic modulus, shear modulus, and fracture energies, were estimated through established literature correlations. This methodology enabled a comprehensive assessment of degradation effects on structural performance, demonstrating how aging leads to a progressive reduction in both lateral capacity and stiffness over time.

Despite the importance of estimating the compressive strength of degraded masonry, few studies in literature provide specific formulations for its assessment. One of the few examples is the work of Tomor et al. (2023), which analyzed the influence of moisture content on the uniaxial compressive strength of sandstone (Figure 12). Their study provides correlations between dry and partially saturated compressive strengths, offering a framework for understanding how moisture exposure contributes to material degradation.

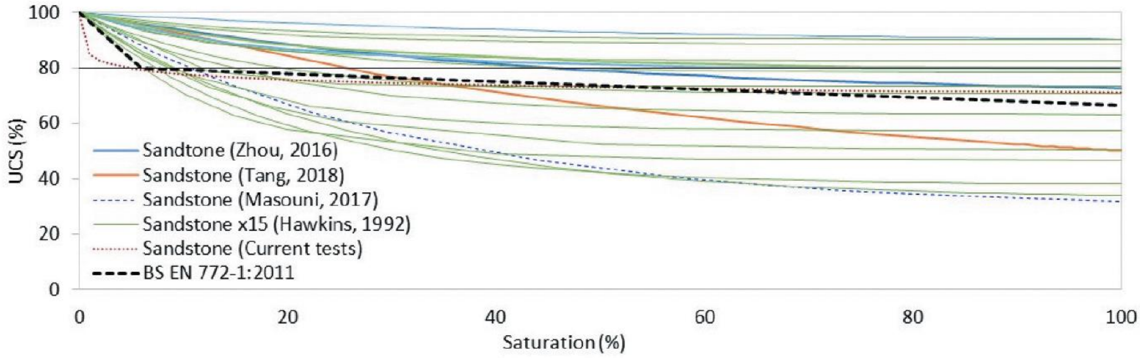

Figure 12 - Uniaxial Compressive Strength (UCS) Trend (%) as a Function of Masonry Saturation Level (%).

Additionally, they examined the long-term evolution of compressive strength under varying moisture conditions, integrating empirical formulations available in literature. Such studies are crucial for refining numerical models that incorporate degradation effects, bridging the gap between experimental findings and predictive modeling.

An increasingly important form of deterioration in historic masonry bridges is fatigue, resulting from the rising speed, density, and weight of modern traffic. The cyclic loading induced by repeated vehicle passages generates progressive damage in the masonry bridge, weakening its structural integrity over time. This phenomenon compromises the long-term durability and stability of these structures, making fatigue assessment a crucial aspect of masonry bridge analysis. As traffic demands continue to increase, integrating fatigue considerations into masonry bridge analysis will be crucial for preserving these historic structures and extending their service life. An example of a methodology addressing this issue is the approach proposed by Laterza et al. (2017), who employed FEM modeling to perform a post-analysis fatigue verification using S-N (Stress-Number of cycles) curves to estimate the fatigue life of masonry structures. Among the various formulations available in the literature, Roberts et al. (2006) proposed a lower-bound fatigue strength curve for dry, submerged, and wet brick masonry based on quasi-static and high-cycle fatigue tests on brick masonry prisms. Another formulation was introduced by Casas (2009), who reprocessed the experimental data from Roberts et al., adopting a Weibull distribution to refine fatigue life predictions. More recently, Koltsida et al. (2018) proposed a novel model using a logarithmic normal distribution to establish a set of S-N-P (Stress level - Cycles to failure - Probability of survival) curves, enabling fatigue life estimation at any desired confidence level.

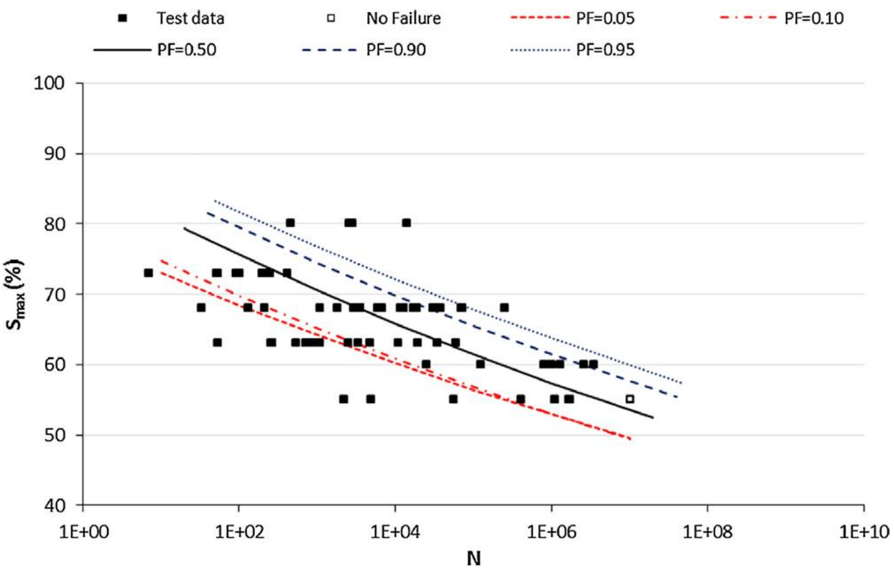

Figure 13 - Experimental data and predicted S-N curves for different probabilities failure. (Tomor et al. 2018).

5.3 Steel Bridges (Raffaele Landolfo)

The structural performance of existing steel critical infrastructures (CIs) such as steel bridges is strongly affected by the occurrence of typical degradation phenomena (DP) that can impair their ultimate and fatigue performance (*Milone & Landolfo, 2022*).

To this end, while addressing degradation of existing steel bridges, it is convenient to first categorize such phenomena depending on their main source, i.e., distinguishing among environmental DP and anthropic (or man-induced) DP. It is worth remarking that such classification should be intended as general as possible, as both kind of sources can detrimentally interact and affect the performance of the CI of concern.

In the following Sections, some of the most relevant DP for steel CIs are first addressed from a theoretical and phenomenological point of view (Section 5.3.1). Subsequently, established modelling techniques for structural assessment of steel CIs affected by DP are presented (Section 5.3.2)

5.3.1 Review of Deterioration Phenomena at Material Scale

5.3.1.1 Generality

While addressing environmental DP in steel structures, the most common occurrence is represented by corrosion. Key factors affecting corrosion development in steel structures and infrastructures are discussed in Section 5.3.1.2.

Moving to the field of man-induced DP, some key remarks on fatigue cracking (i.e., induced by transient applied loads) are hence discussed in Section 5.3.1.3.

Finally, few hints on interaction among corrosion and fatigue ("corrosion fatigue" or "CF" phenomenon) are provided in Section 5.3.1.4.

5.3.1.2 Corrosion

Among environmental DP, the most common issue occurring in steel bridges is undoubtedly represented by (metallic) corrosion. Corrosion consists of progressive material loss due to an electrochemical process which is extremely sensitive to local environmental conditions (i.e., temperature, relative humidity, salinity, etc.) (*Burstein et al, 2004; Harsimran et al., 2021*).

More specifically, in case of steel, material loss is caused by the erosion of metallic iron Fe due to the formation of iron oxides and/or hydroxides due to redox reactions occurring in presence of air and moisture:

$$2\,Fe + O_2 + 2\,H_20 \rightarrow 2\,Fe(OH)_2$$
$$4\,Fe + 3\,O_2 + 6\,H_20 \rightarrow 4\,Fe(OH)_3$$
$$4\,Fe + 3\,O_2 + n\,H_2O \rightarrow 2\,Fe_2O_3 + n\,H_2O$$

Reaction products accumulate on exposed steel surfaces in the form of red-brownish coloured layers commonly known as "rust". Rusting represents a recurring issue for structural steel components due to Fe (and metals in general) being more thermodynamically stable in its compound state (oxide, hydroxide) than in its elemental (metallic) state (*Vedavyasan, 2013*).

The extent and rapidity of corrosion in structural steel depends on several factors which are briefly summarized in the following (*Harsimran et al., 2021*):

- Environmental temperature – It has been experimentally observed that corrosion rate increases with increasing rise in temperature T. Approximately, the corrosion rate almost doubles for every ×10 increase of T, i.e., provided that other conditions are kept constant (*Levy, 1995*);

- Environmental humidity – Corrosion rate sharply increases is the level of relative humidity RH is beyond a material-depending threshold defined as “critical humidity”. For structural steels, typical values are in the range of 60% – 80% RH.
  The observed increment of corrosion rate with increasing RH descends from the tendency of iron oxide films to absorb moisture, which in turn fosters further electrochemical corrosion. Indeed, on one hand, the atmospheric moisture provides water which is essential for setting up of an electrochemical cell. On the other hand, the solubility of iron hydroxides (reaction products) in water reduces their local concentration on the component surface, resulting in a further acceleration of the redox reaction speed.
- Contact with other metals – If steel is in contact with a different metal, corrosion can occur due to the electrochemical potentials of such materials being different. Namely, corrosion rate is directly proportional to the difference among potentials, i.e., more the difference, faster is the corrosion rate. This phenomenon is known as “galvanic corrosion” and can be prevented by avoiding direct contact among structural steel and a more “noble” metal (e.g., such as lead Pb, titanium Ti, copper Cu and relevant alloys).
  Conversely, steel can also act as a galvanic corrosion trigger for less “noble” metals such as aluminium Al alloys, which recently found application for civil structural purposes.
- Steel composition and purity – If quality control on structural steel is inadequate, the presence of numerous impurities will result in an increase of the corrosion rate. This is due to such impurities forming localized electrochemical cells in which the anodic part gets corroded;
- Presence of a surficial oxide film – All the metals, including structural steel, get covered with a thin surface film of metal oxide in an aerated atmosphere. The so-called “specific volume ratio”, i.e., the ratio of volumes of metal oxide to the metal is inversely proportional to the corrosion rate.
  Such ratio can be regarded as an intrinsic material property, and it can be properly manipulated by steel alloying. That is the case of the well-known weathering steel, i.e., a low-alloy steel which includes copper (0.2 – 0.5% Cu), chromium (0.5 – 1.5%) and phosphor (0.1 – 0.2%) to promote the formation of a thin iron oxide layer which prevents further corrosion.

It is clearly understandable that all the above factors can sensibly vary for structural components belonging to steel bridges, i.e., resulting in a very unpredictable corrosion evolution in most aggressive environments. In particular, from a spatial perspective, extensive portions of exposed structures can be affected by degradation or, conversely, damage can take place in highly localized spots (non-uniform corrosion or “pitting” – *Velasquez et al., 2009*; *Popov*, *2015*). At the same time, the material loss rate can significantly vary in time during structural service life in dependence on the above parameters.

For a given degree of material loss, it can be easily inferred that the most critical condition from a structural safety perspective is represented by severe pitting corrosion. Indeed, when material loss is highly localized, the subsequent variation of geometrical features results in very strong stress amplifications that facilitate premature and brittle cracking. Pitting can either arise in “electrochemically active” steels (i.e., steels in which the surficial film cannot effectively passivate the underlying metal) or in “electrochemically passive” steels such as stainless steel, i.e., provided that some additional factors are present (e.g., halogen ions such as chloride ions Cl^- – *Popov, 2015*).

Furthermore, if pitted components are also subjected to significant tensile stresses (e.g., a typical condition for strands in cable-stayed bridges located in aggressive environments, *Milone et al., 2022*), corrosive phenomena can further accelerate until sudden collapse. Such condition is known as “stress corrosion cracking” (*Harsimran et al., 2021*).

5.3.1.3 Fatigue cracking

Among anthropic DP, one of most common issues occurring in steel bridges is represented by fatigue. Fatigue is a mechanical phenomenon of brittle failure of a component when subjected to repeated loads, i.e., even if their magnitude is far below the static resistance of the base material (*Anderson, 2017*).

For ductile materials such as structural steels, two main behavioural regimes can be identified while addressing fatigue issues, i.e.:

- High-cycle fatigue (HCF), which is characterized by small stress fluctuations Δσ (i.e., when compared to the material yield strength f_y) associated with a significantly high number of cycles at failure N_f;
- Low-cycle fatigue (LCF) and Very low cycle fatigue (VLCF), which are characterized by high stress fluctuations $\Delta\sigma \geq f_y$ associated with a low or very low number of cycles at failure N_f.

In both cases, progressive material degradation is caused by the nucleation and propagation of (micro-)cracks which can either start from material defects (inclusions or second phase particles) or from macroscopic trigger sites such as notches (geometrical stress amplifiers).

Crack nucleation in steel components is a complex process that can be idealized through four consecutive steps (*Anderson, 2017*). *i*) Initially, as a response to applied external loads, steel develops cell structures and hardens. This induces a local increase in terms of amplitude of applied stresses due to the new restraints on strains. Such cell structures eventually break down resulting in *ii*) the formation of persistent slip bands (PSBs). Concentrated and elevated slip in the material occurs in PSBs, resulting in a further concentration of stresses that may be enough for a crack to form.

PSB-induced slip planes hence result in *iii*) pairs of intrusions and extrusions along the material surface with propagation of dislocations within the material. PSB-induced surface slip can in turn cause *iv*) fractures to initiate.

After nucleation, progressive crack growth occurs while being mainly driven by the magnitude of cyclic loads (i.e., it is proportional to Δσ – *Anderson, 2017*). Nevertheless, additional factors such as tensile mean stresses may also strongly accelerate the crack growth rate. Contrariwise, crack growth may stop if the loads are small enough to fall below a critical threshold, or in case of compressive mean stresses (“crack closure effects”).

In non-welded structural details which can be commonly found in steel bridges (e.g., double covered joints, gusset plate joints), nucleation of cracks accounts for most of the detail fatigue life. This is especially true in case of thin and only mildly notched steel components. It is for this reason that cyclic fatigue failures occur so abruptly. Indeed, fatigue-related changes in the material are usually not visible without destructive testing, and only after collapse some feature signs of fatigue crisis (e.g., beach marks) can be recognized.

Contrariwise, welded structural details are characterized by fatigue life being almost completely dominated by crack propagation. This outcome descends from the fact that the abovementioned crack nucleation steps can be entirely bypassed if the cracks form at a pre-existing stress concentrator, i.e., such as re-entrant corners delimited by fillet welds’ toes. Moreover, the alteration of the base material in the neighbourhood of the weld (heat affected zone – HAZ) due to the thermomechanical process results in a strong local embrittlement of the component which further reduces its fatigue life.

5.3.1.4 Hints about corrosion fatigue

When corrosive phenomena occur in combination with cyclic loadings, corrosion-induced damage does not simply add up to fatigue damage, but rather, the two processes influence each other. Multiple factors underlie this mutual interaction, namely (*Wang et al., 2019*):

- On one hand, corrosion induces a localized reduction of the resisting cross-section, resulting in stress amplifications which accelerate fatigue cracking. Secondarily, the fatigue strength of iron oxides and hydroxides is negligible as respect to that of pristine steel;
- On the other hand, fatigue cracking creates preferable spots for corrosion development as the cracks can penetrate through the oxide film and/or protective layers, if present.

Corrosion fatigue can represent a critical issue for steel bridges if they are not properly protected, i.e., due to their typical destination of use (*Milone et al., 2022*). Indeed, the constant presence of transient loads due to traffic and wind is combined with the typically aggressive environment in which such infrastructures are placed (e.g., moist or marine environment).

5.3.2 Modeling of Deterioration Phenomena at Structural Scales

In the previous Sections, some of the most relevant DP for steel CIs have been addressed from a phenomenological perspective. In this last Section, each phenomenon is discussed with reference to its modelling at structural scale, i.e., in order to account for it in structural safety assessment.

Accordingly, Section 5.3.2.1 presents some established techniques for corrosion modelling in structural steel details, i.e., with a peculiar focus on non-uniform corrosion (pitting).

Therefore, basics of fatigue analysis and crack propagation modelling are briefly illustrated in Section 5.3.2.2. Finally, some modelling aspects regarding corrosion fatigue in CIs are discussed in Section 5.3.2.3.

5.3.2.1 *Corrosion modelling in steel CIs*

Corrosion modelling for steel bridges encompasses numerous methods having variable complexity.

Simplest models involve the assumption of uniform corrosion, i.e., a constant reduction of the component size due to material loss through the length. Time-depending evolution of corrosion is hence only analysed within the component cross-section i.e., through a progressive reduction of thickness $s = f\,[\eta(t)]$ where $\eta = \Delta m/m_0$ is the corrosion degree expressed in terms of mass loss Δm over the initial mass m_0 of the component (*Milone & Landolfo, 2022*).

To this end, it is worth remarking that similar recommendations are provided in ISO 9224 standard (*ISO, 2012* – see Figure 14), in which a thickness reduction rate for steel components in aggressive environments is given in function of the so-called "corrosivity category" CX, which ranges from 1 (very low corrosivity) to 5 (very high corrosivity). According to ISO 9224, the corrosion development in time is approximated by a polyline with two branches (i.e., with a piecewise constant corrosion rate).

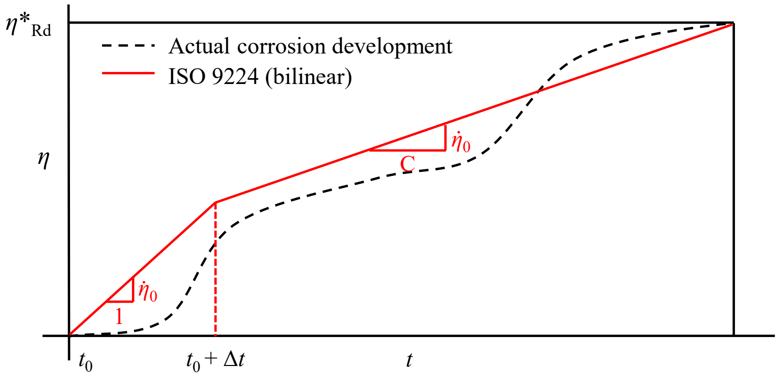

Corrosivity Category	Exposition	C [-]
C1	Very low	5
C2	Low	3.5
C3	Medium	2.5
C4	High	1.5
C5	Very high	1

Figure 14 – Qualitative corrosion development in time on a steel CIs and relevant prescriptions according to ISO 9224 standard.

The knee point of the bi-linear curve is assumed to occur Δt years after construction time t_0, while $\eta(t = t_0)$ is assumed null. In absence of more precise information, Δt = 10 years is recommended.

The ratio among the slopes of the consecutive branches is equal to C : 1, with C ≥ 1 depending on the corrosivity category of concern. The suggested values of parameter C for each category are summarized in Figure 14.

Although being very handy and useful for rough residual life estimations, the above technique is typically not suitable for a realistic assessment of the influence of corrosion on the structural performance of steel bridge details. Indeed, due to the typically high values of aspect ratio in exposed surfaces of details, the corrosion is usually non-uniform and localized (pitting). This results in local stress concentrations that severely impair both the static and fatigue performance of components as respect to uniformly worn elements sharing the same overall value of η (*Milone et al., 2022*).

Generally speaking, two approaches can be used to overcome this important issue, i.e., *i*) introducing the influence of non-uniform corrosion in semi-empirical capacity models which only depend on η or *ii*) attempting to model corrosion in a more detailed and physically consistent way via complex algorithms. To this end – as it will be discussed more in detail in Section 5.3.2.3 – it is worth mentioning that the former approach is established in corrosion fatigue assessment, while the latter technique is more used for static purposes.

As discussed in *Reinoso-Burrows et al., 2023*, some of the complex techniques that proved to be particularly beneficial for corrosion modelling are *i*) cellular automata, *ii*) non-homogeneous Poisson point processes (NHPPPs) and *iii*) Monte Carlo techniques.

In the field of corrosion, cellular automata were proven valuable in providing information on the behavior of structural steels placed in aggressive environments (see Figure 15). Namely, cellular automata models simulate interactions between electrochemical and mechanical processes to provide insights about initiation, propagation, and evolution of corrosion.

A Cellular Automata model is an idealization of a physical system in which both time and space are treated as discrete quantities that may take a finite set of values. Namely, space is represented by a 2D or 3D grid of cells, i.e., with each cell having a specific state at a given time $t = t^*$ (e.g., "dead" – 0 – or "alive" – 1 – in the simplest case). An evolution rule **R** is introduced to link the current state of each cell at $t = t^*$ with its following state evaluated at $t = t^* + 1$. This rule involves the states at $t = t^*$ of a small neighbourhood of a cell *C* which is typically represented by its eight surrounding cells; **R** is simultaneously applied to all cells at each time-step. In light of the above, the overall state **S** of the system at a time $t = t^*$ is completely determined if the initial state of the system $\mathbf{S_0}$ and the evolution rule are known.

In the context of corrosion modelling, the cell state can represent the presence of an element, a compound, or a corrosion product. Clearly, the evolution rules and the initial configuration of the Cellular Automata model in corrosion simulations are specific to each phenomenon to be studied.

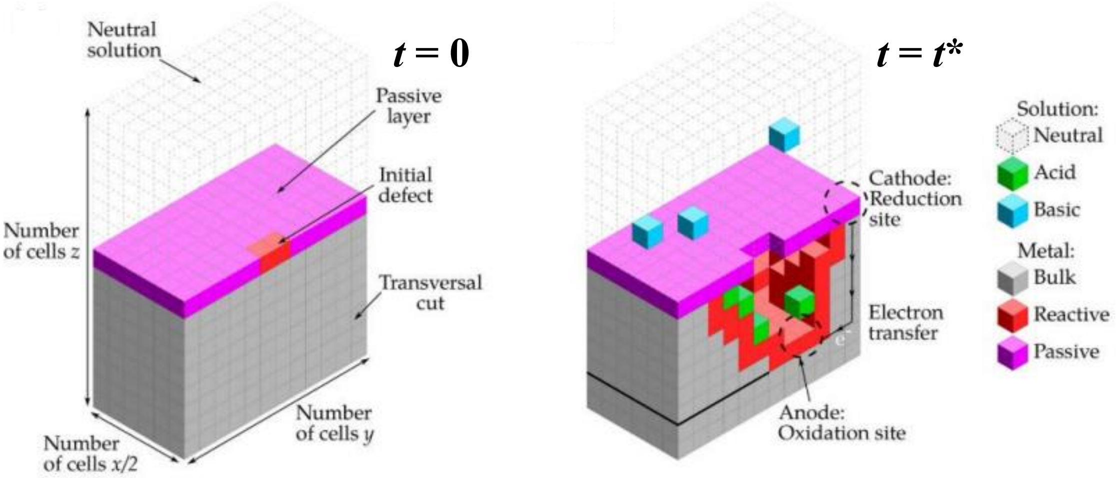

Figure 15 – Cellular Automata model for corrosion modelling in steel Cis (adapted from *Reinoso-Burrows et al., 2023*).

NHPPPs are a kind of stochastic process in which a base space is randomly and progressively filled with points, i.e., with the clause of points occurring independently of one another. The process's name descends from the the number of points in a given finite region following the well-known Poisson discrete probability distribution. The evolution of the system state depends on a key parameter λ defined as “intensity”. To this end, inhomogeneity of NHPPPs relates to λ being not constant, but rather behaving as a location-dependent function in the underlying space on which the Poisson process is defined. This expedient enables a more realistic modelling of corrosive processes in light of the numerous factors affecting their development in space and time.

A successful example of application of NHPPP for corrosion analysis is reported in *De La Cruz et al., 2008* with reference to oil pipelines affected by severe pitting corrosion (see Figure 16). The analytical framework relates to the pioneering work of *Brix et al., 2001*.

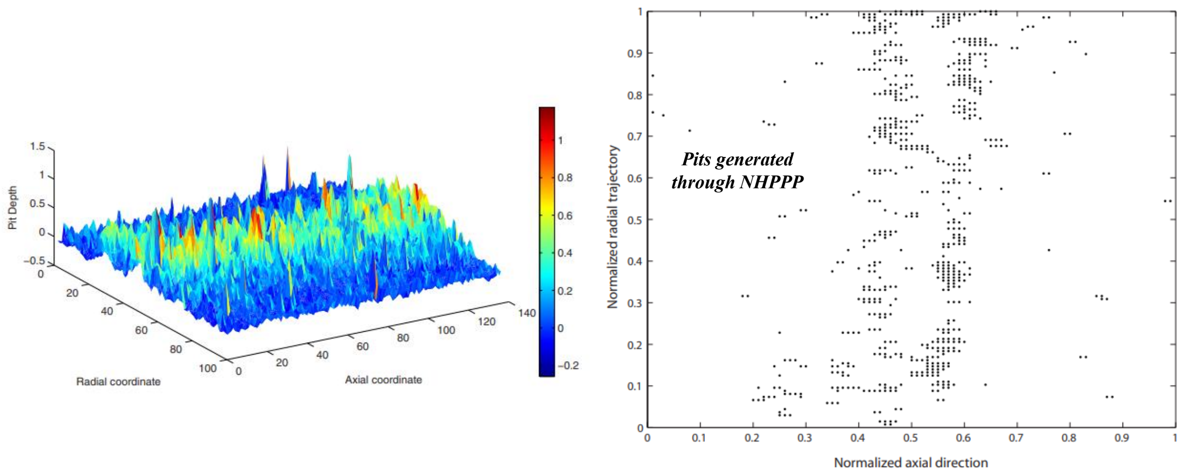

Figure 16 – NHPPP for corrosion modelling in steel CIs (adapted from *De La Cruz et al., 2008*).

Monte Carlo simulations (MCSs) are a well-known class of computational algorithms based on repeated random sampling. MCSs find wide application in the modelling of complex phenomena whose inputs are affected by a significant degree of uncertainty. Therefore, their use in the field of corrosion analysis should not surprise.

As highlighted by *Guessasma et al., 2007*, corrosion process can be modelled as a sequence of discrete events governed by statistical laws describing the system "metal/film/electrolyte". Such system progressively evolves by following a minimum energy path. The basic idea is to identify the relationship between dissolution process (energy balance requirement), kinetic (probabilistic behaviour) and the macroscopic response (dissolution current).

Such an idea is implemented in the MCS by first discretizing the component surficial layer into a 3D grid, with each cell being labelled with a time-depending state identified as "0" (inert), "1" (active), "2" (dissolved). The dissolution probability $P = [1 + \exp(-kV)]^{-1}$ is assumed to depend on the electrochemical potential V via a positive kinetic parameter k to be calibrated (see Figure 17).

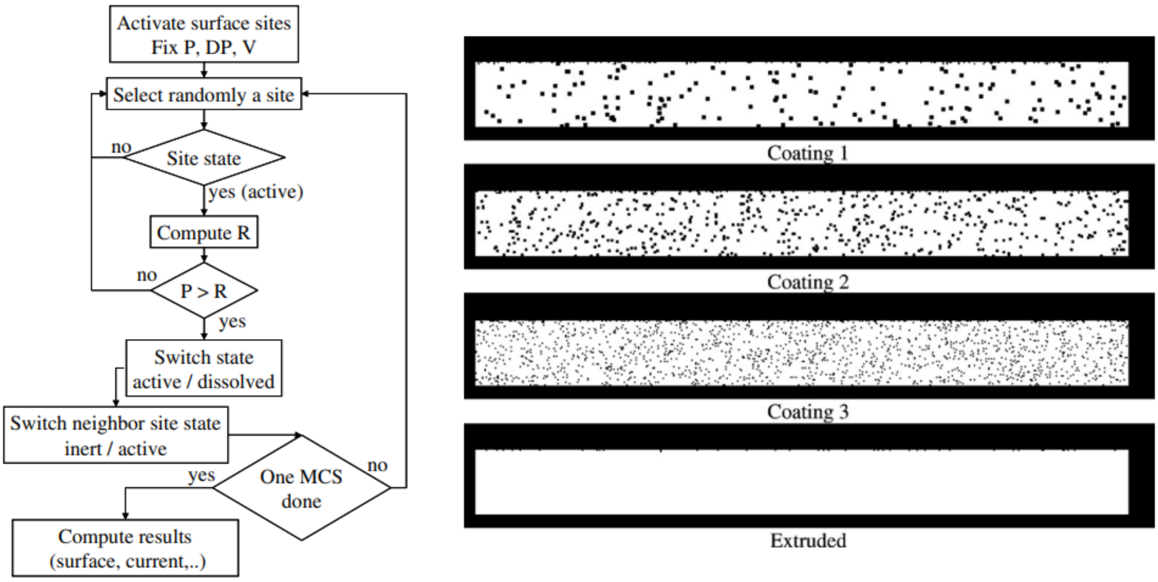

Figure 17 – MCS for corrosion modelling in steel CIs (adapted from *Guessasma et al., 2007*).

Further approaches worth of being mentioned involve the combination of empirical analysis and numerical techniques for corrosion management, e.g., as reported in *Tzortzinis et al., 2022*. The Authors explored the use of three-dimensional laser scanning to evaluate deteriorated steel bridge girders due to corrosion. Thickness contour maps were developed for mapping the remaining material of corroded parts and hence introduced in a numerical model for the mechanical analysis of the component. According to reported results, a good agreement between experimental and predicted failure loads can be matched with this technique.

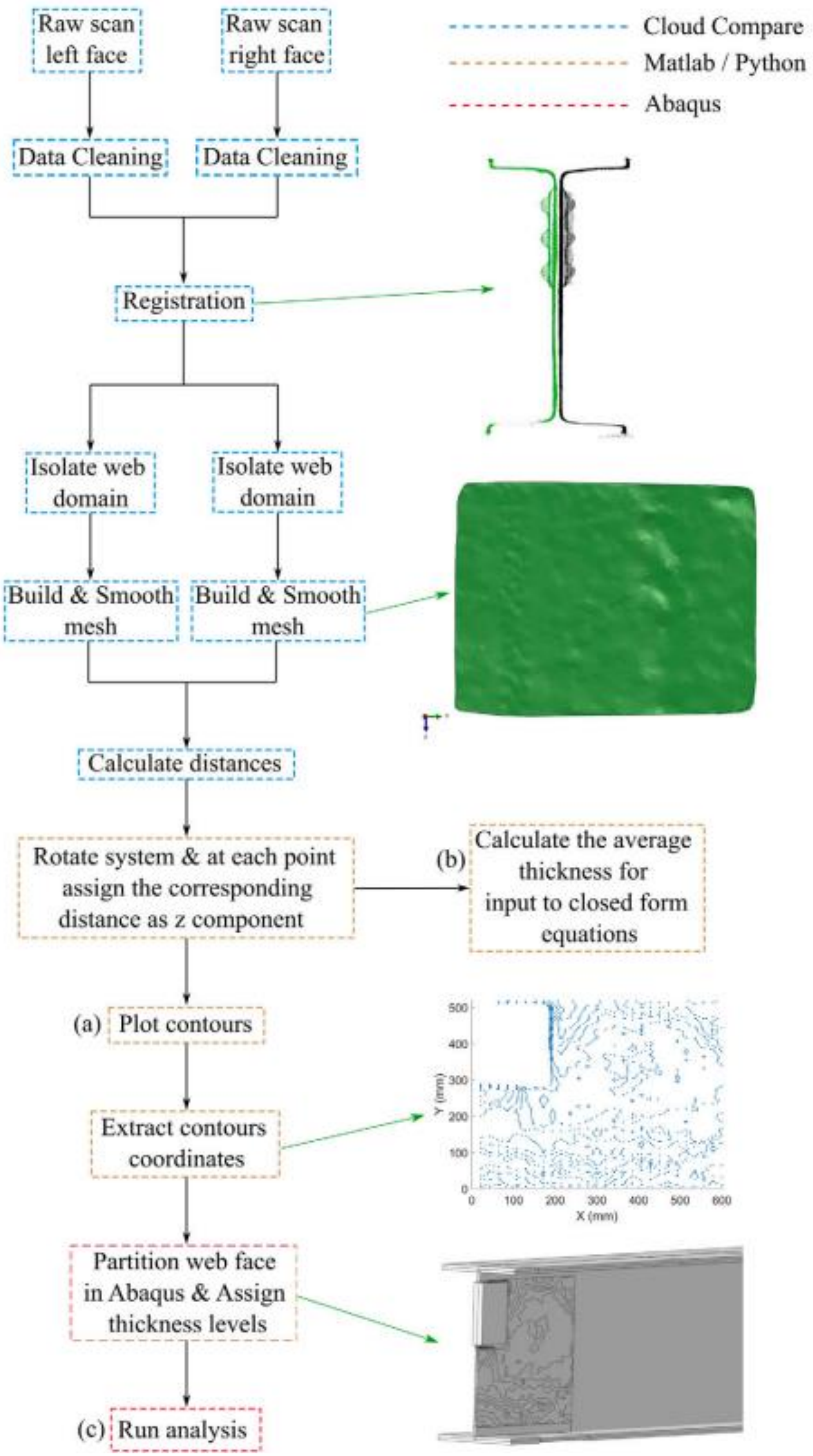

Figure 18 – Laser scanning-based algorithm for corrosion modelling in steel CIs (adapted from *Tzortzinis et al., 2022*).

5.3.2.2 Fatigue modelling in steel CIs

While addressing fatigue modelling in civil CIs, three main families of methods are widely established, i.e., *stress-life methods* (or *S-N methods*), *strain-life methods* (or *ε-N methods*) and linear elastic fracture mechanics (LEFM) based methods. Nevertheless, only the former assessment philosophy is currently encoded in European normative provisions (i.e., EN1993:1-9 for structural steel – *CEN, 2005*).

The main concept behind the whole family of stress-life methods derives from the already mentioned inverse proportionality among applied stress ranges and observed number of cycles at failure for basically any kind of structural detail. In light of this, stress-life methods attempt to derive a functional link between fatigue life in terms of cycles to failure (N) and applied stresses (S), which are regarded as the main parameter influencing fatigue performance.

Comprehensive experimental campaigns dating back up to 150 years ago, starting from pioneering works of *Wohler (1860)* on rail car axes, revealed that fatigue cracks rarely occur and propagate in the base material remotely from any geometrical discontinuity or constructional detail, e.g., sharp corners, holes, mechanically fastened and welded connections. Such details remain critical spots for fatigue performance even if their static resistance is higher than assembled members, as they act as “stress raisers” (*ECCS, 2018*).

Within the framework of S-N methods, two alternative approaches can be followed to deal with such issue, namely (Figure 19 – *ECCS, 2018*):

- the definition of “detail categories”, each one of them characterized by a given geometry, for which fatigue strength domains are defined in terms of nominal applied stresses and derived based on experimental tests;
- the characterization of base material fatigue properties (regarded as an intrinsic material parameter) and the subsequent estimation of fatigue life based on actual maximum stresses attained nearby a given constructional detail.

The former option is referred as “Nominal Stress Method” (NSM – *CEN, 2005*; *ECCS, 2018*) and it arguably represents the simplest option for engineers addressing fatigue design, since the complex task of deriving the fatigue strength domain for a given detail is unrequired in many real situations, as it can be easily found within documents of sanctioned validity (i.e., normative codes and/or standards).

Therefore, after global structural analysis is performed, elastic stresses in parent members nearby the detail can be easily calculated and used for fatigue verifications.

Currently, within the framework of steel structures, a wide list of 114 detail categories is encoded in EN1993:1-9 (*CEN, 2005*), ranging from plain members to mechanically fastened joints, welded connections, stiffening details, tubular joints, orthotropic bridge decks, etc… Additionally, 5 fatigue categories are reported in EN1993:1-11 (*CEN, 2006*) for tension structural components (e.g., wires, strands, ropes, or prestressing bars).

The latter option is instead referred as “*Hot-Spot Stress Method*” (HSSM – *CEN, 2005*; *ECCS, 2018*), and it is usually adopted for critical structural details in which fatigue cracking is a-priori regarded as a design-governing phenomenon (e.g., load carrying welded joints). In this case, the aid of refined FEAs is allowed and fatigue checks are performed through few “master” fatigue strength domains. Notably, although a single domain should be sufficient for a given base material, multiple curves are usually available to account for the effect of different manufacturing processes.

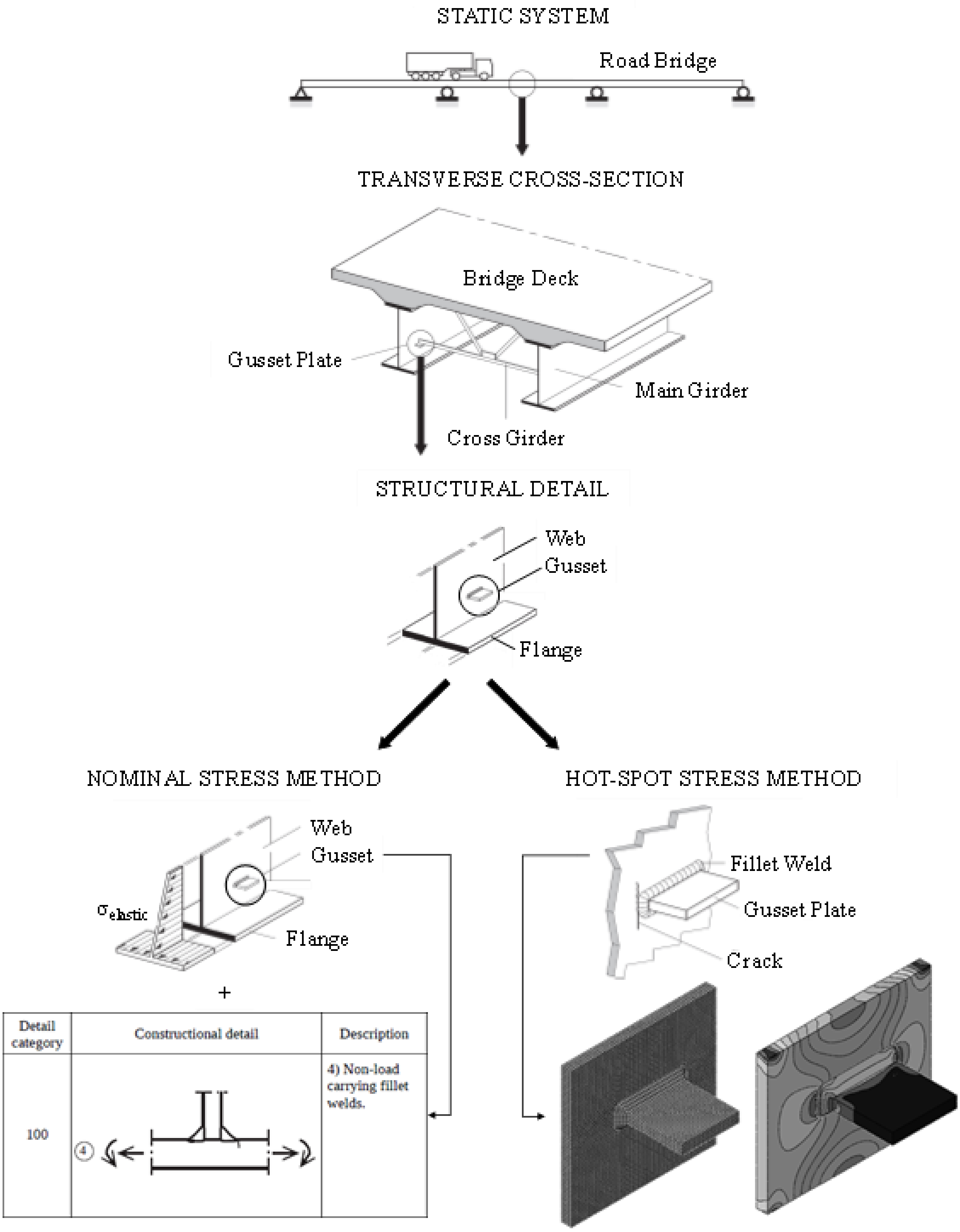

Figure 19 – Stress-Life methods for fatigue modelling and residual life estimations (adapted from *Milone, 2023*).

5.3.2.2.1 Nominal Stress Method (NSM)

NSM is based on the fundamental assumption of adopting nominal stress ranges referred to the gross cross-section of the detail of interest as the main fatigue demanding parameter. Fatigue domain is hence constructed in the form of *S-N* (or *Wohler*) *curves* linking the nominal stress range $\Delta\sigma$ to the observed number of cycles at failure N* (Figure 20 – *Milone, 2023*).

S-N curves graphically summarize the outcomes of an experimental program for the detail of concern, which shall involve a sufficient amount of specimens in order to properly measure the results scatter. Indeed, even nominally identical test conditions for apparently identical test specimens systematically result in different values of N*. This occurs due to ineradicable small differences in parameters governing fatigue life (misalignments, tolerances, … – *ECCS, 2018*).

Remarkably, earlier experimental campaigns already proved how this scatter becomes larger for lower stress ranges (*Schijve, 2009*). Nevertheless, mean values of constant-amplitude fatigue tests results appear to order themselves on straight lines when plotted on a double logarithmic scale (Figure 3.13 – bold dashed line). This property – which is not coincidental as it can be derived according to fracture mechanics considerations (*Anderson, 2017; ECCS, 2018*) – is used to provide an handy analytical description of S-N curves:

$$N^* = C\,(\Delta\sigma)^{-m} \leftrightarrow \log N^* = \log C - m \log \Delta\sigma$$

with C, m being logarithmic regression coefficients representing the influence of the structural detail (i.e., the fatigue strength of the detail for a conventional number of cycles at failure N_C) and the reciprocal (log-)slope of the mean results line, respectively. This expression is often referred as "*Basquin formula*", as it was first proposed by *Basquin* (1910).

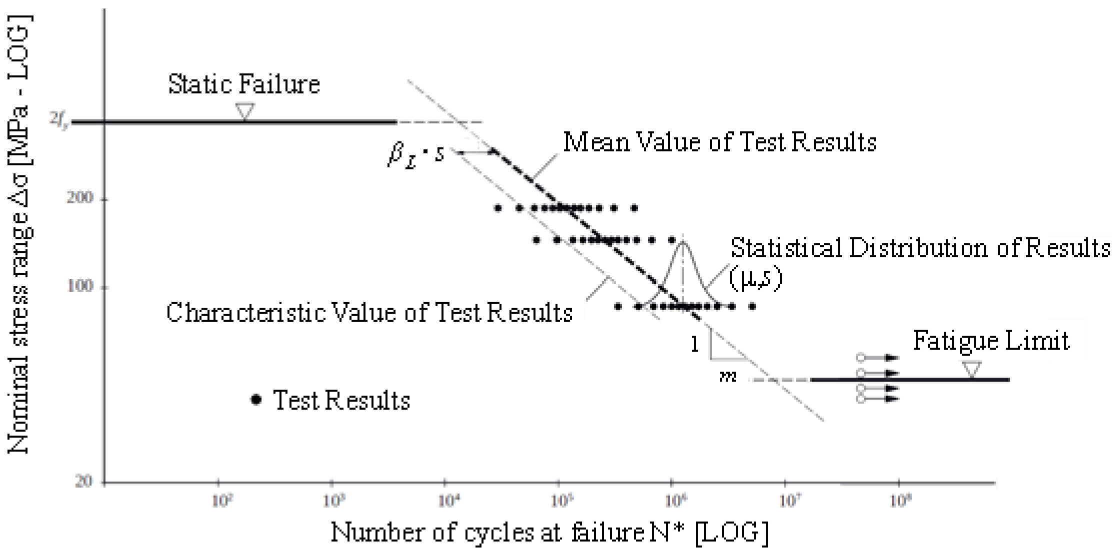

Figure 20 – S-N curves for the application of NSM.

5.3.2.2.2 Hot Spot Stress Method (HSSM)

HSSM aims at estimating the real stress acting on a potential crack spot, i.e. including all possible sources of stress rising associated to the structural detail of concern (*ECCS, 2018*).

Hot-spot stress method is particularly suitable for welded details in which the main principal stress is normal to the weld toe and thus fatigue cracking is expected to initiate from such spot (e.g., non-load carrying fillet welded details – *Niemi et al., 2006*).

To this end, standard procedures are available to extrapolate the hot-spot stress σ_{hs} at the weld toe starting from nearby locations, as a direct measure of weld-toe hot-spot stress is unfeasible. Accordingly, local stress measures derived from testing or refined FEAs can be linearly projected up to the surface perpendicular to the weld toe (see Figure 21 – *Schumacher, 2003*; *Niemi et al., 2006*; *ECCS, 2018*).

The extension of the extrapolation regions, within which the stresses to be projected should be estimated, is currently defined in different documents of sanctioned validity for each relevant case (e.g., *IIW, 2000* for welds or *DNV, 2024* for FEM-based extrapolation). Nevertheless, all indications will be recollected in the upcoming new version of EN1993-1-9 and in the newly introduced EN1993-1-14 devoted to FEM-assisted analysis of steel structures.

It is worth remarking that, in both cases, microscopic effects (i.e., notch effects due to weld type and shape, flaws, etc…) cannot be directly accounted for even with highly refined measures. Therefore, a restricted, yet multiple set of hot-spot S-N curves should be used for fatigue checks to account for such effects (*ECCS, 2018*). To this end, 7 hot-spot welded detail categories are provided by EN1993:1-9, Annex B (*CEN, 2005*), which are variously associated to 3 detail classes ($\Delta\sigma_{C,hs}$ = 90, 100 or 112 N/mm^2, respectively).

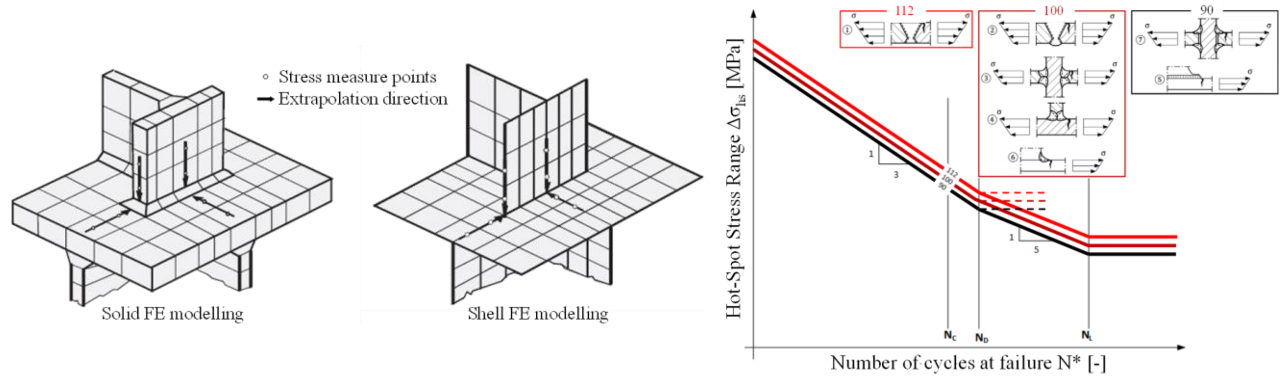

Figure 21 – HSSM for welded details in steel bridges.

5.3.2.2.3 Strain Life Methods

The main limit of all stress-life approaches is represented by the assumption of materials indefinitely behaving as linear elastic (*Osgood, 1982*). Indeed, even though some sources of non-linearity are (more or less explicitly) accounted for, e.g. contacts, friction, etc…, material plasticity is completely overlooked while performing fatigue analyses.

To partially overcome this issue, the range of validity for normative S-N curves is superiorly limited to 1.5 f_y (*CEN, 2005*). However, when dealing with details featuring sharp stress raisers, localized plasticity can occur even for rather small nominal stresses.

While it is true that this aspect is implicitly addressed by EN1993:1-9 with respect to encoded details (*ECCS, 2018*), it is worth mentioning that, in the general case, neglecting plasticity can lead to highly non-conservative fatigue life estimations, especially with low-tenacity metals (*Schijve, 2009*).

The idea of addressing strain (half-)cycles to assess fatigue performance of components was first introduced by *Basquin* (*1910*). Further, crucial developments were provided independently by *Manson* (*1953*) and *Coffin* (*1954*). Namely, while Basquin attempted to relate fatigue life to elastic strain reversals $\Delta\varepsilon_e/2$, Coffin & Manson focussed on the influence of plastic reversals $\Delta\varepsilon_p/2$, and hence to total strain reversals (hence also referred as *strain amplitude* ε_a) (*Dowling, 2004*).

Accordingly, the strain-life *Basquin-Manson-Coffin* (BMC) model can be expressed according to the following equations:

$$\varepsilon_a = \frac{\Delta\varepsilon_{tot}}{2} = \frac{\Delta\varepsilon_e}{2} + \frac{\Delta\varepsilon_p}{2}$$

$$\text{BMC:} \quad \varepsilon_a = \frac{\Delta\varepsilon_e}{2} + \frac{\Delta\varepsilon_p}{2} = \frac{\sigma_f'}{E}\left(2\,N^*\right)^b + \varepsilon_f'\left(2\,N^*\right)^c$$

with σ'_f [F L^{-2}], ε'_f [-] being the so-called *fatigue strength coefficient* and *fatigue ductility coefficient*, respectively and *b*, *c* being the so-called *fatigue strength exponent* and *fatigue ductility exponent*, respectively. BMC coefficients are intended as intrinsic material parameters that can be calibrated based on experimental, constant-amplitude, strain-control tests on round or flat smooth coupons (*Anderson, 2017*).

Usual values of *c* are in the range –0.5 ÷ –0.7 (the greater is |*c*|, the longer is fatigue life), while σ'_f ranges among 500 ÷ 1000 N/mm^2 for mild steels (*Schijve, 2009*).

It can be easily noticed that, while σ'_f and *b* govern HCF regime, ε'_f and *c* account for LCF material behavior. A convenient graphical interpretation of this fact can be provided in the double-logarithmic *strain-life diagram* ε_a – N* (see Figure 22), namely:

- for very high ε_a values, LCF failure points asymptotically follow a straight line *l* having a slope equal to $c < 0$ and passing through the point L = (ε'_f, 1);
- for rather small ε_a values, HCF failure points asymptotically follow a second straight line *h* having a slope equal to $b < 0$ and passing through the point H = (σ'_f/E, 1);
- for intermediate ε_a values, failure points follow a parabolic arc *m* gradually changing slope from *c* to *b*.

In absence of dedicated experimental testing, some literature correlations for a rough estimation of BMC parameters based on static base material properties can be used. Among the different expressions proposed, *Boller-Seeger's formulas* (*Boller & Seeger, 1987*), based on interpretation of experimental tests for various metals, are quite commonly used. Relevant formulas for mild steels adopted in steel bridges are given in the following as a function of the material ultimate tensile strength f_u and of its Young Modulus E:

$$\text{Mild steels:} \quad \begin{cases} \sigma_f' = 1.5\, f_u \\ \varepsilon_f' = 0.59\,\min(1\,;\,1.375 - 125\;\, f_u/E) \\ b = -0.087 \\ c = -0.57 \end{cases}$$

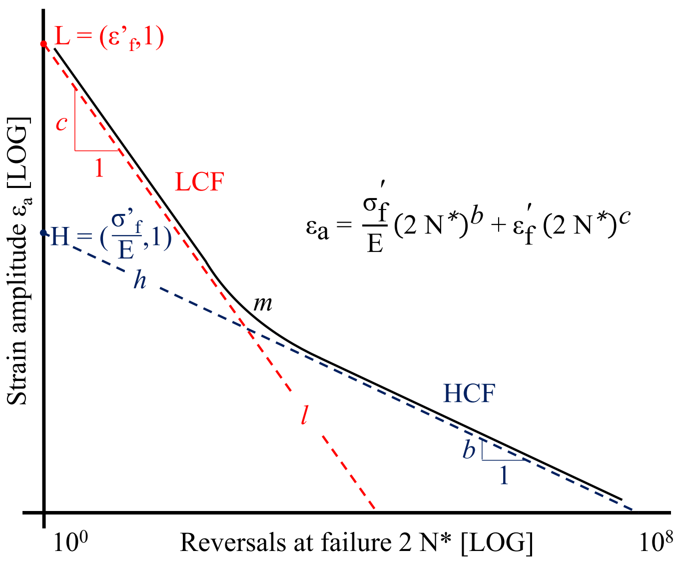

Figure 22 – Graphical interpretation of the BCM fatigue life criterion (strain-life diagram – *Milone, 2023*).

5.3.2.2.4 LEFM-based methods for crack propagation analysis

All the previous formulations address the topic of *total* fatigue life of structural components N*. More properly, fatigue life can be regarded as composed by two subsequent stages, namely *i*) the crack initiation life N^*_i and *ii*) the crack propagation life N^*_p.

The relative influence of crack initiation stage (CIS) and crack propagation stage (CPS) on the total fatigue life depends on many different factors (base material properties, manufacturing process, geometrical features, etc… – *Anderson, 2017*). For instance, in plain and narrow components $N^*_i \gg N^*_p$, while fatigue life of welded and/or severely notched elements is mainly governed by crack propagation (*ECCS, 2018*).

To separately deal with CIS and CPS when relevant, two aspects should be addressed, namely: *i*) clearly identifying the boundary between the two stages and *ii*) introducing a reliable crack propagation model (*Anderson, 2017*).

On one hand, the former aspect can be easily handled by performing constant-amplitude, displacement-control fatigue tests on plain narrow coupons.

On the other hand, crack propagation modelling is a rather complex topic which is still an open field of research nowadays, especially for two- or three-dimensional problems (*Anderson, 2017*). Therefore, only some related hints are summarized in this Section.

The basic formulation addressing CPS was introduced by Paris (*Paris et al., 1961*; *Paris & Erdogan, 1963*), which proposed the homonymous crack growth equation:

$$\text{Paris: } \frac{d}{dN} a = C\,(\Delta K)^m$$

where a is the crack length, da/dN is the crack growth rate against the number of loading cycles N, $\Delta K = K_{max} - K_{min}$ is the *stress intensity factor range* and C, m are experimental regression parameters depending on *i*) material composition, *ii*) environmental conditions (temperature, corrosivity) and *iii*) applied stress ratio R. Further insights about ΔK and *stress intensity factors* (SIFs, usually also referred as “K”) are provided in the following.

Paris parameters for one-dimensional fracture propagation in tension (i.e., *Mode I*, crack opening – *Anderson, 2017*) are usually determined by means of compact-tension (CT) specimens with standard shape and size (Paris law traces a straight line in the bi-logarithmic da/dN – ΔK plane, notably resembling Basquin’s formula (Figure 3.25). The range of validity for Paris law is defined as *stable crack propagation region* (or *region II*), and it refers to intermediate ΔK values (*Anderson, 2017*).

For rather small values of ΔK, cracks do not propagate at all (that is, $da/dN = 0$). This condition occurs up to a threshold value ΔK_{th} which separates region II from the *inhibited crack propagation region* (or *region I*). Contrariwise, for large values of ΔK (i.e., larger than a critical value ΔK_c) crack propagation greatly accelerates until failure. This behaviour range is defined ad *instable crack propagation region* (or *region III – Anderson, 2017*). It is worth remarking that both ΔK_{th} and ΔK_c are functions of the same variables affecting C and m values.

Provided that Paris parameters have been accurately determined for the boundary conditions of concern, N^*_p can be easily estimated by integrating Paris law over a given load history LH:

$$N^*_p = \int_{LH} \frac{da}{C\,(\Delta K)^m}$$

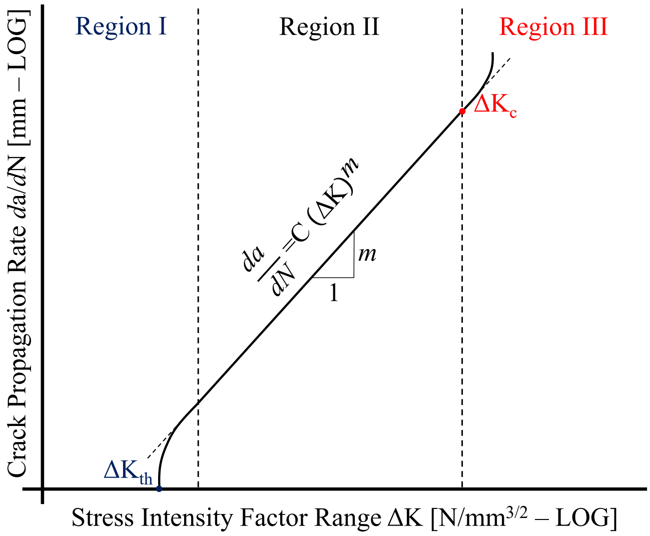

Figure 23 – Graphical interpretation of the Paris law (*Milone, 2023*).

The above equation provides an approximate estimation of N^*_p as it assumes a *region II* behaviour for the entire LH. A more accurate estimation of crack propagation life can be immediately performed by disregarding LH phases for which $\Delta K \leq \Delta K_{th}$ and arresting integration as soon as a value of $\Delta K \geq \Delta K_c$ (i.e., by conservatively assuming $m \rightarrow \infty$ for region III – Anderson, 2017). Nevertheless, several modifications of Paris Law attempting at capturing all the three behaviour regions can be found in scientific literature (e.g., *Forman & Mettu, 1992*), although neither of them gained the same popularity as the original formulation in light of their complexity.

The physical meaning of the stress intensity factor range ΔK relates to basic concepts of LEFM. ΔK is defined as the difference between the extremal SIFs (usually also referred as "K") associated to a given load cycle $K_{max} - K_{min}$.

The concept of stress intensity factor was first introduced by *Irwin* (*1956*) while extending the pioneering work of *Griffith* (*1920*) on brittle fracture of materials featuring sharp cracks in tension (Mode I). Namely, it was well-known at the time that regarding a sharp crack as a limit case of elliptical hole in a wide plate ($w/2a \gg 0$), infinite tensile stresses $\sigma_A \rightarrow \infty$ at the crack tip would be predicted by the classic elasticity theory, as they inversely depend on the curvature radius $\rho \rightarrow 0$ (Figure 3.26a-b – *Anderson, 2017*).

This outcome clearly contrasts with experimental observations, as ideally brittle materials (e.g. glass, PMMA, etc…) would instantaneously break for any small value of the far-field stress σ_0, while they exhibit a finite, yet reduced tensile resistance even in presence of sharp cracks. While *Griffith* (*1920*) proposed an enlightening solution involving an energetic balance among potential and surface material energies, *Irwin* (*1956*) introduced a closed form expression for stresses in polar coordinates (r, θ) centred at the crack tip (Figure 3.26c).

Accordingly, singular stresses σ_{ij} on a given director sweeping an angle θ with respect to the crack bisector can be expressed as a power series of the polar radius r (i.e., with first exponent = $-{}^1/_2$ and following ones > 0). Hence, for $r \rightarrow 0$, higher order terms can be conveniently neglected, leading to the following expression for σ_{ij}:

$$\sigma_{ij}(r, \theta) = \frac{K_I}{\sqrt{2\pi r}} f_{ij}^{(I)}(\theta) \rightarrow \lim_{r \to 0} \sigma_{ij} = \infty$$

with K_I being a constant defined as the stress intensity factor for Mode I (i.e., in pure tension) and $f_{ij}^I(\theta)$ being a dimensionless, Mode I-related function of the angular coordinate θ.

Equivalent formulations can be derived for Mode II (in-plane shear) and Mode III (out-of-plane shear), with the superposition principle being valid for mixed-Mode fracture (*Anderson, 2017*).

K_I is hence defined as the (finite) limit of singular stresses multiplied by *r*- and θ- depending terms as follows (Equation 3.46):

$$K_I = \lim_{r,\,\theta \to 0} \frac{\sigma_{ij}(r,\theta)}{f_{ij}^{(I)}(\theta)} \sqrt{2\pi\, r} < \infty$$

Existence and finiteness of limit featured in the above equation is granted by the $\sqrt{2\pi\, r}$ term, which eliminates stress singularity at crack tip $\propto r^{-1/2}$. Several closed forms for K_I exist for elastic isotropic bodies featuring variously shaped cracks (*Anderson, 2017*).

5.3.2.3 Corrosion fatigue modelling in steel CIs

As mentioned in previous Sections, both corrosion and fatigue phenomena are characterized by a significant degree of randomness (*Anderson, 2017*; *Burstein et al., 2004*; *Popov, 2015*; *Wang et al., 2019*), which further intensifies when fatigue and corrosion damage are combined.

To address this aspect, two main approaches have been followed in the scientific literature, namely (*i*) implementing stochastic procedures to account for both fatigue and corrosion intrinsic randomness and (*ii*) using simplified techniques to deal with corrosion fatigue in a deterministic way, usually based on experimental data.

Unsurprisingly, very few codified procedures for the corrosion fatigue analysis of steel constructions are available at present time. Nevertheless, some relevant contributions dealing with the corrosion fatigue analysis of steel structures can already be found in the scientific literature.

With regard to the stochastic approaches, *Lehner et al., 2019* adopted Monte Carlo simulations for the corrosion fatigue analysis of a riveted crane support truss that had been in service for nearly 100 years.

Li et al., 2020 modelled corrosion fatigue as a stochastic process in order to assess the time-dependent failure probability of corroded riveted connections employed in a steel bridge. The results highlighted that, as expected, corrosion greatly increases failure probability at a given time with respect to lone fatigue damage. Moreover, the authors proposed a modification of S-N curves (i.e., increasing the logarithmic slope of Wohler curves proportionally to the corrosion degree η) to account for this effect for both high-cycle (HCF) and low-cycle fatigue (LCF). This approach is comparable with recommendations reported in DNVGL-RP-C203 standard (*DNV, 2024* – see Figure 24, solid line), which also prescribe a downgrade of S-N curves for worn details by reducing the corresponding DC, instead.

This outcome has indeed been experimentally confirmed by several authors. For instance, *Adasooriya et al., 2019* demonstrated that steel components in aggressive environments show a significant decline of fatigue performance. According to the authors, the logarithmic slopes of both the LCF and the HCF branches of the S-N curves can reach up to ≈1.6 times their original values in the worst conditions, i.e., in the case of exposure to saline water (see Figure 24, dashed line).

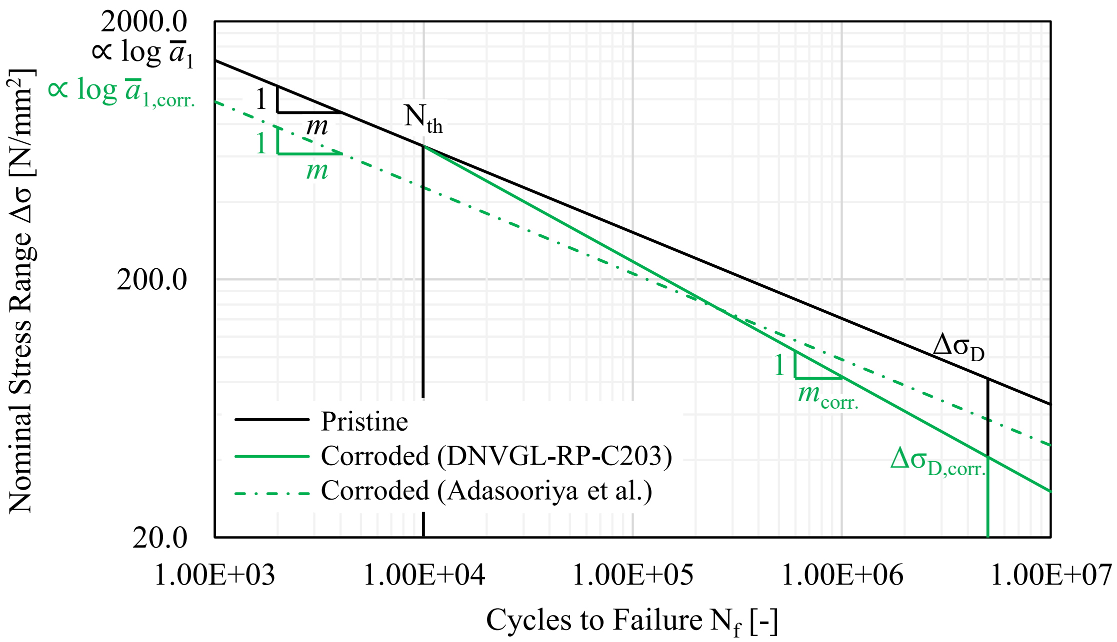

Figure 24 – Modification of S-N curves to account for corrosion fatigue crisis (*Milone et al., 2024*).

In the same fashion, *Jiang et al., 2017* proposed a corrosion fatigue domain for strands adopted in cable-stayed bridges in which the shape of the S-N curves depends on the corrosion degree η, such as with the logarithmic slope linearly increasing for increasing values of η.

Within the framework of simplified fatigue assessment procedures, *Landolfo et al., 2010* investigated the fatigue performance of an existing riveted railway bridge affected by ongoing corrosion, i.e., considering the effect of progressive thickness reduction on the fatigue demand. Accordingly, relevant cross-section properties for transient stress analysis were updated in step with ongoing degradation, and total damage was hence estimated through the Palmgren-Miner's rule.

5.4 Integral bridges under corrosion (Giuseppe Quaranta)

5.4.1 Review of Deterioration Phenomena in Integral Abutment Bridges

Integral abutment bridges (IABs) have become a common choice in modern bridge engineering due to their inherent advantages over traditional designs. By eliminating expansion joints and bearings, IABs provide a seamless connection between the superstructure and the abutments, reducing maintenance demands, improving structural performance, and enhancing durability. These features make them particularly attractive for highway and railway applications where long-term reliability is crucial. The use of reinforced concrete is very common in IABs construction, but it is inherently susceptible to various deterioration mechanisms caused by environmental, mechanical, and chemical factors. Over time, the exposure of IABs to harsh environmental conditions such as temperature fluctuations, deicing salts, moisture, and pollutants can lead to significant material degradation. One prominent issue is carbonation, a process where carbon dioxide penetrates the concrete surface and reacts with calcium hydroxide, reducing the alkalinity of the concrete and exposing steel reinforcement to the risk of corrosion. Another critical factor is chloride-induced corrosion, commonly initiated by deicing salts or marine environments, which can accelerate the deterioration of reinforcement bars and compromise structural integrity. In colder climates, freeze-thaw cycles also pose a significant challenge. These cycles cause water ingress into concrete to freeze and expand, leading to cracking, scaling, and spalling of the concrete surface. Over time, this repetitive action can weaken the structure and expose the reinforcement to further damage. Similarly, alkali-silica reaction can occur when alkali hydroxides in the cement react with reactive silica in the aggregate, forming a gel that expands in the presence of moisture. This phenomenon can lead to cracking and significant reductions in concrete strength and durability.

The unique design of IABs introduces additional considerations. The integral connection between the superstructure and abutments subjects the structure to continuous movement due to thermal expansion and contraction. In regions with significant temperature variations, this movement can induce additional stresses in the concrete and reinforcement, potentially exacerbating existing degradation mechanisms or leading to fatigue over time. Soil-structure interaction at the abutments, caused by seasonal variations in soil moisture and thermal movements, can also contribute to the aging process by imposing additional loads and stresses on the structure. Moreover, long-term loading and repeated traffic-induced vibrations can cause fatigue damage to the concrete and reinforcement, gradually reducing the load-carrying capacity of the bridge.

Understanding these degradation and aging phenomena is essential for ensuring the durability, safety, and serviceability of IABs throughout their intended lifespan. At the design stage, this requires a holistic approach that encompasses the identification of primary deterioration mechanisms, the accurate simulation of their effects, and the implementation of effective preventive measures.

5.4.2 Modeling of Chloride-induced Corrosion in Ordinary Rebars and Post-tensioned Tendons

The numerical modeling of degradation and aging effects in IABs is conducted using a relevant case study to analyze their impact on structural performance. A real post-tensioned reinforced concrete integral abutment roadway bridge is examined. The bridge is in a coastal city and, as such, serves as an ideal case study to evaluate the effectiveness of design standards in ensuring the required durability for integral abutment bridges subjected to chloride-induced corrosion because of the exposure to a marine environment. Figure 25 shows the lateral view and a transverse section of the bridge. The structure features two parallel decks, each 17 m wide, positioned side by side with a 2 m gap between them.

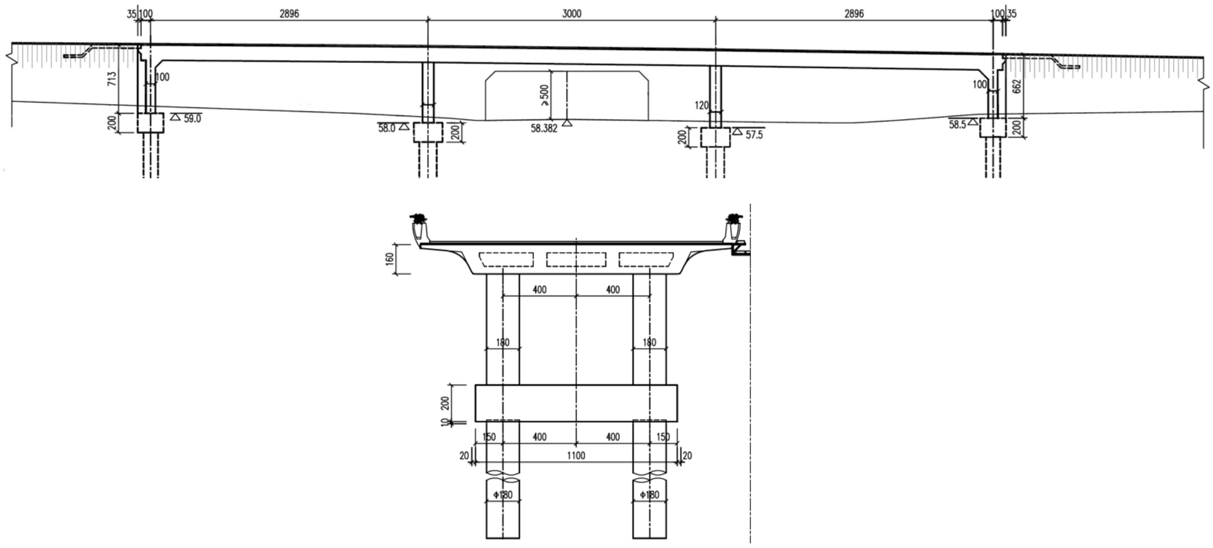

Figure 25 - Lateral view and transverse section of the bridge.

Each deck supports four traffic lanes and has no sidewalks. It is composed of three spans, totaling approximately 88 m in length. The two outer spans each measure approximately 29 m, making them slightly shorter than the central span, which is about 30 m long. Each span features two transverse beams positioned at its ends. There are two types of girder cross-sections, see Figure 26. The first type, featuring webs 0.45 m wide, is used in the middle of the deck. This section spans 13.71 m in the lateral spans and 15.5 m in the central span. Beyond this section, there is a variable cross-section extending 8 m towards the supports, where the web width gradually increases from 0.45 m to 0.75 m. The key geometric characteristics of the girder include a cross-sectional area of 9.73 m^2 and a moment of inertia of 3.42 m^4 at the central span. The deck is seamlessly supported by intermediate columns and abutments at the end. The heights of the two piers range from 6.20 m to 6.40 m. The pier consists of two circular columns, each with a diameter of 1.2 m and supported by two piles. At either end of the bridge, there are abutments with heights of 9.10 m and 8.60 m. These abutments are supported by piles beneath them. The connection between the superstructure and the infrastructure is made at the midpoint of the abutment stem. Each abutment is also equipped with two wing walls. The soil behind the abutments is moderately dense sand.

The bridge deck is constructed with C50 concrete. As shown in Figure 25Figure 26, each span employs post-tensioning using 24 tendons made of high-strength harmonic steel, which are arranged in three rows with variable heights and evenly distributed within the cross-section webs. Each tendon comprises 16 strands, with an equivalent diameter of 15.24 cm. Additionally, the girder primarily uses 25 mm and 16 mm diameter rebars on the top and bottom of the cross-section. On the lateral sides and internal parts, 16 mm and 12 mm diameter rebars are predominantly employed. The concrete cover of the ordinary rebars ranges from 4 to 6 cm. The position of the ordinary rebars in a cross-section of the bridge is illustrated in Figure 27. It is highlighted that, with a minimum concrete cover for ordinary rebars of 4 cm and a concrete class of C50, the bridge girder complies with common recommendations intended to ensure the target durability for reinforced concrete structures exposed to marine aerosols without direct contact with seawater.

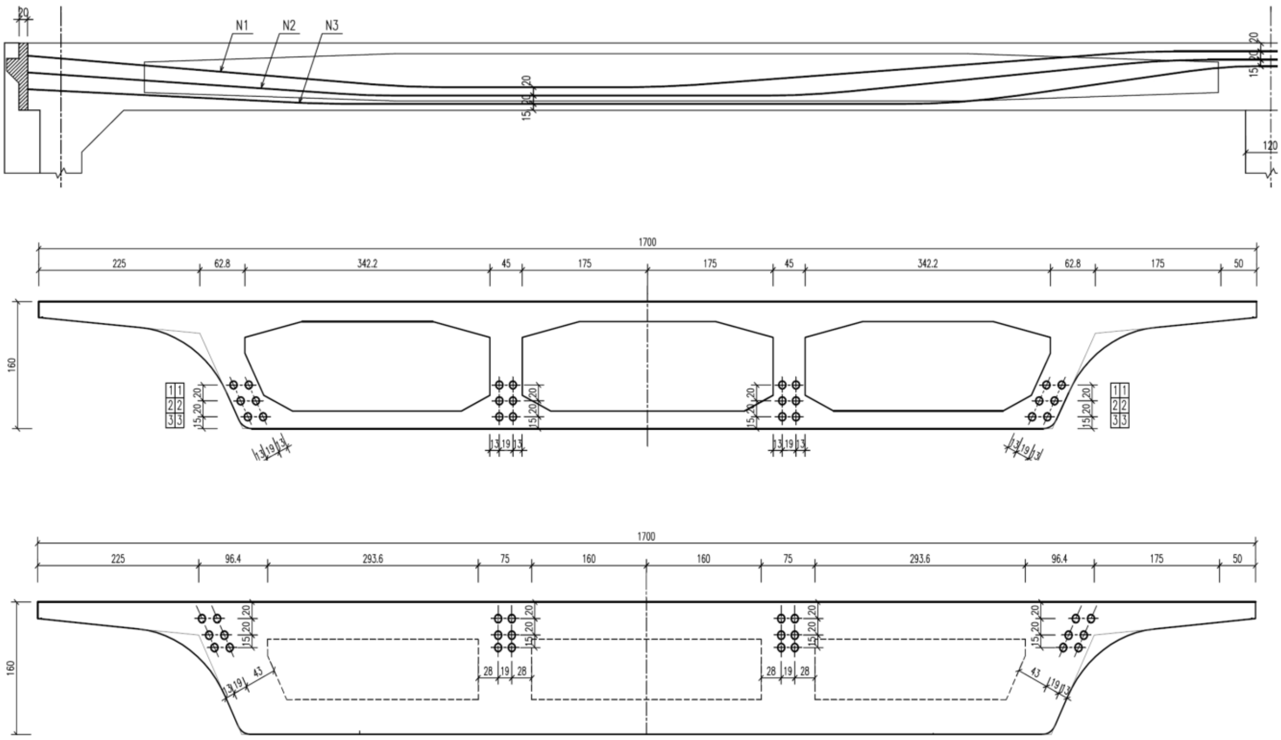

Figure 26 - Cross-sections of the girder in the middle of the deck and close to the supports, together with the position of the longitudinal post-tensioned tendons in the lateral spans.

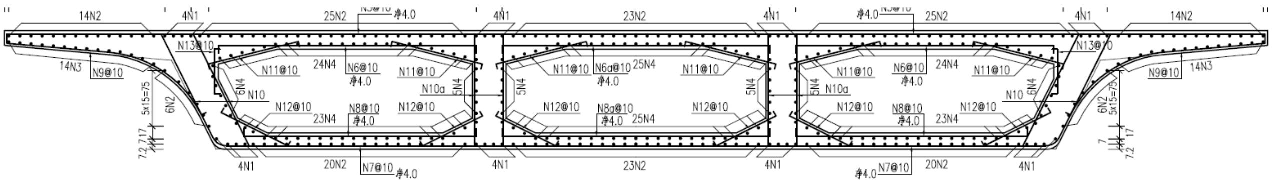

Figure 27 - Position of the rebars in the midspan cross-section.

The structural numerical model of the bridge aligns with the goal of assessing its serviceability under normal operating conditions including traffic load, thermal load, and reinforcement corrosion, alongside with long-term effects in both concrete and post-tensioned tendons. In agreement with common technical guidelines and previous research, the serviceability of the bridge is investigated through a linear elastic analysis. The linear elastic finite element model that has been developed for this task employs standard Euler-Bernoulli beam elements. Since the serviceability assessment of the bridge is here conducted under normal loading conditions, a refined model for the soil-foundation-structure interaction is dubbed not necessary for the current study. Hence, piers and abutments are assumed to be fixed at the base while the interaction between abutments and backfill is replaced by equivalent linear springs. Traffic loads and post-tensioning effects are modeled as concentrated forces and distributed loads applied on the girder, while temperature effects are accounted for using the thermal coefficient.

The activities detailed in this intermediate report primarily focused on modeling steel corrosion. It is assumed that both ordinary rebars and post-tensioned tendons of the girder are subjected to chloride-induced corrosion. Chloride penetration in both concrete and filling grout is simulated as one-dimensional diffusion process by means of the Fick's second law (Poulsen 2014), which general governing equations reads:

$$\frac{\partial C}{\partial t} = \frac{\partial}{\partial x}\left(D \frac{\partial}{\partial x} C\right), \tag{1}$$

where C is the chloride concentration at penetration distance x and D is the diffusion coefficient. Equation (1) is solved by imposing the boundary chloride concentration C_s and initial chloride concentration C_0. Let c be the distance of the steel reinforcement from the source of chloride. As soon as the chloride concentration C calculated according to Eq. (1) exceeds a critical threshold value C_{th} at $x = c$, the corrosion propagates and i_c rules the corrosion current density of the underlying electrochemical process. Generalized and pitting (aka localized) corrosion are considered independently for ordinary rebars and post-tensioned tendons (Val and Melchers 1997), with no overlap between the two.

Generalized corrosion manifests as a uniform reduction of the cross-section area of the ordinary rebar or wire. In this case, the diameter of the generic corroded rebar or wire ϕ_g in [mm] at time t in [years] can be estimated for i_c in [μA/cm²] as follows:

$$\phi_g = \phi_0 - 0.0232 \int_{t_c}^{t>t_c} i_c(\tau)\, \mathrm{d}\tau, \tag{2}$$

where ϕ_0 represents the initial diameter in [mm] while t_c and τ are the corrosion initiation time and the time integration variable in [years], respectively. Given the current diameter ϕ_g from Eq. (2), the residual area of the corroded ordinary rebar or wire affected by generalized corrosion is directly determined as follows:

$$A_g = \pi \frac{{\phi_g}^2}{4}. \tag{3}$$

Pitting corrosion concentrates over small areas of ordinary rebar or wire cross-section. The pit penetration δ_ℓ in [mm] is determined for the generic corroded rebar or wire given i_c in [μA/cm²] as follows:

$$\delta_\ell = R \cdot 0.0116 \int_{t_c}^{t>t_c} i_c(\tau)\, \mathrm{d}\tau, \tag{4}$$

where R denotes the pitting factor, which represents the ratio between the maximum and uniform corrosion. The residual area of the corroded rebar or wire affected by pitting (localized) corrosion is calculated assuming a hemispherical shape of the pit given its depth δ_ℓ from Eq. (4) as follows (Val and Melchers 1997):

$$A_\ell = \begin{cases} \pi \frac{{\phi_0}^2}{4} - A_1 - A_2 & \text{if } \delta_\ell \le \phi_0/\sqrt{2} \\ A_1 - A_2 & \text{if } \phi_0/\sqrt{2} < \delta_\ell \le \phi_0 \\ 0 & \text{if } \delta_\ell > \phi_0 \end{cases}, \tag{5}$$

where

$$A_1 = \frac{1}{2}\left[\vartheta_1 \left(\frac{\phi_0}{2}\right)^2 - a \left|\frac{\phi_0}{2} - \frac{{\delta_\ell}^2}{\phi_0}\right|\right], \tag{6a}$$

$$A_2 = \frac{1}{2}\left[\vartheta_2 {\delta_\ell}^2 - a \frac{{\delta_\ell}^2}{\phi_0}\right], \tag{6b}$$

$$\vartheta_1 = 2\arcsin\left(\frac{2a}{\phi_0}\right), \tag{6c}$$

$$\vartheta_2 = 2\arcsin\left(\frac{a}{\delta_\ell}\right), \tag{6d}$$

$$a = 2\delta d \sqrt{1 - \left(\frac{\delta_\ell}{\phi_0}\right)^2}. \tag{6e}$$

The spatial uncertainty of the pits distribution is also taken into account. In particular, a Poisson process with rate λ_ℓ is assumed to model the occurrence of the pit corrosion along each ordinary rebar or each tendon. For post-tensioned tendons, pit corrosion is modeled with the assumption that only a single strand will be affected at any specific location along the tendon, and the affected strand is randomly selected. For the sake of completeness, it is highlighted that such probabilistic model of the spatial variability of the pits carries out some simplifications. In detail, it is known that pits in the ordinary rebars are more frequent close to the stirrups. Furthermore, the assumption of identical and independent distributions of the pits in each reinforcement element does not reflect the diverse orientation and exposure conditions as well as the spatial correlation of the corrosion phenomenon. Nonetheless, the adopted simplifications are deemed acceptable in the context of the current analysis.

The current area of the corroded reinforcement A_s or A_p is thus calculated either according to Eq. (3) in case of generalized corrosion, or Eq. (5) in case of pitting corrosion. The estimation of the corrosion current density i_c in Eqs. (2) and (4) is detailed hereafter, differing for ordinary rebars and post-tensioned tendons.

It is assumed that chloride-induced corrosion of ordinary rebars is due to the exposure to marine aerosol. Chloride penetration in concrete is simulated as one-dimensional diffusion process by means of Fick's second law as per Eq. (1). So doing, C is the chloride content at distance x and time t from the concrete surface, where airborne chloride accumulates, whereas D is the diffusion coefficient of concrete. For concrete surfaces exposed to marine aerosol, it has been recognized that chloride concentration is not constant while it exhibits an asymptotic value. Therefore, Eq. (1) is solved numerically under the assumption of time-dependent boundary chloride content C_s, which value in [% of binder] is calculated as follows (Yang et al. 2017):

$$C_s = C_{s1}\left(1 - e^{-\theta_{Csa} t_e}\right), \tag{7}$$

where C_{s1} is the initial value of the boundary chloride concentration in [% of binder], θ_{Csa} is a regression parameter equal to 1.25, and t_e is the exposure time in [years]. The mean value of C_{s1} is related to both exposure conditions and concrete mix as follows (Yang et al. 2017):

$$\mu_{C_{s1}} = 0.64\theta_{Csb} e^{-0.01d} v^{0.61} r_w, \tag{8}$$

where θ_{Csb} represents a correction coefficient depending on the binder type, which is equal to 2.57 for ordinary Portland cement. Moreover, d denotes the distance from the coast in [m], v represents the wind speed in [m/s] in the direction of the shoreline distance, and r_w is the water-to-binder ratio. A null initial chloride concentration C_0 is considered for the girder concrete. The diffusion coefficient D generally depends on several influencing factors (Shafei et al. 2012). Herein, the effects due to concrete aging and cracking only are taken into account in agreement with previous studies as follows:

$$D = D_0 \psi_t \psi_w, \tag{9}$$

where D_0 is the reference value of the diffusion coefficient for concrete, while ψ_t and ψ_w are two corrective factors that account for the effects due to concrete aging and cracking, respectively. The corrective factor ψ_t accounting for concrete aging is expressed as follows (Yang et al. 2018):

$$\psi_t = \left(\frac{t_0}{t + t_0}\right)^n, \tag{10}$$

where t_0 stands for the age of the concrete when first exposed to the chloride environment. The parameter n is the so-called aging factor and mainly depends on the concrete mix (Thomas Bamforth 1999). For low to moderate crack widths, chloride penetration in cracked materials can still be effectively modeled as a diffusion-like process using the following corrective factor proposed by Zhang et al. (2011):

$$\psi_w = \max(1{,}47.18w^2 - 8.18w + 1), \tag{11}$$

where w is the crack width in [mm]. Crack opening in concrete girder can be attributable to two concurrent factors, namely the pressure due to the rust generated by the corrosion of ordinary rebars and unintentional tension stress caused by the loss of prestress force in the post-tensioned tendons. Since detailed mechanical modeling of cracking phenomena in concrete would result into a prohibitive computational effort in the context of a reliability analysis, simplified formulations are here preferred. The width of concrete cover cracking w_s in [mm] resulting from reinforcement corrosion is modeled according to the empirical formulation proposed by Vidal et al. (2004):

$$w_s = \theta_{w_s}(\Delta A_s - \Delta A_s^*), \tag{12}$$

where $\theta_{w_s} = 0.0575$ represents a regression coefficient, ΔA_s denotes the steel cross-section area loss of the ordinary rebar in [mm^2], and ΔA_s^* is its value corresponding to the onset of corrosion crack in [mm^2]. Depending on the corrosion type, $\Delta A_s = A_{s0} - A_s$, where A_s is either A_g or A_ℓ given by Eq. (3) or Eq. (5) for generalized and pitting corrosion, respectively. The value of ΔA_s^* is calculated as follows:

$$\Delta A_s^* = A_{s0}\left\{1 - \left[1 - \frac{\theta_s}{\phi_0}\left(7.53 + 9.32\frac{c}{\phi_0}\right)10^{-3}\right]^2\right\}, \tag{13}$$

where the regression parameter θ_s is equal to 2 for generalized corrosion and to 6 for pitting corrosion. Moreover, c is the concrete cover.

The crack width due to loss of prestress force w_p in [mm] is estimated as recommended in (Nawy 1985), using the following formulation:

$$w_p = 8.51 \cdot 10^{-5}\frac{A_{ct}}{\Sigma_o}\Delta\sigma_p^*, \tag{14}$$

where A_{ct} is the concrete area in tension in [cm^2], Σ_o is the sum of the tendons' circumferences in [cm], and $\Delta\sigma_p^*$ is the net stress in the tendons in [MPa] obtained as the difference between the current tension generated by the applied loads and the stress corresponding to the decompression condition.

Equations (13) and (14) provide an estimate of the crack widths due to corrosion of ordinary rebars and prestressing force reduction individually. However, the coalescence of individual cracks and repeated loads can widen the crack. The inherent uncertainty related to cracking must be thus considered. Since the acceleration of the chloride ingress is governed by the widest crack, Eqs. (13) and (14) are thus considered to estimate the min value of w as follows:

$$w_{min} = \max(w_c, w_p), \tag{15}$$

and the condition $w \leq 0.4$ mm is imposed to ensure the validity of the diffusion-like mechanism.

A ordinary rebar placed at a distance c from the concrete surface exposed to chloride corrodes once the critical value of the chloride content C_{th} is here exceeded. The corrosion current density i_c in Eqs. (2) and (4) is determined by means of the well-known empirical formulation proposed by Liu and Weyers (1998), which was later on implemented into a fully probabilistic framework by Papakonstantinou and Shinozuka (2013). In detail, it is estimated as follows:

$$\ln(1.08 i_c) = 17.89 + 0.7771\ln(1.69C) - \frac{3006}{T} - 0.000116R_c + 2.24(t - t_c)^{-0.215}, \tag{16a}$$

$$\ln(R_c) = 8.03 + 0.549\ln(1 + 1.69C). \tag{16b}$$

In Eq. (22), C is the chloride concentration in [kg/m^3], T is the temperature in [K], R_c is the ohmic resistance of concrete in [Ω], t and t_c are the current time and the corrosion initiation time in [years], respectively. The reference value of 293.15 K (20 °C) is adopted for T.

As far as the corrosion of post-tensioned tendons is concerned, it is known that ingress and movement of moisture, oxygen and chloride can be promoted by incomplete filling grout as well as poor detailing and maintenance of the joints. A certain quantity of chloride is also latent in the grouting. Both sources of chloride contribute to the corrosion of the tendons. In agreement with Nguyen et al. (2013), chloride penetration into filling grout is simulated by means of the Fick's second law as per Eq. (1). The chloride content C at distance x from the surface inside the duct at time t is directly calculated by assuming time-independent values for all model parameters, including the diffusion coefficient of the filling grout D, boundary chloride content (i.e., constant chloride concentration in the air within the voids of the duct) C_s, and initial chloride content to which the wires are exposed in the duct C_0.

The wire in the tendon which surface is placed at a distance c from the top of the filling grout corrodes once the critical value of the chloride content C_{th} is here exceeded. The corrosion current density i_c in Eqs. (2) and (4) for post-tensioned tendons is determined by means of the formulation proposed by Wang et al. (2023):

$$i_c = \theta_t C^{0.308} r_w^{2.326} e^{\frac{-6417+5.829\cdot 10^{-8}\sigma_p}{T}}, \tag{17}$$

where σ_p is the average tension value in the tendon in [Pa]. In Eq. (17), θ_t is a regression parameter equal to $2.092\cdot 10^{10}$. The empirical formulation in Eq. (17) is adopted for post-tensioned tendons because it was purposely calibrated by Wang et al. (2023) for prestressed steel accounting for the influence of the tension. It is highlighted that σ_p in Eq. (17) is calculated considering the effects of traffic and thermal loads together with those due to the corrosion as well as concrete creep, shrinkage, and steel relaxation.

6. Modeling of deterioration and residual life prediction for water infrastructures

6.1 Water supply infrastructures (Cristina Bragalli, Elena Toth)

Water infrastructures systems intrinsically recall the systemic nature being defined as the set of elements distinct in terms of properties and functions, mutually interconnected, interacting with each other and with the external environment, to allow the collection, adduction, purification and distribution of water resources; they react or evolve as a whole connected to the environmental, economic and social context in a bidirectional way. This definition is consistent with the identification of water systems as critical infrastructures because of their impact on the socio-economic context of the environment in which they develop (Mohammed et al., 2022).

Understanding the long-term performance and predicting the service life of water pipelines are essential for facilitating early replacement, avoiding economic losses, ensuring safe transportation of drinking water from treatment plants to consumers and thus for a proactive management strategy of the water distribution network (Fan et al., 2022). A key factor for achieving this is improving the accuracy of pipe failure prediction models. However, the underlying mechanisms of incorporating explanatory variable data into the models still need to be better understood as well as the developing of suitable models that could be used for cases where data are insufficient or incomplete (Almheiri et al., 2021; Forero-Ortiz et al., 2023).

6.1.1 Collection and Validation of Data for Water Pipe Systems

The importance of substantial and reliable dataset can permit to better understand how all the variables interact, a crucial prerequisite before assessing the performance of pipe in failure rate prediction models. (Forero-Ortiz et al., 2023). However, incomplete and inaccurate data entries are very common in pipe databases. Data quality tests can be done to ensure that data is reasonable. Moreover, data can be cleaned by removing entries with missing data, or missing entries can be filled using data-imputation techniques developed for water distribution utilities (Kerwin et al., 2023).

Overall, the available data can be divided into different categories: *Physical data*, *Operational data*, *Maintenance interventions data*, *Environmental data* and *Social-economic data*. In Figure 28a, descriptive statistics of the main influencing factors are presented (Taiwo et al., 2023).

Generally, pipe information and break records are provided in the formats of two different layers in the Geographic Information Systems (GIS). As shown in Figure 28b, the pipe-information dataset is represented by edges and the break-records dataset is represented by points. Close examination indicated that these two types of data are not strictly overlapped. It is because the pipelines are based on actual laydown, while break locations (maintenance locations) are recorded manually or by GPS devices which do not align with the water pipes (Fan et al., 2022).

The water distribution system (WDS) of Parma (Figure 29) was identified as case study within the area managed by IREN SpA. The city has 198,931 inhabitants (31/07/2024) and is located in Northern Italy, more precisely in the western part of Emilia Romagna Region, between the Apennines and the Po Valley; the city is crossed by the Parma stream, a tributary of the Po river. The WDN analyzed is represented by a graph composed of 24020 nodes of which 23990 junctions, 5 tanks, and 25 reservoirs and 25052 links of which 18503 pipes, 6476 valves and 73 pumps. The length of the pipes is 832.7 km. The average demand allocated to the nodes is 612 l/s of which 68% water consumption and 32% leakage.

An advanced hydraulic (physically-based) model of a real-world water supply network has been implemented in WNTR Python package able to perform multiple analysis using the pressure-driven model Epanet 2.2. as hydraulic model. The reservoirs represent suction tanks of a pumping station and 24 wells. In order to model the drawdown of a water table due to withdrawal depending on the pumping rate, the well was modeled as a reservoir with a pump that has a linear characteristic curve which at zero flow rate gives a head equal to the height of the water table without withdrawal and which at the maximum withdrawal rate gives a head corresponding to the lowering of the water table for that withdrawal. WDS in the modeled scenario is supplied by 13 active wells and the reservoir, that represent a suction tank of pumping station. There are 3 junctions in the hydraulic model, which are transfer nodes that supply other water distribution systems.

Category	Predictors	Frequency	Normalized frequency
Physical and pipe related	Age	26	0.546
	Burial depth	4	
	Coating	2	
	Crack depth	4	
	Diameter	35	
	Length	22	
	Material type	27	
	Number of hydrants	2	
	Number of valves	2	
	Elastic modulus	8	
	Thickness	14	
Total		146	
Environment-related	Bedding condition	2	0.288
	Cold days	2	
	Corrosion depth	3	
	Corrosion length	2	
	Surface load	3	
	Frost load	4	
	Groundwater condition	1	
	Hot days	2	
	Land use	2	
	Precipitation	2	
	Soil corrosivity	13	
	Soil elastic modulus	5	
	Soil type	6	
	Temperature	9	
	Traffic load	13	
	Unit weight of soil	8	
Total		77	
Operation-related	Internal pressure	25	0.161
	Number of previous breaks	12	
	Water age	1	
	Water pH	2	
	Water temperature	1	
	Water velocity	2	
Total		43	
Social-related	Population	1	0.003
Total		1	
Grand total		267	

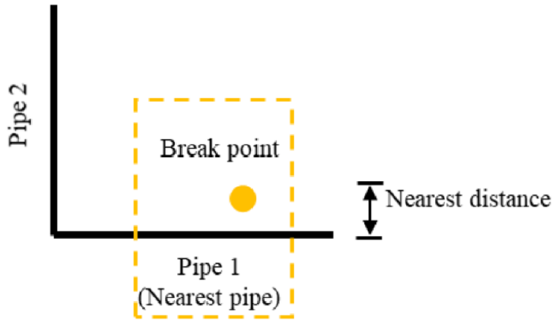

(b)

a) b)

Figure 28 - Descriptive Statistics of the Influencing Factors (Taiwo et al., 2023); (b) pipe break dataset aggregated based on nearest distance of break point to the pipe (Fun et al., 2022).

The material of a pipeline is a fundamental characteristic to investigate its fragility and the failure modes to which it is subject. In fact, the resistance to atmospheric agents, internal or external loads and interaction with the soil changes based on the type of material. In the WDN of Parma, the pipeline percentage of length divided by material is presented as summarized in Table 2. Table 2 shows the analysis of the breaks in the period 2022-2023 that affected the pipelines present in the Parma water distribution network model in relation to the material; the percentage of the total breaks that occurred for each material and the relative percentage in terms of length of the network corresponding to each material are indicated; furthermore, the average break rate (number of breaks per km in a year) in the observation period 2022-2023 is also indicated. Table 3 shows the analysis of the breaks in the period 2022-2023 that affected the pipes present in the

Parma water distribution network model in relation to the diameter; the percentage of the total breaks that occurred for each diameter class and the relative percentage in terms of length of the corresponding network are indicated; furthermore, the average break rate (number of breaks per km in a year) in the observation period 2022-2023 is also indicated.

The operational data refers to the results obtained in WNTR PDA by the hydraulic model. In Figure 30 the maps of maximum, average and minimum pressures and relative percentage distribution at the nodes of the Parma WDS model are shown, respectively, in (a), (b) and (c). In Figure 31 the statistical metrics of pressure is presented.

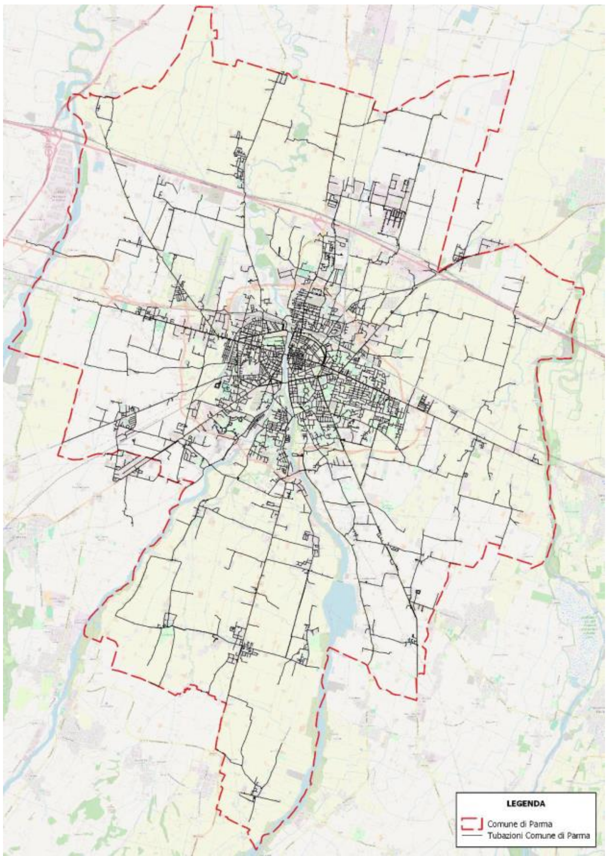

Figure 29 - Case study: water distribution network of the city of Parma.

Table 2 - Case study of Parma WDN: distribution of breaks as a function of the pipe material

Material	%breaks	% relative length	Rate of failure breaks/(km*year)
Cast iron	28,6	9,5	0,308
Asbestos cement	39,2	47,7	0,155
Polyethylene	25,4	17,5	0,189
Welded Steel	6,8	25,3	0,134

Finanziato dall'Unione europea
NextGenerationEU
Ministero dell'Università e della Ricerca
Italiadomani
PIANO NAZIONALE DI RIPRESA E RESILIENZA

Table 3 - Case study of Parma WDN: distribution of breaks as a function of the diameter

Diameter (mm)	% relative length	% breaks	Rate of failure breaks/(km*year)
D≤50	1,6%	7,9%	0,927
50≤D<90	14,8%	50,3%	0,651
90≤D<125	39,0%	33,3%	0,163
125≤D<175	27,3%	3,5%	0,024
175≤D<300	9,0%	1,3%	0,027
D≥300	8,3%	3,8%	0,086

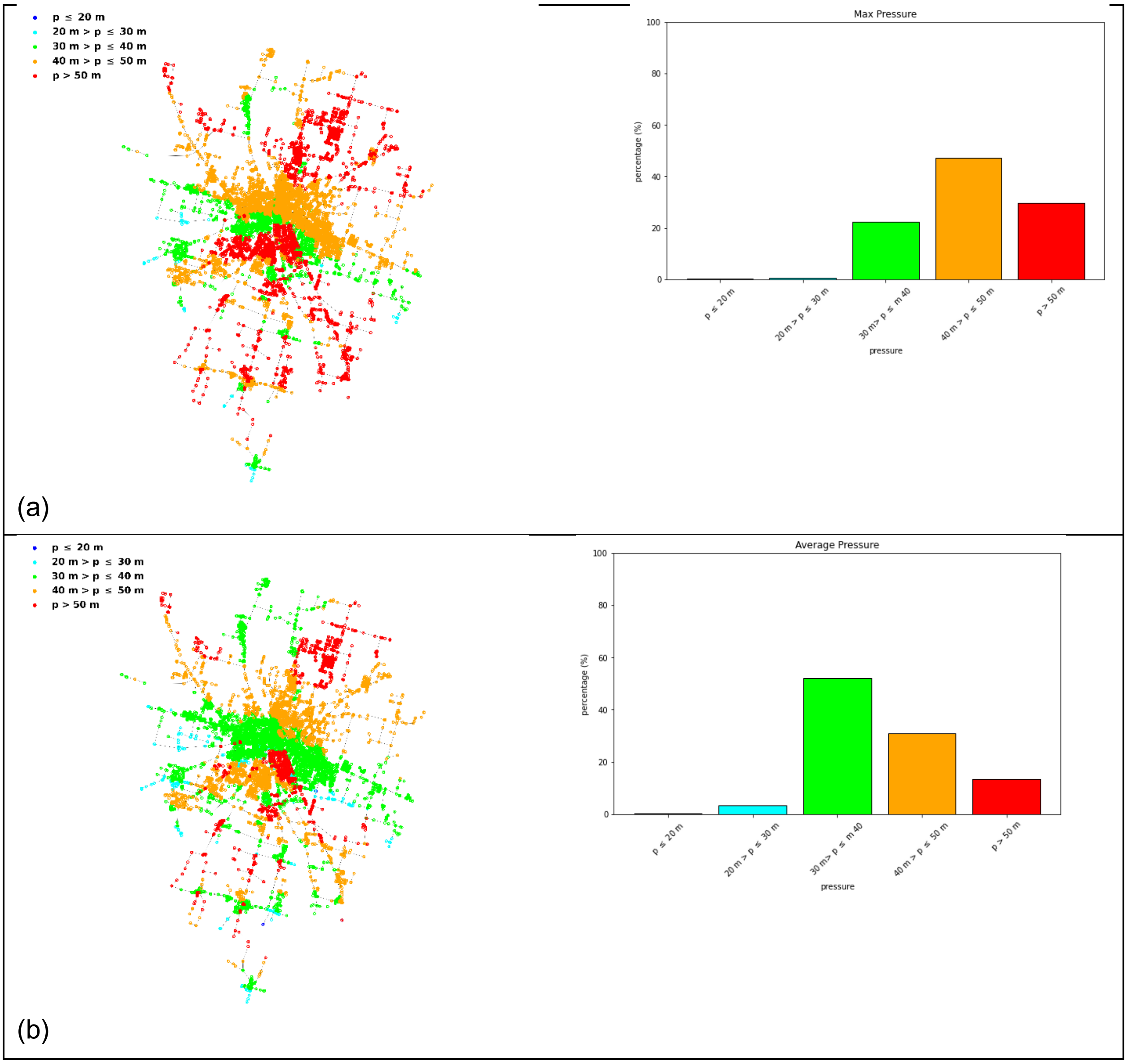

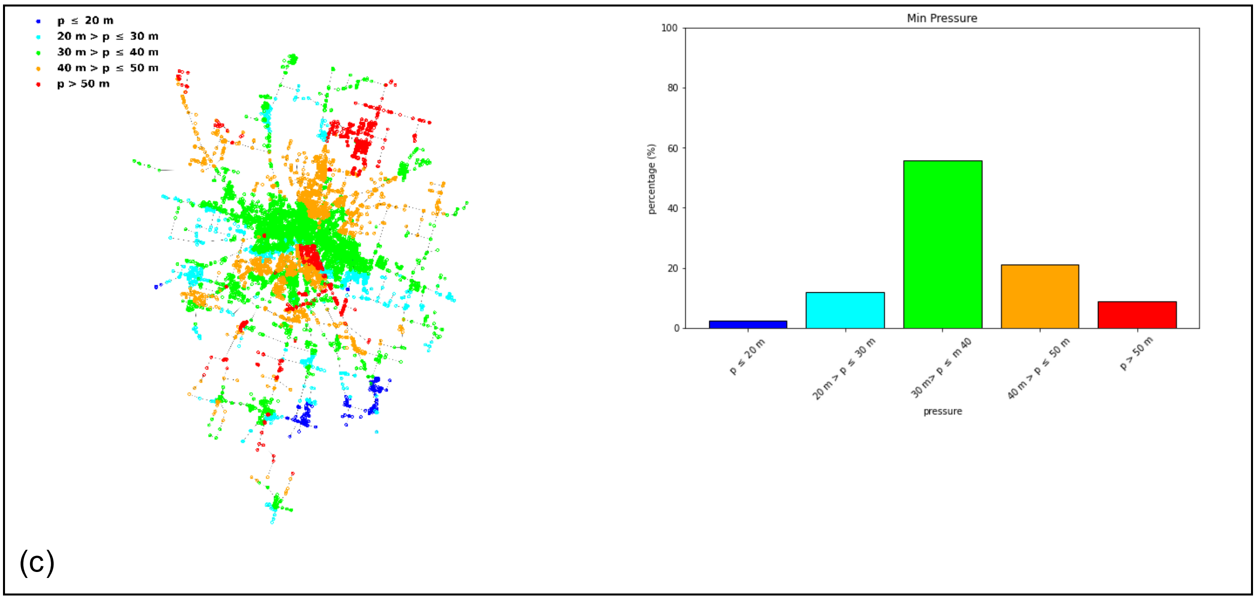

Figure 30 - WNTR PDA results: maps of maximum, average and minimum pressures and relative percentage distribution at the nodes of the Parma water distribution system model, respectively in (a), (b) and (c).

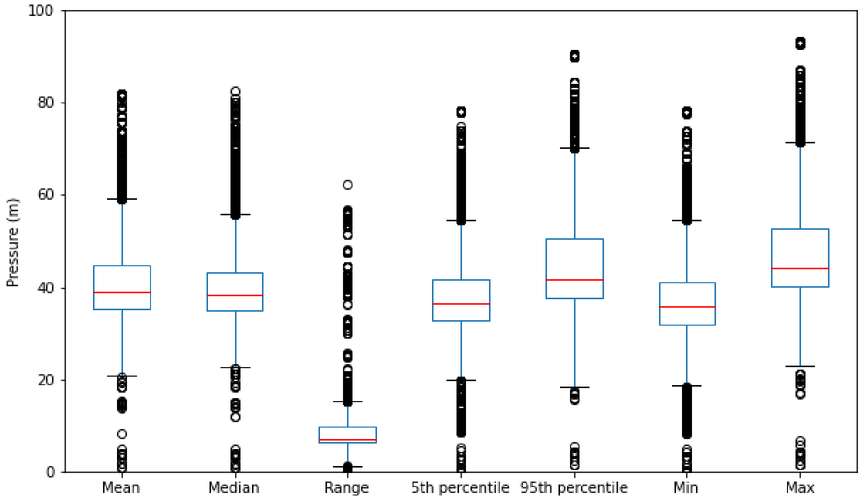

Figure 31 - WNTR PDA results: statistical metrics of pressure in the case study of water distribution network of Parma.

For a more in-depth analysis of the failure, the database of the interventions provided by IREN SpA in the period 2022-2024 was processed in the open source QGIS environment (https://www.qgis.org/) which allows to visualize, organize, analyze and represent spatial data. Thanks to the geo-localization of the interventions, it was possible to have an overlapping analysis of the pipelines with the associated interventions (Figure 32b). The purpose of this processing is to extract from the data provided the data useful for conducting a study on the degradation of the pipeline, trying to understand its main causes.

The data were processed in the open source QGIS environment (https://www.qgis.org/) which allows to visualize, organize, analyze and represent spatial data. For a more in-depth analysis of the state of the water infrastructure, the breaks shapefile of the years 2022 and 2023 was uploaded into the QGIS project. Thanks to the potential of QGIS and the geo-localization of the interventions provided by IREN SpA, it was possible to have an overlapping view of the water distribution model of Parma with the associated interventions (Figure 32b). The purpose of this processing is to extract from the data provided the information useful for conducting a study on the fragility of the network, trying to understand the main causes. Furthermore, this analysis creates the base for attempting to interpret the degradation phenomena and therefore can provide information on the priority of interventions. Figure 32a shows the analyses of georeferenced breaks in the water distribution networks of Parma in the period 2022-2023.

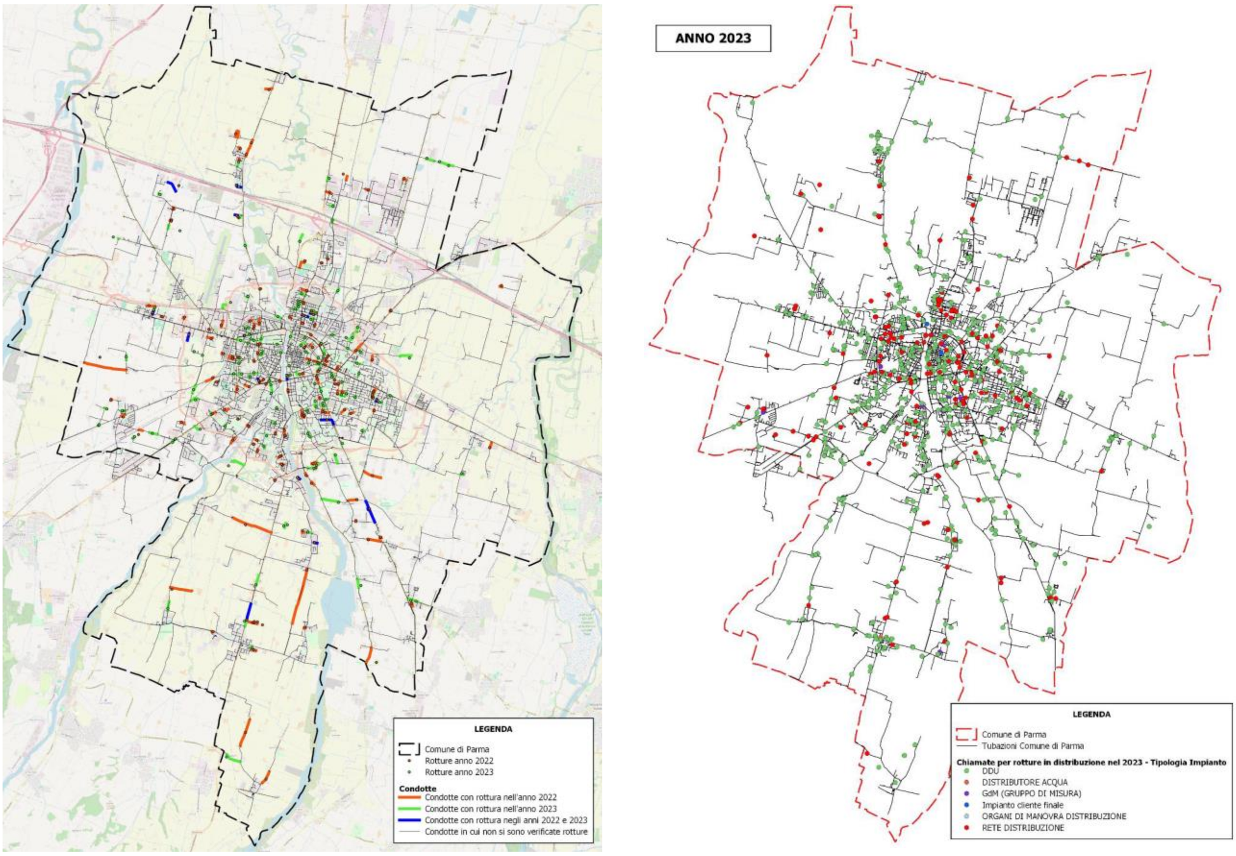

(a) (b)

Figure 32 - (a) grouping of pipelines that did not suffer any breaks in the period 2022-2023 (black line), that suffered breaks in 2022 (orange line), in 2023 (green line) or that suffered breaks in both years (blue line); (b) interventions on water network in 2023 based on the type: breaks on water pipelines (red dots) and breaks on user connections (green dots)

6.1.2 Key Parameters Influencing Deterioration

In the modeling of the structural dimension, identifying the key factors that influence the pipe failure is a key task in developing reliable prediction models (Farmani et al., 2017). According to a recent review, these factors can be generally grouped into four types according to their attributes in WDS: physical, operational, environmental, social and economic (Fan et al., 2022; Taiwo et al., 2023). In Figure 4a a brief discussion about the frequency analysis of the factors that influence the failure of water pipes, which are resultantly used in developing the prediction models and material types used in prior investigations, are shown. These four types of factors interplay and there is a need to better understand the interplay between these contributing factors and pipe failure probabilities. Although previous studies have examined the impacts of different factors on pipe failure probabilities, the relative importance (i.e., degree of the impacts) is yet to be well understood. Therefore, the interpretability consideration is also very important in developing a pipe failure prediction model (Fan et al., 2022).

Zangenehmadar et al. (2016) aim to benefit from Delphi method to prioritize the factors affecting the failure based on their significance (Figure 33). Delphi technique is a decision-making method based on opinions of experts concentrating on a certain issue to analyze, evaluate and forecast the solution. Three rounds of questionnaires were sent to the pre-selected experts and factors were arranged based on their importance in deterioration.

Different and unique failure modes may occur in water mains based on their material types. As water pipes are commonly buried underground, the role of soil-pipe play an important interaction on pipe failures. In particular, the pipes may suffer failures resulting from the differential ground settlement. The pipe deterioration process due to different soil corrosivity can also affect the pipe failure probability. Significant seasonal influence on the pipe's break has been observed (air temperature, precipitation) pointing out how the pipes suffered more breaks during extremely cold or hot days, possibly due to the soil-pipe interaction (Fan et al., 2022).

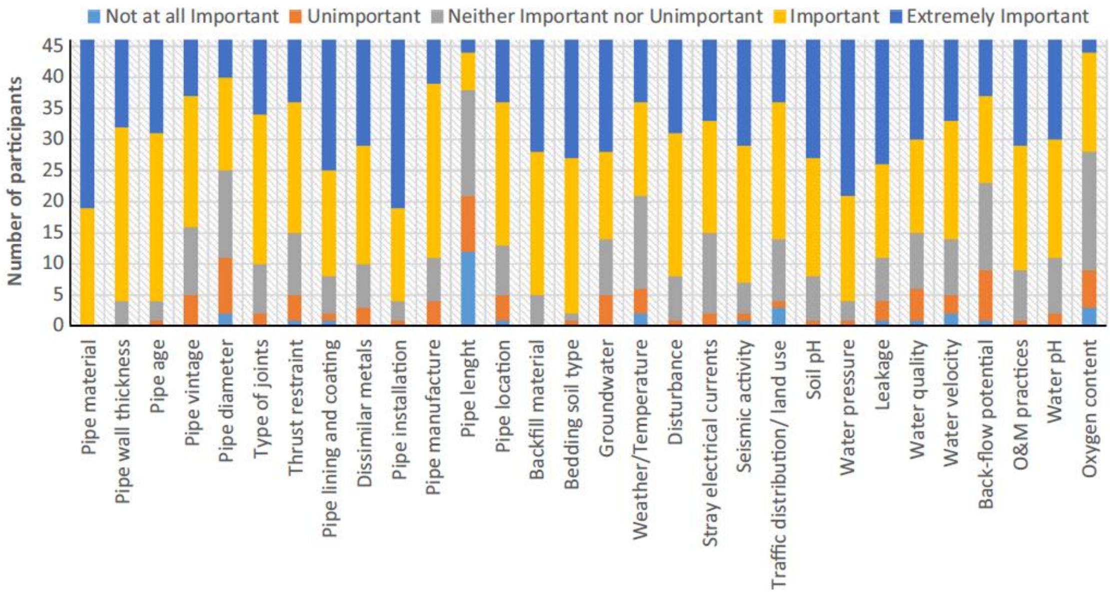

Figure 33 - Prioritization of the failure factors affecting the pipeline in water distribution networks by Delphi survey conducted in Zangenehmadar et al. (2016).

6.1.3 Predictive Models for Residual Life Estimation

Systematic reviews of the techniques used in modeling the failure probability of water pipes (Figure 34a), including physical, statistical, machine-learning (ML)-based and combined models are presented in literature (Forero-Ortiz et al., 2023; Taiwo et al., 2023; Philip & Aljassmi, 2020).

Physical-based models consider physical factors with empirical or semi-empirical feature equations that compare the allowable strength of a pipe to the real-world loading (Fan et al., 2022). Since physical models are based on equations, the contribution of each factor to the failure probability can be easily inferred. However, the location of the pipes (i.e., underground) makes the data collection needed to develop the physical models a considerable challenge (Taiwo et al., 2024).

Several statistical models have been proposed to study effects of different covariates in the failure of water pipes. In Kimutai et al. (2015) three statistical models, the Weibull proportional hazard model (WPHM), the Cox proportional hazard model (Cox-PHM), and the Poisson model (PM), were considered. This study recommends that a combination of models rather than a single model be used in assessing pipe network conditions based on the rate of deterioration and material type of the system. The probability of water pipe failure is estimated using a physical probabilistic approach in Mazumder et al. (2021). The failure probability of a pipeline is estimated as a fragility function and the consequence of the failure is determined through a fuzzy hierarchical process. However statistical models can only handle limited variables and require expert experience to formulate the statistical equations (Taiwo et al., 2024).

In recent years, machine learning (ML) approaches have been widely used for water pipe condition assessment and failure prediction (Dawood et al., 2020; Fan et al., 2022; Zali et al., 2024), as shown in Figure 34b. Machine learning-based models have emerged as a powerful tool in enhancing the predictive capabilities of water distribution network models (Forero-Ortiz et al., 2023). These methods require a considerable amount of data from water distribution networks. Kerwin et al. (2020) a systematic, iterative approach to the development of ANN failure prediction models to aid decision-makers in short-term prioritization. Imbalanced and missing data, whether asset or failure data, compromise a model's prediction performance. In Zali et al. (2024) three ML methods—XGBoost, random forest and logistic regression—were used to prioritize asset rehabilitation. To address the issue of imbalanced data, a method of semi-supervised clustering is proposed to leverage the domain knowledge in combination with unsupervised learning to divide the data set into homogeneous categories and enhance the classification accuracy.

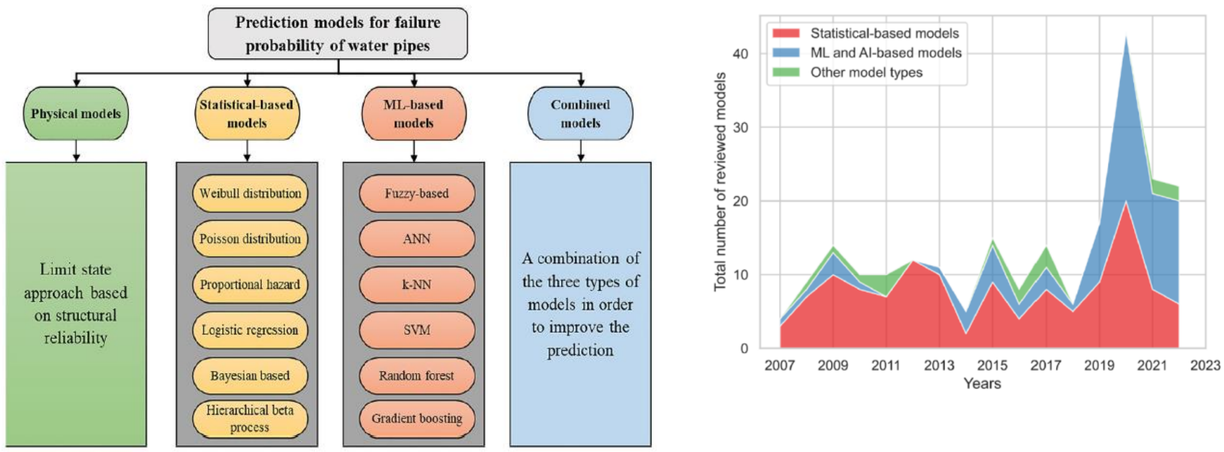

(a) (b)

Figure 34 - (a) Prediction models for failure probability of water pipes (Taiwo et al., 2023); (b) comparison of trends in model types between 2007 and 2022 with a substantial increase in the utilization of Machine Learning-based models in the last four years (Forero-Ortiz et al., 2023).

6.2 Urban drainage infrastructures (Maria Sambito, Gabriele Freni)

The present section is focused on urban drainage infrastructure deterioration and investigating the efficiency of prediction models. After a classification and the identification of advantages and disadvantages of different approaches, the chapter focuses on the data needs of each approach and the definition of compelling developments of existing approaches to be applied to urban drainage pipes. On the operational front, pipelines face an array of physical, chemical, and biological threats, including corrosion, abrasion, root intrusion, and material fatigue. Inadequate maintenance and insufficient periodic inspections exacerbate these challenges, increasing both the risk of sudden failures and the probability of chronic issues like repeated blockages. The deterioration of drainage networks adversely impacts public safety, disrupts critical services, and causes environmental harm by promoting water contamination. Accurate and consistent data collection proves pivotal in modeling deterioration. Inspection logs and maintenance records yield essential insights about failures, while environmental data—including soil properties, climatic variables, and demographic patterns—help pinpoint underlying causes and hot spots. Nevertheless, issues such as missing values, uneven inspection coverage, and lack of standardized protocols hamper modeling accuracy. The chapter underscores the importance of advanced data acquisition techniques (e.g., CCTV inspections, real-time sensor monitoring, and geophysical surveys) and centralized geographic information systems for improved decision-making. A range of modeling techniques is explored. Empirical (Statistical) Models, including regression-based and probabilistic survival analyses, can effectively leverage historical datasets to predict failure patterns. While these methods often excel at system-level or short-term forecasts, their reliance on consistent, high-quality data limits their applicability when records are sparse or conditions diverge from historical norms. Physically Based (Mechanistic) Models emphasize fundamental processes like corrosion kinetics, structural loading, and hydraulic behavior. Though highly informative, these models can be computationally expensive and are sensitive to parameter uncertainties, especially in large or complex drainage networks. Machine Learning Approaches offer a complementary perspective, capable of managing high-dimensional datasets and capturing nonlinear interactions among multiple variables. Methods such as random forests, neural networks, and hybrid ML-transient-based models have demonstrated excellent performance in predictive tasks like leak detection and failure risk assessment. Key challenges include preventing overfitting, ensuring model interpretability, and sustaining adequate labeled data for training. Lastly, the chapter examines model evaluation and validation through metrics commonly used in classification tasks (e.g., accuracy, precision, recall, F1 score, and AUC-ROC) and real-world testing scenarios. It highlights the value of comprehensive calibration and pilot testing—often using in situ data—to improve model reliability.

6.2.1 Background on Urban Drainage Pipe Deterioration

Urban drainage systems are key infrastructures for stormwater management and preventing flooding in urban areas. However, managing these systems presents several challenges, as urbanisation has caused an increase in impermeable surfaces, reducing the natural absorption of rainwater and overloading existing drainage systems. Monitoring and prevention actions of sewage systems are crucial to guarantee public health and environmental sustainability (Sambito et al. 2019). The intensification of extreme weather events due to climate change, such as torrential rains, also subjects networks to more significant pressures, often exceeding their design capacities.

This scenario is further aggravated by the aging process that many drainage systems are reaching the end of their life cycle, with materials that progressively deteriorate; the absence of scheduled maintenance and regular interventions increases the risk of failures and obstructions, worsening the performance of the networks (Berardi et al., 2009).

These issues not only set the system's functionality at risk but also increase the probability of phenomena such as urban floods, with negative impacts on the protection of the environment, property and human lives.

Urban drainage pipes, despite being designed to last decades, are subject to various deterioration processes that progressively compromise their functionality. These mechanisms include physical, chemical and biological phenomena that can act individually or in combination, accelerating the degradation of infrastructures.

Corrosion is one of the main factors of deterioration, especially for metal pipes. Galvanic corrosion phenomena or interaction with acidic or polluted waters can corrode the internal and external surfaces of pipes (Frehmann et al., 2002).

Since it is wastewater, the presence of solid materials, such as sediments or debris, also causes damage in terms of abrasion of the internal surfaces of the pipe. Other substances that tend to accumulate such as grease, oil, limestone or sediments can progressively reduce the transport capacity of pipes, promoting obstructions and even causing structural damage (Banik et al., 2020).

In many urban areas, tree roots also represent a significant threat to pipes. In fact, they can penetrate through small cracks or unsealed joints, causing flow obstructions and deformations or breaks in the walls of the pipelines.

Other factors that should not be underestimated are thermal variations and material fatigue. In fact, temperature fluctuations, especially in extreme climates, can cause repeated expansions and contractions in the materials of the pipelines, weakening them over time. Regarding material fatigue, repeated loads, both internal (variable hydraulic pressures) and external (traffic or weight of the overlying soil) cause cyclical stress that can lead to micro-cracks that progressively widen, causing breakages.

Insufficient maintenance, the absence of periodic inspections and the lack of adjustments to face the growing challenges posed by climate change and the phenomenon of urbanization further aggravate an often already critical situation.

The deterioration of urban drainage networks has a direct and significant impact on urban areas, causing various problems involving the environment, public health and the economy. The deterioration of pipes reduces their capacity to convey rainwater, causing frequent flooding in urban areas, especially during intense weather events. In turn, flooding compromises the safety of people and property, damaging buildings, roads and infrastructure, and can interrupt essential services such as public transport. The deterioration of urban drainage networks also poses a health risk as well as a hydraulic one; in fact, deteriorated pipes can favor the stagnation of water, creating ideal habitats for the proliferation of mosquitoes, bacteria and other pathogens. In the event of a break, contaminated water can rise to the surface or infiltrate water networks, increasing the risk of waterborne diseases.

The environmental impact is well known, compromised pipelines can release untreated wastewater into natural bodies of water, such as rivers or lakes, causing serious damage to ecosystems as well as the infiltration of pollutants into the soil can alter the quality of groundwater, making it unusable for drinking or agricultural purposes.

All these factors have repercussions in economic terms, as the interruption of essential services and environmental degradation generate both direct and indirect economic impacts. The lack of preventive interventions also often leads to costly emergencies, such as sudden repairs or replacements of entire sections of the network. Flooding and the loss of functionality of the pipelines can cause damage to infrastructure and private property.

In general, deteriorated drainage networks make cities less capable of adapting to the changes to which they are continuously subjected and of dealing with extreme events, increasing the overall vulnerability of the territory. The deterioration of urban drainage pipelines represents a complex challenge that requires timely and integrated interventions. Failure to address these issues not only exacerbates the consequences listed above but progressively increases the difficulty and cost of future solutions.

6.2.2 Data Requirements and Sources (MS 2p)

To model the deterioration of urban drainage pipelines, it is essential to have complete and accurate data that describes the condition of the infrastructure and the factors that influence its degradation. Among the main types of data commonly used are pipeline inspection logs; these data are derived from periodic inspections and provide detailed information on the condition of the pipeline, such as the presence of cracks, corrosion, blockages or structural deformations. They are essential to identify the most vulnerable areas and estimate the remaining life of the infrastructure.

Maintenance logs contain information on past maintenance activities, such as repairs, cleaning or replacements. They are useful for identifying the sections of the network most prone to recurring failures and for evaluating the effectiveness of the maintenance strategies adopted ((Yang & Su, 2006).

Keeping track of environmental variables is another important aspect. These data include information on the climate (for example, frequency and intensity of precipitation), temperature and humidity, which can accelerate phenomena such as corrosion or erosion. Climate change is making these variables increasingly relevant in deterioration modeling.

Fundamentally, it is important to know the soil properties, such as pH, salt content, or geotechnical instability, that directly influence the degradation of pipelines, especially those made of metal or concrete. Geotechnical and geological data help to understand the specific risks related to local conditions.

Finally, population density and traffic intensity above are key factors that increase stress on pipelines. This data provides context for the pressure on the network, helping to predict deterioration in the most critical areas.

Data collection is a key step in understanding and modeling the deterioration of urban drainage pipes. Different techniques and tools are used to acquire detailed information on the condition of the infrastructure and the factors that influence its degradation. Traditional visual inspections, used to identify surface problems, are often limited in their ability to detect internal defects. For this reason, different techniques have been implemented.

Among the most common methods are CCTV (Closed Circuit Television) inspections. This method consists of inserting robotic cameras inside the pipes to acquire high-resolution images and videos of the internal surfaces. It provides a direct view of the condition of the pipes, allowing to identify problems such as cracks, corrosion, blockages and deformations but the cameras can only reach certain sections of the network; furthermore, it is an expensive technique, especially for large networks and requires highly trained personnel for image analysis.

Another solution is active monitoring through a network of sensors. Sensors are installed inside or near the pipes to monitor in real time parameters such as pressure, flow, temperature, humidity and corrosion level. Continuous monitoring provides real-time data to identify emerging problems before they become critical and reduces the need for frequent manual inspections. However, sensor installation and maintenance require specific skills and sensors can be subject to failure or malfunction, affecting the quality of the data collected. Furthermore, instrumental costs should not be underestimated if sensors are not strategically positioned to reduce their number but at the same time ensure rapid interception of the source of contamination that generates the failure.

Other investigations involve data collection through geophysical methods (such as ground-penetrating radar) or structural tests to assess the bearing capacity and integrity of pipelines.

Detailed analysis allows to assess the structural health of pipelines and the risk of failure and can be used on different types of materials and in difficult conditions. On the other hand, investigations can take weeks or months to complete and there is a need for specific, often expensive, instrumentation.

Using geographic databases to integrate information on infrastructure with environmental, demographic and topographic data allows to merge data of different nature (topography, urbanization, soil characteristics) in a single system, facilitating the identification of risk areas. The accuracy of the GIS depends on the quality and updating of the data entered.

Overall, the most common challenges in data collection concern accessibility, costs and standardization. Reaching all sections of the network can be complicated, especially in densely urbanized or difficult to excavate areas. Collecting reliable data on a scale requires significant investments.

Finally, there is often a lack of uniform protocols to ensure the consistency of data collected from different sources.

Data quality is one of the most critical aspects in modeling the deterioration of urban drainage pipelines. Incomplete, inconsistent or unreliable data can compromise the accuracy of the analyses and lead to ineffective design decisions. Among the main issues related to data quality and their implications are missing values; they are frequent in inspection or maintenance records, often due to lack of regular inspections in some sections of the network and/or errors in data collection or storage.

Lack of information can make it difficult to identify the critical points of the system. Incomplete models lead to less precise estimates of deterioration. For example, the use of estimates based on averages or predictive models is often a solution to fill these gaps. However, the implementation of more rigorous and regular data collection protocols appears to be the most correct path.

Regarding protocols, the lack of standardization in the methods of data collection and recording can generate discrepancies between different sources or time periods. For example, two successive inspections may use different criteria to assess the same type of damage. The implications include difficulty in making temporal or spatial comparisons across the network and increased uncertainty in model results.

It is therefore important to define standardized guidelines for data collection and storage and train inspection personnel to ensure consistency in methods.

Other issues include data collected through methods such as CCTV inspections or sensors that can be subject to interpretation or measurement errors. For example, CCTV image quality may vary depending on internal conditions of pipelines (e.g. sediment or stagnant water) or sensors may detect inaccurate data due to malfunctions or environmental interference.

Inaccurate results may negatively impact maintenance or repair decisions, and deterioration modeling may under- or overestimate the actual risk.

Integrating multiple data sources to validate results (e.g., combining visual inspections and sensor data) and using advanced analysis tools to manage data uncertainty, such as probabilistic models or Monte Carlo analysis, can be some of the solutions.

An equally relevant issue is large-scale data. Data collection on large urban networks can be hampered by time and resource constraints as well as logistical difficulties in accessing certain areas or sections of the network. The lack of complete network coverage can generate models that do not correctly represent real conditions.

For this reason, it is necessary to prioritize the most critical areas for targeted data collection and exploit technologies such as drones or radar to increase coverage more quickly and cost-effectively.

Finally, there are errors in data storage and management since inadequate storage of historical data, often in paper or non-digitized format, can cause the loss of relevant information.

This leads to a series of difficulties in creating useful historical series to identify trends and deterioration dynamics.

Digitizing all available data and organizing them in centralized databases and implementing integrated GIS systems for a more effective and accessible management of information are effective strategies.

In conclusion, data quality is essential for modeling pipeline deterioration and for planning maintenance and repair activities. Addressing issues such as missing values, inconsistencies, and uncertainties improves the models' reliability and allows optimisation of resources and strategies to ensure sustainable and resilient management of urban drainage networks.

6.2.3 Empirical (Statistical) Models

Traditional statistical approaches for predicting pipe deterioration in urban drainage systems include deterministic, probabilistic, and machine learning models (Barton et al., 2022). Deterministic models, such as regression models, are simple and require minimal data. They perform well for predicting failure rates at the network level or for large groups of pipes, especially over shorter intervals to capture seasonal influences (Barton et al., 2022). Probabilistic models like survival analysis can account for randomness and are useful for predicting time-to-failure, interarrival times, and failure probabilities for individual pipes (Barton et al., 2022). Examples include the non-homogeneous Poisson process, zero-inflated Poisson process, Weibull accelerated lifetime model, and linear extended Yule process (Santos et al., 2016). Some interesting contradictions emerge in model performance. While deterministic models work well at the network level, probabilistic models are better suited for individual pipe predictions (Barton et al., 2022). The linear extended Yule process and zero-inflated Poisson process showed the best overall results in one study, while the Weibull model performed well for medium-term predictions but less so for shorter windows (Santos et al., 2016). In summary, choosing the most appropriate statistical model requires careful consideration of variables, prediction interval, spatial level, response type, and inference level needed (Barton et al., 2022). While these traditional approaches have proven useful, they each have strengths and limitations depending on the specific application and data available. Newer machine learning techniques are also emerging to handle more complex data relationships in pipe deterioration modeling (Barton et al., 2022).

Statistical approaches for pipe deterioration often rely on several underlying assumptions: Parametric lifetime models are commonly used for statistical analysis and prediction of failure rates in water distribution pipes. These models assume that pipe lifetimes follow certain probability distributions, and the resulting theoretical failure rates are time-invariant (Dehghan et al., 2008). This implies an assumption of stationarity in the failure rate process. However, empirical evidence from Melbourne, Australia, shows that pipe failure rates can vary over time, potentially influenced by factors like rainfall patterns (Dehghan et al., 2008). Another assumption is that population characteristics can be used to model degradation paths for individual pipe sections. This data-driven approach simulates various aspects of pit growth progression and spatial distribution of pits, assuming that these characteristics are representative of individual pipe behavior (Yarveisy et al., 2023). The model also assumes that corrosion-related parameters such as pit dimensions, initiation probability, and location can be accurately modeled based on field data and understanding of corrosion behavior. Interestingly, some approaches acknowledge the lack of historical data and propose alternative methods. The Thomas model, for instance, estimates failure rates using available information on vessel shape, size, thickness, and construction details, assuming these factors are indicative of failure likelihood (Medhekar et al., 1993). This model can incorporate maintenance and inspection history, assuming their impact on predicted failure rates can be accurately reflected.

In conclusion, while statistical approaches provide valuable insights into pipe deterioration, their underlying assumptions may not always hold in real-world scenarios. The time-varying nature of failure rates and the influence of external factors like environmental conditions challenge the assumption of stationarity. To address these limitations, regular updating of model parameters or developing non-parametric techniques for modeling pipe failure rates may be necessary (Dehghan et al., 2008).

Pipe deterioration in urban drainage systems is a critical issue that requires accurate prediction and assessment for effective management. While empirical methods have been widely used, they face several limitations, particularly when extrapolating to new conditions. One of the primary limitations of purely empirical methods is their reliance on historical data and CCTV inspection reports, which can be prone to errors due to their subjective nature and human involvement (Salihu et al., 2023). This subjectivity can lead to inconsistencies in deterioration assessments and may not accurately reflect the true condition of the pipes. Additionally, the lack of sufficient data to develop prudent deterioration models is a significant challenge (Salihu et al., 2023). This data scarcity limits the ability of empirical methods to provide accurate predictions, especially when dealing with new or unfamiliar conditions. Another limitation is the difficulty in capturing the complex interactions between various factors affecting pipe deterioration. Empirical methods often struggle to account for the dynamic nature of urban environments, climate change impacts, and evolving infrastructure systems (Abebe & Tesfamariam, 2020; Xu et al., 2023). As a result, these methods may fail to accurately predict deterioration patterns in changing urban landscapes or under different environmental conditions. To address these limitations, researchers are exploring more advanced approaches. For instance, Salihu et al. (2023) propose an AI-based model that integrates unsupervised multilinear regression and Weibull analysis to improve deterioration predictions. Abebe and Tesfamariam (2020) suggest a Dynamic Bayesian Network model to capture dependencies among indicators and quantify uncertainty. These approaches aim to provide more robust and adaptable deterioration models to handle new conditions and limited data scenarios better. By incorporating a wider range of data sources and advanced analytical techniques, these methods offer promising alternatives to purely empirical approaches in urban drainage pipe deterioration assessment.

6.2.4 Physically Based (Mechanistic) Models

Engineering models based on physical laws have been developed to understand and predict deterioration processes in urban drainage systems. These models integrate life-cycle cost optimisation with structural deterioration, considering both progressive degradation (e.g., corrosion, fatigue) and sudden events (e.g., earthquakes) (Sanchez-Silva et al., 2012). For instance, corrosion in reinforced concrete pipes, commonly used in storm sewer systems, can be modeled using chemical kinetics and thermodynamic principles (Zheldakov et al., 2021). Interestingly, while most models focus on degradation, some innovative approaches explore ways to mitigate these issues. For example, perforated concrete sewer pipes have been proposed to alter moisture conditions and potentially reduce degradation in urban watersheds (Ni et al., 2022). This approach, while promising, requires careful consideration of the trade-off between drainage performance and structural integrity. Engineering models for urban drainage deterioration processes combine physical principles, from corrosion kinetics to structural mechanics. These models help predict system performance over time and inform maintenance strategies. However, as urban environments evolve, new approaches like perforated pipes may offer alternative solutions to traditional drainage problems, necessitating further research and modeling efforts to understand their long-term impacts and benefits fully.

Material properties play a crucial role in pipe deterioration. For instance, concrete and vitrified clay pipes have different helpful service lives, with concrete pipes lasting approximately 79 years compared to 48 years for vitrified clay pipes (Salihu et al., 2023). Physical aging is extensively detected in PVC pipes, while other degradation mechanisms have minimal effects (Makris et al., 2021). Concrete's tensile and compressive strength are identified as the most influential parameters over the entire service life of sewer pipes (Zamanian & Shafieezadeh, 2021). Flow characteristics, such as water velocity and surface angle, impact pipe deterioration. The extraction and reuse of greywater can alter flow characteristics in water and sewer pipe networks, potentially affecting their performance (Chowdhury & Rajput, 2016).

Additionally, the presence of dissolved sulfide concentration and pH-dependent factors in wastewater significantly affect infiltration/exfiltration for pipes older than 30 years (Zamanian & Shafieezadeh, 2021). Environmental conditions, including soil properties, groundwater levels, and external loads, contribute to pipe deterioration. Traffic loads, represented mainly by truck weight and multiple presence factors, represent traffic loads as significant variables in deterioration models (Zamanian & Shafieezadeh, 2021). The hostile environment in which PVC sewer pipes operate raises concerns about their longevity (Makris et al., 2021). Furthermore, land use changes, such as the expansion of sealed surfaces, impact the distribution and volume of urban flooding, which can indirectly affect pipe deterioration (Liu et al., 2022). Pipe deterioration models for urban drainage systems must consider the complex interplay between material properties, flow characteristics, and environmental conditions. These factors collectively influence the structural integrity, hydraulic performance, and overall lifespan of sewer pipes. By incorporating these variables into deterioration models, urban planners and engineers can better predict and manage the maintenance needs of drainage systems, ultimately contributing to more sustainable and resilient urban water management.

While widely adopted for urban drainage system design and operations, mechanistic models face challenges due to the complexity of dynamic processes and high computational demands (Duan et al., 2024). These models often involve numerous parameters representing complex hydrodynamic processes, making effective and robust calibration difficult, especially with limited observations (Huang et al., 2022). The calibration and verification approach to testing model performance can give an exaggerated sense of certainty, as model structure and parameters are often not identifiable based on available data series, leading to elements of guesswork (Harremoës & Madsen, 1999). Interestingly, some studies have found that models with less complexity might perform equally well with reduced establishment and computation time (Chang et al., 2019). For instance, calibrated models with different resolutions showed similar performances, although peak flows exhibited noticeable scale effects of up to 30% (Chang et al., 2019).

Additionally, considering effective impervious area as a calibration parameter only marginally increased performance during calibration but slightly decreased performance in validation, highlighting the importance of detailed identification (Chang et al., 2019). To address these challenges, researchers are exploring alternative approaches. Knowledge-informed data-driven modeling offers a unique solution that reduces data requirements and enhances model interpretability by integrating existing mechanistic knowledge into data-driven models (Duan et al., 2024). This approach balances model complexity with dataset size, enabling more efficient and interpretable modeling in urban water systems. Furthermore, innovative modeling software like Simuwater combines multiple principles, simulates various components, and incorporates optimised control functions, demonstrating significant results in reducing combined sewer overflow in real-time case-control studies (Wang et al., 2021).

6.2.5 Machine Learning Approaches

Machine learning techniques have been increasingly applied to urban drainage pipe deterioration prediction and risk assessment, offering improved accuracy and efficiency over traditional methods. Random forest algorithms have shown promising results in risk assessment for municipal pipe networks. A study optimized the random forest learning model and compared it with other centralized learning methods, demonstrating better prediction accuracy and robustness on the dataset (Cen et al., 2023). The model identified key risk factors affecting pipe failure, with pipe material, soil properties, service life, and the number of past failures being the most influential. Neural networks have also been employed for predicting pipe deterioration. Probabilistic Neural Networks (PNN) were used to divide the deterioration degree of pipes into 5 levels, estimating the maximum residual service time for each pipe and diameter (Baek et al., 2005). This approach enables quantitative management of water distribution systems and optimal scheduling of rehabilitation efforts. Interestingly, some studies have explored hybrid approaches combining machine learning with other techniques. For instance, a hybrid Machine Learning/Transient-Based (ML/TB) leak detection method for pipe networks was developed, utilizing hydraulic responses in the frequency domain and machine learning feature selection techniques (Ayati & Haghighi, 2023). This approach outperformed existing methods in leak detection accuracy with fewer sampling sites. In conclusion, machine learning techniques, particularly random forests and neural networks, have demonstrated significant potential in improving urban drainage pipe deterioration prediction and management. These methods offer enhanced accuracy, robustness, and the ability to handle complex datasets, making them valuable tools for infrastructure managers and decision-makers in urban water management.

Machine learning (ML) approaches offer several strengths in handling large-scale urban drainage systems and high-dimensional data: ML methods, particularly neural networks (NN), excel at learning input-output relationships in large complex systems based on extensive datasets (Scheinker, 2021). This capability is especially valuable for urban water drainage systems, which represent complex networks with nonlinear dynamics and various interactions (Baumann et al., 2022). ML algorithms can effectively process huge datasets (Big Data) that require special tools and approaches, making them well-suited for handling the high-dimensional data often associated with urban drainage systems (Rybczak et al., 2024). One of the key strengths of ML approaches is their ability to capture nonlinear relationships in complex systems. This is particularly important for vascular flow modeling, which involves solving nonlinear Navier-Stokes equations in complex anatomies with physiological boundary conditions (Macraild et al., 2024). By extension, this capability is highly relevant to urban drainage systems, which exhibit similar complexities. ML-based models can provide instant predictions of complex phenomena, making them appealing for speeding up large parameter space searches that would otherwise require computationally expensive simulations (Scheinker, 2021). However, it's important to note that conventional urban drainage system (UDS) models, which are mechanistic, can be slow-running, difficult to calibrate and re-calibrate in real-time, and struggle with handling noisy data (Norreys & Cluckie, 1997). In contrast, ML approaches can overcome these limitations by offering faster computation times and better handling of noisy data, making them more suitable for real-time control and monitoring of urban drainage systems. In conclusion, ML approaches demonstrate significant strengths in handling large-scale urban drainage systems and high-dimensional data, particularly in their ability to capture nonlinear relationships, process big data efficiently, and provide rapid predictions. These capabilities make ML methods valuable tools for improving urban water management, especially in the face of challenges such as rapid urbanization and climate change (Ramos & Besharat, 2021).

Urban drainage systems face several challenges in modeling and management, particularly when leveraging data-driven approaches. The need for large labeled datasets is a significant hurdle, as highlighted by the limitations of mechanistic models in capturing complex dynamic processes (Duan et al., 2024). This challenge is compounded by the high computational demands of these models, which can hinder their practical application in real-world scenarios. Overfitting is another critical concern, especially when dealing with high-dimensional representations of urban systems. Chen et al. (2022) noted that "high-dimensional representation often causes overfitting problems and leads to poor model performance." This issue is particularly acute when working with diverse structures within small datasets, which is often the case in urban drainage systems. Interpretability of models remains a key challenge, as emphasised in Duan et al. (2024). While data-driven models offer opportunities to capture system complexities, their lack of interpretability can hinder wider adoption. This is particularly important in urban water systems, where understanding the underlying processes is crucial for effective management and decision-making. There is a growing emphasis on integrating domain knowledge with data-driven approaches to address these challenges. Duan et al. (2024) advocates for a "knowledge-informed approach" that balances model complexity with dataset size, enabling more efficient and interpretable modeling in urban water systems. Similarly, Wu et al. (2024) discusses integrating Bayesian regularisation techniques with deep learning to enhance model performance and reliability while providing probabilistic insights. These approaches aim to leverage existing mechanistic knowledge to reduce data requirements, enhance interpretability, and improve overall model accuracy in urban drainage system management.

6.2.6 Model Evaluation and Validation

The provided papers do not specifically address pipe maintenance or related decision-making processes. However, they offer insights into various performance metrics used in evaluating machine learning and deep learning models across different domains, which could be applicable to pipe maintenance scenarios. Several common evaluation metrics are mentioned across the papers, including accuracy, precision, recall, F1 score, and Area Under the Receiver Operating Characteristic curve (AUC-ROC) (Chen et al., 2024; Kundu et al., 2023; Liang et al., 2023; Pekşen et al., 2024). These metrics are widely used to assess the performance of classification models in various fields, including medical imaging and diagnostics. Interestingly, some papers highlight the importance of considering multiple metrics for a comprehensive evaluation. Senousy et al. (2023) introduces a novel approach called Actionable Uncertainty Quantification Optimization (AUQantO) to improve deep learning model performance by optimizing uncertainty quantification techniques. In conclusion, while the papers do not directly address pipe maintenance, the evaluation metrics and approaches discussed could be adapted to assess models for pipe maintenance decision-making. Accuracy, precision, recall, F1 score, and AUC-ROC could be used to evaluate the performance of models predicting pipe failures or maintenance needs. Additionally, considering multiple metrics and incorporating uncertainty quantification techniques could enhance the reliability and decision-making capabilities of such models in the context of pipe maintenance.

Makana et al. (2022) emphasizes the need for broader and richer data sets, including both asset and surrounding environment data, to inform the development and application of deterioration modeling approaches. This underscores the importance of comprehensive data for validation purposes, as more diverse and representative data can lead to more robust cross-validation and out-of-sample testing (Makana et al., 2022). Interestingly, Rinas et al. (2020) presents a real-world case study where sediment transport inside a pressure pipe was monitored using online total suspended solids measurements. This in situ data was used for the development and calibration of a sediment transport model, which can be considered a form of real-world pilot testing. The resulting simulation over 30 days of pumping operation demonstrated the model's ability to predict sediment transport under various conditions, highlighting the value of real-world validation (Rinas et al., 2020). In conclusion, while the papers do not explicitly discuss validation techniques, they emphasize the importance of accurate modeling, comprehensive data collection, and real-world testing. These elements are fundamental to effective validation processes, which are essential for ensuring the reliability and applicability of urban drainage pipe deterioration models in practice.

6.2.7 Final remarks

Urban drainage infrastructure is vital for safeguarding urban environments from flooding and public health hazards; however, these systems are increasingly strained by urbanization, climate change, and aging materials. As detailed in this chapter, deterioration of drainage pipelines arises from a range of physical, chemical, and biological processes—often exacerbated by deferred maintenance and evolving environmental pressures. Preventative strategies, therefore, require a comprehensive and systematic approach that prioritizes data quality, robust modeling, and ongoing validation.

A critical foundation for understanding and predicting pipe deterioration lies in data collection and management. Reliable inspection logs, maintenance records, and auxiliary information (e.g., climate data, soil characteristics, and population density) enable more accurate modeling of deterioration processes. Yet issues such as inconsistent collection protocols, missing values, and incomplete network coverage remain significant challenges. Standardized data collection methods, greater adoption of sensor technologies, and advanced GIS platforms are all vital to improving data availability and consistency.

Modeling approaches for pipe deterioration vary in complexity and scope:

- Empirical (Statistical) Models draw on historical data to capture trends in pipe failures. They can be deterministic—suitable for system-level failure rates—or probabilistic, which better handle time-to-failure and uncertainty. Although these methods are often straightforward to implement, they can struggle when extrapolating beyond conditions reflected in the training dataset and may be limited by incomplete or noisy historical data.
- Physically Based (Mechanistic) Models rest on the fundamental laws governing degradation processes such as corrosion, fatigue, and structural loading. These approaches excel at illuminating the underlying causes of deterioration and can account for both gradual and sudden events. However, they are frequently computationally expensive, difficult to calibrate for large-scale networks, and highly sensitive to parameter uncertainties—demands that underscore the need for abundant and high-quality data.
- Machine Learning (ML) Techniques offer notable advantages in handling complex, high-dimensional data and have shown promising results in predicting pipe failures and deterioration risk. Methods such as random forests and neural networks can quickly handle large datasets, capture nonlinear relationships, and support real-time analytics. Nonetheless, challenges exist around the need for extensive labeled data, the risk of overfitting, and model interpretability—issues that can be mitigated through domain-informed feature engineering, Bayesian regularization, or hybrid ML-mechanistic frameworks.

Across all approaches, model evaluation and validation are essential to ensure reliability and operational relevance. Metrics such as accuracy, precision, recall, F1 scores, and AUC-ROC, while drawn from fields like medical diagnostics, are equally valuable in assessing classification tasks related to pipe failure prediction. Further steps—such as real-world pilot studies, cross-validation with independent datasets, and uncertainty quantification—offer additional layers of verification and aid in practical, data-driven decision-making.

Overall, maintaining urban drainage networks cost-effectively and sustainably requires a synergistic strategy. Continuous data collection and careful management can support advanced modeling techniques. Statistical methods can provide broad-system insights, physically based models clarify the mechanisms of deterioration, and ML approaches can highlight nuanced, data-driven patterns. Combining these approaches—while addressing data quality and interpretability—will enhance the resiliency of urban drainage infrastructure, ultimately ensuring safer, healthier, and more sustainable urban environments.

7. Conclusions

This document analyses the effect of deterioration on different civil engineering infrastructures. In particular, Section 5.1 investigates the damage and deteriorations in half-joints, known also as Gerber saddles. In this context, a method for the evaluation of the load-bearing capacity of saddles subject to degradation and corrosion is proposed and results explained.

In Section 5.2, the primary physical, chemical, and biological deterioration mechanisms affecting masonry bridges were analyzed, with a focus on their impact on long-term structural performance. The most critical defects, including brick loss, material loss in mortar joints, surface cracking, and exfoliation, were systematically classified, emphasizing their role in reducing the effective cross-section and potentially leading to structural failures. A comparative analysis of modeling approaches was conducted, highlighting the advantages and limitations of different strategies for defect assessment. Limit analysis was presented as an efficient tool for evaluating structural stability under deterioration, while FEM and DEM allow for more detailed simulations. FEM enables direct modeling of crack propagation and stiffness degradation, whereas DEM is particularly suited for capturing the loss of connectivity between masonry components. Case studies were referenced to illustrate the applicability of these methods. Finally, limit analysis will be further developed as a tool for studying large-scale deterioration effects, supporting predictive assessments and conservation strategies for masonry bridges.

In Section 0, typical degradation phenomena for steel bridges were addressed, i.e., with either reference to environmental and man-induced effects. Namely, metallic corrosion was first addressed in Section 5.3.1.2 at material scale, paying particular attention to influencing factors which can affect its development (e.g., temperature, relative humidity, steel composition, environmental conditions, etc…). A key distinction was made among uniform and localized corrosion, with the latter condition being critically detrimental for steel bridges. Subsequently, fatigue cracking in steel components due to transient loads was discussed in Section 5.3.1.3 from a phenomenological perspective. Therefore, established techniques to account for the aforementioned phenomena at structural scale were illustrated. For instance, main features of advanced models for corrosion analysis, e.g., such as cellular automata, Poisson processes and Monte Carlo simulations were summarized in Section 5.3.2.1. Subsequently, stress-, strain- and LEFM-based methods for fatigue modelling in steel infrastructures were shown in Section 5.3.2.2. Finally, interaction among environmental and anthropic degradation phenomena in steel structures (e.g., corrosion fatigue) were briefly discussed with both reference to phenomenological and modelling aspects.

In Section 5.4, the research unit at Sapienza University of Rome has presented ongoing efforts toward developing a comprehensive model to simulate the serviceability conditions of Integral Abutment Bridges (IABs), accounting for the combined effects of traffic loads, thermal gradients, chloride-induced corrosion (affecting both ordinary reinforcement and post-tensioned tendons), and aging phenomena. In particular, this report has outlined the selected case study, detailing the structural model and the numerical methods used to simulate corrosion processes triggered by airborne chlorides. The implemented corrosion models effectively capture critical mechanisms, including chloride diffusion through concrete, the initiation and propagation of steel corrosion, and the resulting loss of cross-sectional area in reinforcement and tendons. By incorporating time-dependent and spatially varying chloride exposure, the model provides realistic predictions of generalized and localized corrosion effects on steel reinforcement. The model is currently undergoing further developments, including the numerical simulation of traffic loads, thermal gradients, steel relaxation, creep, and concrete shrinkage. Numerical simulations will be performed once the model is fully developed.

Then, Section 6.1 showed that a key factor for achieving a proactive management strategy of the water distribution network is improving the accuracy of pipe failure prediction models. However, the underlying mechanisms of incorporating explanatory variable data into the models still need to be better understood as well as the developing of suitable models that could be used for cases where data are insufficient or incomplete. In recent years, machine learning (ML) approaches have been used widely for water pipe condition assessment and failure prediction. Machine learning-based models have emerged as a powerful tool in enhancing the predictive capabilities of water distribution network models. In order to investigate the response of models, they must necessarily developed and validated considering relevant and large case studies such as the water distribution network of Parma.

Finally, Section 6.2 described the urban drainage infrastructure deterioration and investigated the efficiency of prediction models. After a classification and the identification of advantages and disadvantages of different approaches, the chapter focused on the data needs of each approach and the definition of compelling developments of existing approaches to be applied to urban drainage pipes.

8. References

Abebe, Y., & Tesfamariam, S. (2020). Storm sewer pipe renewal planning considering deterioration, climate change, and urbanisation: a dynamic Bayesian network and GIS framework. Sustainable and Resilient Infrastructure, 8(1), 70–85.

Adasooriya, N. D., Pavlou, D., & Hemmingsen, T. (2020). Fatigue strength degradation of corroded structural details: A formula for S-N curve. Fatigue & Fracture of Engineering Materials & Structures, 43(6), 721-733.

Almheiri Z., Meguid M., Zayed T. (2021). Failure modeling of water distribution pipelines using meta-learning algorithms, Water Research 205 (2021) 117680.

Almusallam, A. A. (2001). Effect of degree of corrosion on the properties of reinforcing steel bars. Construction and building materials, 15(8), 361-368.

Anderson, T. L. (2017). Fracture mechanics—Fundamentals and applications (4th ed.). CRC Press: Boca Raton, FL, USA;

Ayati, A. H., & Haghighi, A. (2023). Multiobjective Wrapper Sampling Design for Leak Detection of Pipe Networks Based on Machine Learning and Transient Methods. Journal of Water Resources Planning and Management, 149(2).

Baek, C. W., Kim, E. S., & Kim, J. H. (2005). Estimate of pipe deterioration and optimal scheduling of rehabilitation. Water Supply, 5(2), 39–46.

Banik, B. K., Di Cristo, C., Leopardi, A., & De Marinis, G. (2017). Illicit intrusion characterization in sewer systems. Urban Water Journal, 14(4), 416–426.

Barton, N. A., Tran, T. H., Hallett, S. H., & Jude, S. R. (2022). An evolution of statistical pipe failure models for drinking water networks: a targeted review. Water Supply, 22(4), 3784–3813.

Basquin, O. H. (1910). The exponential law of endurance tests. Proceedings of the American Society for Testing and Materials, 10, 625-630.

Baumann, H., Ravn, N. H., & Schaum, A. (2022). Efficient Hydrodynamic Modelling of Urban Stormwater Systems for Real-Time Applications. Modelling, 3(4), 464–480.

Berardi, L., Giustolisi, O., Savic, D. A., & Kapelan, Z. (2009). An effective multi-objective approach to prioritization of sewer pipe inspection. Water Science and Technology, 60(4), 841–850. https://doi.org/10.2166/wst.2009.432

Biondini, F. (2011). Cellular automata simulation of damage processes in concrete structures. In Soft computing methods for civil and structural engineering (pp. 229-264). Saxe-Coburg Publications.

Biscarini, C., Catapano, I., Cavalagli, N., Ludeno, G., Pepe, F. A., & Ubertini, F. (2020). UAV photogrammetry, infrared thermography, and GPR for enhancing structural and material degradation evaluation of the Roman masonry bridge of Ponte Lucano in Italy. NDT & E International, 115, 102287.

Boller, C., & Seeger, T. (1987). Materials data for cyclic loading – Low alloy steels. Elsevier: Amsterdam, Netherlands.

Brix, A., Senoussi, R., Couteron, P., & Chadoeuf, J. (2001). Assessing goodness of fit of spatially inhomogeneous Poisson processes. Biometrika, 88(2), 487-497.

BS EN 1992-1-1:2023. Eurocode 2 - Design of concrete structures - Part 1-1: General rules and rules for buildings, bridges and civil engineering structures, 2023.

Burstein, G. T., Liu, C., Souto, R. M., & Vines, S. P. (2004). Origins of pitting corrosion. Corrosion Engineering Science & Technology, 39(1), 25-30.

Camuffo, D., Fassina, V., & Havermans, J. (2021). Basic environmental mechanisms affecting cultural heritage – Understanding deterioration mechanisms for conservation purposes. Nardini Editore.

Casas, J.R. (2009) A probabilistic fatigue strength model for brick masonry under compression. Construction and Building Materials, 23(8), 2964-72.

Cavalagli, N., Gusella, V., Severini, L. (2017). The safety of masonry arches with uncertain geometry. Computers and Structures, 188, 17-31. https://doi.org/ 10.1016/j.compstruc.2017.04.003

CEN (European Committee for Standardization). (2005). EN1993-1-9 Eurocode 3: Design of steel structures – Part 1-9: Fatigue. CEN.

CEN (European Committee for Standardization). (2006). EN1993-1-11 Eurocode 3: Design of steel structures – Part 1-11: Design of structures with tension components. CEN.

Cen, H., Huang, D., Liu, Q., Tang, A., & Zong, Z. (2023). Application Research on Risk Assessment of Municipal Pipeline Network Based on Random Forest Machine Learning Algorithm. Water, 15(10), 1964.

Chang, Q., Kazama, S., Touge, Y., & Aita, S. (2019). The effects of spatial discretization on performances and parameters of urban hydrological model. Water Science and Technology, 80(3), 517–528.

Chen, J., Blume, H. P., & Beyer, L. (2000). Weathering of rocks induced by lichen colonization – A review. CATENA, 39(2), 121-146.

Chen, T., Philippi, I., Phan, Q. B., Nguyen, L., Bui, N. T., Dacunha, C., & Nguyen, T. T. (2024). A vision transformer machine learning model for COVID-19 diagnosis using chest X-ray images. Healthcare Analytics, 5, 100332.

Chowdhury, R. K., & Rajput, M. A. (2016). Will greywater reuse really affect the sewer flow? Experience of a residential complex in Al Ain, UAE. Water Supply, 17(1), 246–258.

Coffin, L. F. (1954). A study of the effects of cyclic thermal stresses on a ductile metal. Transactions of ASME, 76, 931-950.

Coronelli, D., & Gambarova, P. (2004). Structural assessment of corroded reinforced concrete beams: modeling guidelines. Journal of structural engineering, 130(8), 1214-1224.

Dawood T., Emad Elwakil E., Novoa H. M., Delgado J. F. G. (2020). Artificial intelligence for the modeling of water pipes deterioration mechanisms, Automation in Construction 120.

De La Cruz, J. L., Kuniewski, S., Van Noortwijk, J. M., & Gutierrez, M. A. (2008). Spatial nonhomogeneous Poisson process in corrosion management. Journal of The Electrochemical Society, 155(8), 396-406.

De Ponti, R. D., Cantini, L., & Bolondi, L. (2021). Edifici in muratura – Caratteristiche costruttive, vulnerabilità e approfondimenti diagnostici. Grafill. (in italian)

Dehghan, A., Mcmanus, K. J., & Gad, E. F. (2008). Statistical analysis of structural failures of water pipes. Proceedings of the Institution of Civil Engineers - Water Management, 161(4), 207–214.

Di Carlo, F., Meda, A., Molaioni, F., & Rinaldi, Z. (2023). Experimental evaluation of the corrosion influence on the structural response of Gerber half-joints. Engineering Structures, 285, 116052.

Dowling, N. E. (2004). Mean stress effects in stress-life and strain-life fatigue. SAE Technical Paper, 2004-01-2227.

DNV (Det Norske Veritas). (2024). DNVGL-RP-C203 - Fatigue design of offshore steel structures: Recommended practice. DNV: Oslo, Norway.

Duan, H., Li, J., & Yuan, Z. (2024). Making waves: Knowledge and data fusion in urban water modelling. Water Research X, 24, 100234.

ECCS (European Convention for Constructional Steelwork). (2018). Fatigue design of steel and composite structures (2nd ed.). Wiley, Ernst & Sohn: Hoboken, NJ, USA.

Fan, X., Wang, X., Zhang, X., Xiong B.Yu (2022). Machine learning based water pipe failure prediction: The effects of engineering, geology, climate and socio-economic factors. Reliability Engineering & System Safety, 219, 108185.

Farmani R., Kakoudakis K., Behzadian K., Butler D. (2017). Pipe Failure Prediction in Water Distribution Systems Considering Static and Dynamic Factors, WDSA Procedia Engineering 186, 117 – 126.

Ferretti, D., & Bazant, Z. P. (2006). Stability of ancient masonry towers: Moisture diffusion, carbonation, and size effect. Cement and Concrete Research, 36(7), 1379-1388.

Forero-Ortiz E., Martinez-Gomariz E., Sanchez-Juny M., Gonzalez J. C., Cucchietti F., Viader F. B., Monton M. S. (2023). Models and explanatory variables in modelling failure for drinking water pipes to support asset management: a mixed literature review, Applied Water Science, 13:210.

fib Bulletin 34 (2006) Model Code for Service Life Design.

fib Model Code 2020 (2024).

Frehmann, T., Nafo, I., Niemann, A., & Geiger, W. F. (2002). Storm water management in an urban catchment: Effects of source control and real-time management of sewer systems on receiving water quality. Water Science and Technology, 46(6–7), 19–26.

Gjorv O.E. (2014), Durability design of concrete structures in severe environments, CRC Press.

Gilbert, M. (1993) The behavior of masonry arch bridges containing defects. PhD Thesis, University of Manchester.

Gonzalez, J. A., Andrade, C., Alonso, C., & Feliu, S. (1995). Comparison of rates of general corrosion and maximum pitting penetration on concrete embedded steel reinforcement. Cement and concrete research, 25(2), 257-264.

Granneman, S. J. C., Lubelli, B., & van Hees, R. P. J. (2016). Lime mortar with mixed in crystallization modifiers to mitigate salt damage. In Proceedings of the 10th International Conference on Structural Analysis of Historical Constructions (SAHC), Leuven, Belgium, 13-15 September.

Griffith, A. A. (1920). The phenomena of rupture and flow in solids. Philosophical Transactions of the Royal Society of London, Series A, 221, 163-198.

Guessasma, S., Elkedim, O., Nardin, P., Hamzaoui, R., & Grosdidier, T. (2007). Monte Carlo simulation of uniform corrosion process under potentiostatic conditions. Corrosion Science, 49(7), 2880-2904.

Harremoës, P., & Madsen, H. (1999). Fiction and reality in the modelling world-balance between simplicity and complexity, calibration and identifiability, verification and falsification. Water Science and Technology, 39(9), 1–8.

Harsimran, S., Santosh, K., & Rakesh, K. (2021). Overview of corrosion and its control: A critical review. Proceedings on Engineering Sciences, 3(1), 13-24.

Huang, Y., Savic, D., Zheng, F., Jia, Y., Kapelan, Z., & Zhang, J. (2022). Exploring the Performance of Ensemble Smoothers to Calibrate Urban Drainage Models. Water Resources Research, 58(10).

IIW (International Institute for Welding). (2000). Fatigue design procedure for welded hollow section joints (Doc. XIII-1804-99, XV-1035-99). IIW: Cambridge, UK.

International Union of Railways (UIC). (2018). Recommendations for the inspection, assessment and maintenance of masonry arch bridges. Paris, France: UIC.

Irwin, G. R. (1956). Fracture dynamics. Fracturing of Metals, 147-166. American Society for Metals.

ISO (International Organization for Standardization). (2012). ISO 9224: Corrosion of metals and alloys – Corrosivity of atmospheres – Guiding values for the corrosivity categories. ISO: Geneva, Switzerland.

Jiang, C., Wu, C., & Jiang, X. (2018). Experimental study on fatigue performance of corroded high-strength steel wires used in bridges. Construction and Building Materials, 187, 681-690.

JSCE. (2007). Standard specifications for concrete – design.

Kerwin S., Garcia de Soto B., Adey B., Sampatakaki K. & Heller H. (2023). Combining recorded failures and expert opinion in the development of ANN pipe failure prediction models, Sustainable and Resilient Infrastructure, 8:1, 86-108.

Koltsida, I.S., Tomor, A.K., Booth, C.A. (2018) Probability of fatigue failure in brick masonry under compressive loading. International Journal of Fatigue, 112, 233-239.

Kimutai E., Betrie G., Brander R., R. Sadiq R. & Tesfamariam S. (2015). Comparison of Statistical Models for Predicting Pipe Failures: Illustrative Example with the City of Calgary Water Main Failure, J. Pipeline Syst. Eng. Pract., 6(4).

Landolfo, R., Cascini, L., & Portioli, F. (2010). Modeling of metal structure corrosion damage: A state of the art report. Sustainability, 2(6), 2163-2175.

Laterza, M., D'Amato, M., Casamassima, V.M. (2017). Stress-Life curves method for fatigue assessment of ancient brick arch bridges. International Journal of Architectural Heritage, 11(6), 843-858. https://doi.org/10.1080/15583058.2017.1315621

Lehner, P., Krejsa, M., Pařenica, P., Křivý, V., & Břozovský, J. (2019). Fatigue damage analysis of a riveted steel overhead crane support truss. International Journal of Fatigue, 128, 105190.

Levy, A. V. (1995). Erosion and erosion-corrosion of metals. Corrosion, 51(11), 872-883.

Li, L., Mahmoodian, M., & Chun-Qing, L. (2020). Prediction of fatigue failure of corrosion affected riveted connections in steel structures. Structural & Infrastructural Engineering, 16(12), 1524-1538.

Liang, H., Wang, M., Wen, Y., Du, F., Jiang, L., Geng, X., Tang, L., & Yan, H. (2023). Predicting acute pancreatitis severity with enhanced computed tomography scans using convolutional neural networks. Scientific Reports, 13(1).

Liu, T., & Weyers, R. W. (1998). Modeling the dynamic corrosion process in chloride contaminated concrete structures. Cement and Concrete Research, 28(3), 365-379.

Made, A. M., Martin, J. V., & Colville, J. (2004). The effects of moisture on compressive strength and modulus of brick masonry. In 13th International Brick and Block Masonry Conference, Amsterdam, July 4-7, p. 8.

Makana, L. O., Schellart, A. N. A., Metje, N., Rogers, C. D. F., Boxall, J. B., Shepherd, W. J., & Tait, S. (2022). Future Inspection and Deterioration Prediction Capabilities for Buried Distributed Water Infrastructure. Journal of Pipeline Systems Engineering and Practice, 13(3).

Makris, K. F., Langeveld, J. G., & Clemens, F. H. L. R. (2021). Extensive testing on PVC sewer pipes towards identifying the factors that affect their operational lifetime. Structure and Infrastructure Engineering, 1601–1613

Manson, S. S. (1952). Behavior of materials under conditions of thermal stress. Heat Transfer Symposium, University of Michigan, 27–28 June. University of Michigan Press.

Mazumder R. M., Salman A. M., Li Y. & Yu X. (2021). Asset Management Decision Support Model for Water Distribution Systems: Impact of Water Pipe Failure on Road and Water Networks, J. Water Resour. Planning and Management, 147(5).

Medhekar, S. R., Bley, D. C., & Gekler, W. C. (1993). Prediction of vessel and piping failure rates in chemical process plants using the Thomas model. Process Safety Progress, 12(2), 123–126.

Milone, A., & Landolfo, R. (2022). A simplified approach for the corrosion fatigue assessment of steel structures in aggressive environments. Materials, 15(6), 2210.

Milone, A., & Berto, F. (2022). Methodologies for the fatigue assessment of corroded wire ropes: A state-of-the-art review. Structures, 37, 787-794.

Milone, A. (2023). On the performance of lap-shear hot-driven riveted connections: Experimental and numerical study (Doctoral dissertation).

Milone, A., Foti, P., Viespoli, L. M., Wan, D., Mutignani, F., Landolfo, R., & Berto, F. (2024). Influence of hot-dip galvanization on the fatigue performance of high-strength bolted connections. Engineering Structures, 299, 117136.

Mohammed A., Kaddoura K., Zayed T., Moselhi O., Hawari A. (2022). Integrated Reliability Assessment Model for Drinking Water Networks: A Case Study of the City of London, Canada, J. Perform. Constr. Facil., 36(5).

Nawy, E. G. (1985, November). Flexural cracking behavior of pretensioned and post-tensioned beams: the state of the art. In Journal Proceedings (Vol. 82, No. 6, pp. 890-900).

Nguyen, V. S., Jeong, M. C., Han, T. S., & Kong, J. S. (2013). Reliability-based optimisation design of post-tensioned concrete box girder bridges considering pitting corrosion attack. Structure and Infrastructure Engineering, 9(1), 78-96.

Ni, P., Mei, G., Shen, L., & Jiang, P. (2022). Load Capacity of Perforated Reinforced Concrete Sewer Pipes. Journal of Pipeline Systems Engineering and Practice, 13(1).

Niemi, E., Fricke, W., & Maddox, S. J. (2006). Fatigue analysis of welded components - Designer's guide to the structural hot-spot stress approach. Woodhead Publishing: Cambridge, UK.

Norreys, R., & Cluckie, I. (1997). A novel approach to the real-time modelling of large urban drainage systems. Water Science and Technology, 36(8–9), 19–24.

Osgood, C. C. (1982). Fatigue design (2nd ed.). Pergamon Press: Oxford, UK.

Paris, P. C., Gomez, M. P., & Anderson, W. E. (1961). A rational analytic theory of fatigue. The Trend in Engineering, 13, 9-14.

Papakonstantinou, K. G., & Shinozuka, M. (2013). Probabilistic model for steel corrosion in reinforced concrete structures of large dimensions considering crack effects. Engineering Structures, 57, 306-326.

Paris, P. C., & Erdogan, F. (1963). A critical analysis of crack propagation laws. Journal of Basic Engineering, 85, 528-533.

Pekşen, M. F., Yurtsever, U., & Uyaroğlu, Y. (2024). Enhancing electrical panel anomaly detection for predictive maintenance with machine learning and IoT. Alexandria Engineering Journal, 96, 112–123

Philip B. E., Aljassmi H. (2020). The Relevance of Water Pipe Deterioration Prediction Models: A review, International Journal of Scientific & Technology Research volume 9, issue 02.

Popov, B. N. (2015). Corrosion engineering: Principles and solved problems. Elsevier: Amsterdam, Netherlands.

Poulsen, E. (2014). Diffusion of chloride in concrete: theory and application. CRC Press.

Powers, T. C. (1945). A working hypothesis for further studies of frost resistance. Journal of the American Concrete Institute, 16(4), 245-272.

Ramos, H. M., & Besharat, M. (2021). Urban Flood Risk and Economic Viability Analyses of a Smart Sustainable Drainage System. Sustainability, 13(24), 13889.

Reinoso-Burrows, J. C., Toro, N., Cortés-Carmona, M., Pineda, F., Henriquez, M., & Galleguillos Madrid, F. M. (2023). Cellular automata modeling as a tool in corrosion management. Materials, 16(6051).

Rinas, M., Koegst, T., Tränckner, J., Frischmuth, K., & Fricke, A. (2020). Sediment Transport in Sewage Pressure Pipes, Part II: 1 D Numerical Simulation. Water, 12(1), 282.

Roberts, T., Hughes, T., Dandamudi, V., Bell, B. (2006). Quasi-static and high cycle fatigue strength of brick masonry. Construction and Building Materials, 20(9), 603-14.

Rybczak, M., Popowniak, N., & Lazarowska, A. (2024). A Survey of Machine Learning Approaches for Mobile Robot Control. Robotics, 13(1), 12.

Salihu, C., Hosseini, M. R., Kineber, A. F., Zayed, T., Mohandes, S. R., & Elghaish, F. (2023). A Deterioration Model for Sewer Pipes Using CCTV and Artificial Intelligence. Buildings, 13(4), 952.

Sambito, M., Di Cristo, C., Freni, G., & Leopardi, A. (2019). Optimal water quality sensor positioning in urban drainage systems for illicit intrusion identification. Journal of Hydroinformatics, HYDRO-D-19-00036R1.

Sanchez-Silva, M., Klutke, G.-A., & Rosowsky, D. V. (2012). Optimisation of the design of infrastructure components subject to progressive deterioration and extreme loads. Structure and Infrastructure Engineering, 8(7), 655–667.

Santos, P., Amado, C., Coelho, S. T., & Leitão, J. P. (2016). Stochastic data mining tools for pipe blockage failure prediction. Urban Water Journal, 14(4), 343–353.

Saviano, F., Parisi, F., Lignola, G.P. (2022). Material aging effects on the in-plane lateral capacity of tuff stone masonry walls: a numerical investigation. Materials and Structures, 55(198). https://doi.org/10.1617/s11527-022-02032-5

Scherer, G. W. (1999). Crystallization in pores. Cement and Concrete Research, 29(8), 1347-1358.

Scheinker, A. (2021). Adaptive Machine Learning for Robust Diagnostics and Control of Time-Varying Particle Accelerator Components and Beams. Information, 12(4), 161.

Schijve, J. (2009). Fatigue of structures and materials. Kluwer Academic Publishing: Amsterdam, Netherlands.

Schumacher, A. (2003). Fatigue behavior of welded circular hollow section joints (Doctoral dissertation).

Senousy, Z., Gaber, M. M., & Abdelsamea, M. M. (2023). AUQantO: Actionable Uncertainty Quantification Optimization in deep learning architectures for medical image classification. Applied Soft Computing, 146, 110666.

Shafei, B., Alipour, A., & Shinozuka, M. (2012). Prediction of corrosion initiation in reinforced concrete members subjected to environmental stressors: A finite-element framework. Cement and Concrete Research, 42(2), 365-376.

Taiwo, R., Ben Seghier, M. E. A., & Zayed, T. (2023). Toward sustainable water infrastructure: The state-of-the-art for modeling the failure probability of water pipes. Water Resources Research 59, e2022WR033256. https://doi.org/10.1029/2022WR033256.

Thomas, M. D., & Bamforth, P. B. (1999). Modelling chloride diffusion in concrete: Effect of fly ash and slag. Cement and Concrete Research, 29(4), 487-495.

Tomor, A.K., Nichols, J.M., Orban, Z. (2024). Evaluation of the loss of uniaxial compressive strength of sandstones due to moisture. International Journal of Architectural Heritage, 18(5), 771-787. https://doi.org/10.1080/15583058.2023.218313

Tuutti, K. (1982) Corrosion of steel in concrete, CBI.

Tzortzinis, G., Chengbo, A., Brena, S. F., & Gerasimidis, S. (2022). Using 3D laser scanning for estimating the capacity of corroded steel bridge girders: Experiments, computations and analytical solutions. Engineering Structures, 265(6), 114407.

UIC Report. (2020). Catalogue of damages in masonry arch bridges. UIC Railway Publications.

Val, D. V., & Melchers, R. E. (1997). Reliability of deteriorating RC slab bridges. Journal of Structural Engineering, 123(12), 1638-1644.

Vidal, T., Castel, A., & François, R. (2004). Analyzing crack width to predict corrosion in reinforced concrete. Cement and Concrete Research, 34(1), 165-174.

Vedavyasan, C. V. (2013). Corrosion. In Encyclopedia of Membranes. Springer: Berlin, Germany.

Velázquez, J. C., Caleyo, F., Valor, A., & Hallen, J. M. (2009). Predictive model for pitting corrosion in buried oil and gas pipelines. Corrosion, 65, 332-342.

Wang, H., Li, J., Qiu, Y., Zhang, L., Jia, H., & Han, G. (2021). Integrated and Control-Oriented Simulation Tool for Optimizing Urban Drainage System Operation. Water, 14(1), 25.

Wang, Y., Pan, Z., Zhao, C., & Zeng, B. (2023). Long-term behavior of prestressed concrete industrial buildings in chloride-based industrial environments. Journal of Building Engineering, 76, 107344.

Wang, Y., & Zheng, Y. (2019). Research on corrosion fatigue performance and multiple fatigue sources fracture process of corroded steel wires. Advances in Civil Engineering, 2019, 4914359.

Wöhler, A. (1860). Versuche zur Ermittlung der auf die Eisenbahnwagenachsen einwirkenden Kräfte und die Widerstandsfähigkeit des Wagen-Achsen. Zeitschrift für Bauwesen, 10, 583-616. [in German].

Winkler, E. M. (1973). Stone: Properties, durability in man's environment. Springer Verlag.

Wu, P., Zhang, Z., Peng, X., & Wang, R. (2024). Deep learning solutions for smart city challenges in urban development. Scientific Reports, 14(1).

Yang, L., Ma, Q., & Yu, B. (2018). Analytical solution and experimental validation for dual time-dependent chloride diffusion in concrete. Construction and Building Materials, 161, 676-686.

Yang, L. F., Cai, R., & Yu, B. (2017). Investigation of computational model for surface chloride concentration of concrete in marine atmosphere zone. Ocean Engineering, 138, 105-111.

Yang, M. D., & Su, T. C. (2006). Automation model of sewerage rehabilitation planning. Water Science and Technology, 54(11–12), 225–232. https://doi.org/10.2166/wst.2006.805

Yarveisy, R., Khan, F., & Abbassi, R. (2023). Data-driven model to predict burst pressure in the presence of interacting corrosion pits. Journal of Pipeline Science and Engineering, 4(1), 100146.

Xu, H., Wang, Y., Fu, X., Wang, D., & Luan, Q. (2023). Urban Flood Modeling and Risk Assessment with Limited Observation Data: The Beijing Future Science City of China. International Journal of Environmental Research and Public Health, 20(5), 4640.

Zampieri, P., Zanini, M.A., Faleschini, F. (2016). Influence of damage on the seismic failure analysis of masonry arches. Construction and Building Materials, 119, 343-355. https://doi.org/10.1016/j.conbuildmat.2016.05.024

Zangenehmadar Z., Moselhi O. (2016). Prioritizing deterioration factors of water pipelines using Delphi method, Measurement 90 (2016) 491–499.

Zali R. B.; Latifi M.; Javadi A. A.; and Raziyeh Farmani R. (2024) Semisupervised Clustering Approach for Pipe Failure Prediction with Imbalanced Data Set, J. Water Resour. Plann. Managem., 150(2).

Zamanian, S., & Shafieezadeh, A. (2021). Temporal global sensitivity analysis of concrete sewer pipes under compounding corrosion and heavy traffic loads. Structure and Infrastructure Engineering, 19(8), 1108–1121.

Zheldakov, D., Mustafin, R., Sinitsin, D., Bulatov, B., Gaysin, A., & Kozlov, V. (2021). Durability Control of Brickwork's Material Including Operation Parameters of the Building Enclosure. Mathematical Modelling of Engineering Problems, 8(6), 871–880.

Zhang, S. F., Lu, C. H., & Liu, R. G. (2011). Experimental determination of chloride penetration in cracked concrete beams. Procedia Engineering, 24, 380-384.